Preparation, Crystal Chemistry and Electrical Properties of Double Metal Nitrides Containing Lithium

Hisanori YAMANE

Contents

Chapter 1.

General Introduction

The phenomena of ionic conduction in solids have been known since the nineteenth century (1). The materials having high ionic conductivity are called as superionic conductors or solid electrolytes. About twenty years ago, the knowledge of superionic conductors was limited only about a few materials such as ZrO_2 and AgI. The research concerning superionic conductors has been promoted after the comprehensive study conducted by Yao and Kummer in 1967 (2) for β-Al_2O_3 which has high conductivitiy of Na^+ ion at ambient temperature. It was utilized to the sodium-sulfur battery as a solid electrolyte. Recently various kinds of new battery system have been proposed such as lithium-sulfur battery, fuel cell, lithium intercalation battery and so on. More efficient energy supply and storage require improvements of batteries in terms of energy and power density. The finding of new solid electrolytes is crucial for the improvements. Solid electrolytes have possibilities to be used in some other electric devices such as gas sensors. From this viewpoint, survey of new superionic conductors is an exciting problem and one of the most important tasks for material scientists.

A lithium battery is fairly interesting because of its high energy density and its long term stability. The high energy density is due to a low equivalent weight of Li metal and its high generated cell voltages. Solid lithium battery is in a next step of the battery development. Therefore, many kinds of lithium ion conductors have been studied. Lithium nitride has the highest conductivity of 10^{-1} Sm^{-1} at room temperature (300 K) among the various lithium ionic conductors (3). The structure of Li_3N is composed of hexagonally dense packed "Li_2N" layers connected by other lithium ions. Lithium ions migrate easily in the layer (4). Lithium β-alumina $LiAl_{11}O_{17}$ is a superionic conductor at ambient temperature (5). In this case, lithium ions move between the layers of spinel block. Another famous lithium ion conducter is $Li_{14}Zn(GeO_4)_4$ called LISICON, which has a framework built of corner-sharing ZrO_6 tetrahedra, GeO_4 tetrahedra and a three-dimensional network of tunnels in which Li^+ ions reside (6, 7).

A number of anion conductors such as ZrO_2, CaF_2 and β-PbF_2 have the fluorite structure which is considered to be favorable for ionic conductions (1). Their anionic conductivities are very high at elevated temperature and can be enhanced by doping other kinds of cations to generate anion vacancy. Antifluorite structure, in which the roles of cation and anion are opposite to the case of fluorite, might be a good structure type for cationic conductor. The anions construct face-centered cubic lattice and are surrounded by eight cations as illustrated in Fig. 1. Each cation is tetrahedally coordinated by anions. This structure has octahedral cation vacancies through which cations migrate generating Frenkel-type defects. Li_2O and Li_2S crystallize in the antifluorite structure, whose conductivities are low at ambient temperature (8, 9). Intrinsic vacancies were introduced in antifluorite-type structure of $Li_6\square Zn^{2+}O_4$ and $Li_5\square_2M^{3+}O_4$ (M = Al, Ga, Fe) (10, 11). The conductivity was enhanced in comparison with that of Li_2O. $Li_9N_2Cl_3$ ($Li_{1.8}N_{0.4}Cl_{0.6}$) also has the antifluorite structure with 10% vacancy of lithium site. Its lithium ion conductivity is relatively high at room

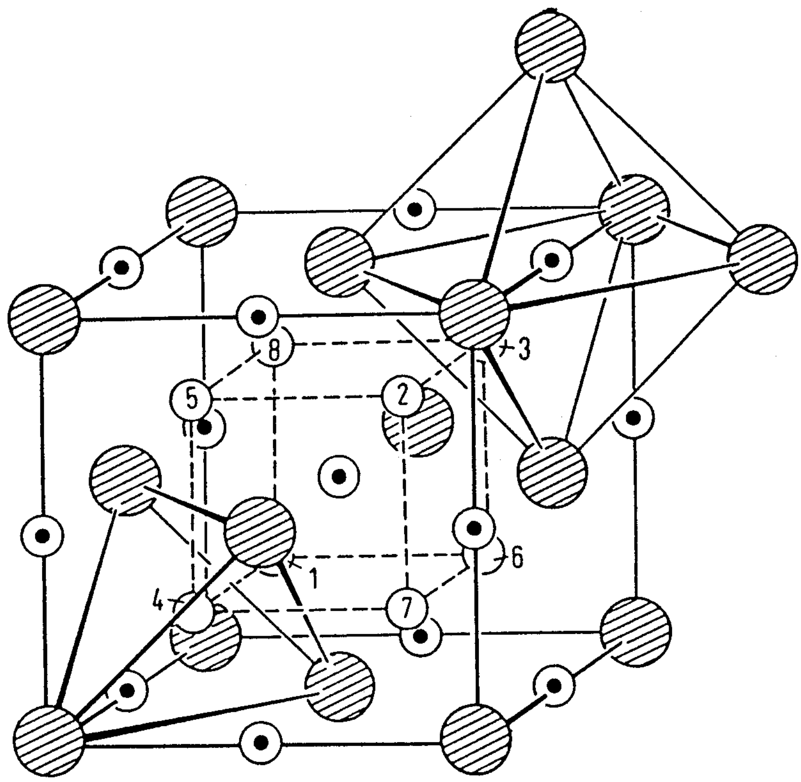

Fig. 1. Antifluorite-type structure. ▨ anion,
① - ⑧ cation, ⊙ octahedral vacancy.

temperature (10^{-4} Sm^{-1} at 300 K) (12). Figure 2 shows ionic conductivity for some kinds of lithium ion conductiors. The temperature dependence of ionic conductivity σ is generally given by the equation:

$$\sigma = n \frac{A}{RT} \exp(-\frac{Ea}{RT}) \quad ,$$

where T is the absolute temperature, R the gas constant, E_a an activation energy, n a number of mobile ions and A an inherent constant for each material. Plots of $\ln\sigma T$ against T^{-1} should give straight lines of slope $-E_a/R$.

Double metal nitrides containing lithium were systematically investigated by Juza et al. some twenty years ago (13). They described the structure as the antifluorite structure or its superstructure. The formula can generally be represented as $Li_{2x-3}M^{x+}N_{x-1}$ (M = Mg, Zn, Al, Ga, Si, Ti, Nb and so on). Two examples of the compounds are given in Fig. 3 for LiMgN (14) and in Fig. 4 for Li_3AlN_2 (15). Lithium and magnesium ions distribute statistically in tetrahedra of nitrogen ions. In the case of Li_3AlN_2, lithium and aluminum ions are ordered in the tetrahedral sites and construct an antifluorite-type superstructure with 32 nitrogen ions.

Lang et al. studied double metal nitrides such as $MgSiN_2$, $BaSiN_2$ and $LiGe_2N_3$ (16). Their structures are related to wurtzite-type. Table 1 summarized the previous studies concerning double metal nitride with lithium. The crystal structures were assumed using their powder X-ray diffraction data. Many compounds take the antifuorite-type structure. Other structural

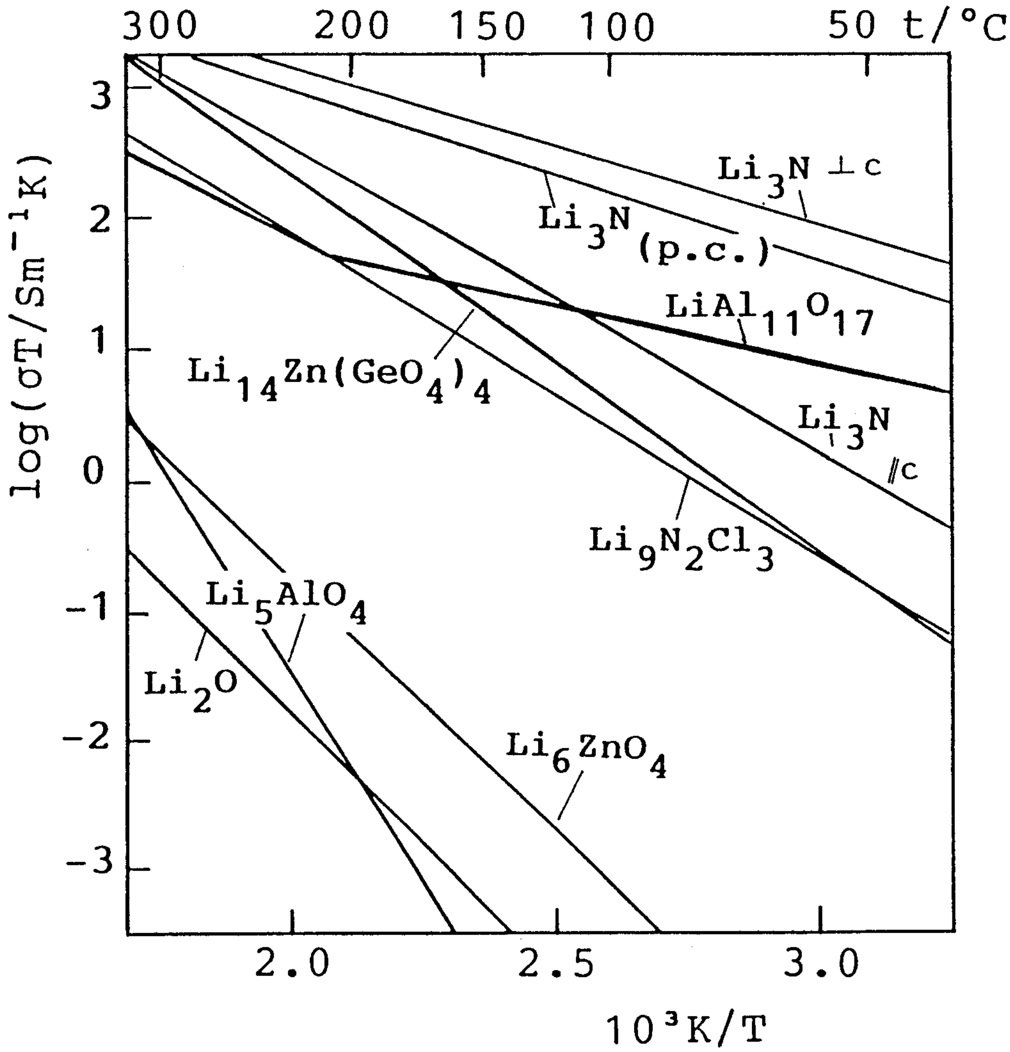

Fig. 2. Compilation of representative solid lithium ion conductors. The product of the conductvity σ and the absolute temperature T is plotted against the inverse absolute temperature.

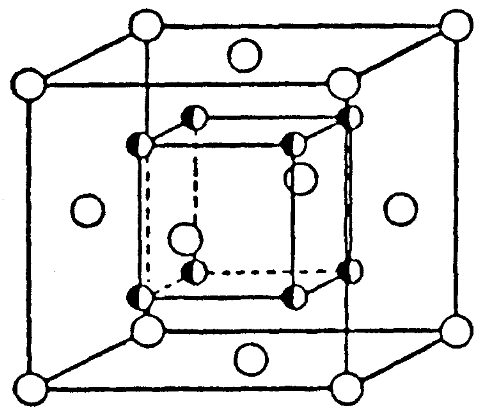

Fig. 3. Crystal structure of LiMgN. ○ nitrogen, ◐ disordered lithium and magnesium.

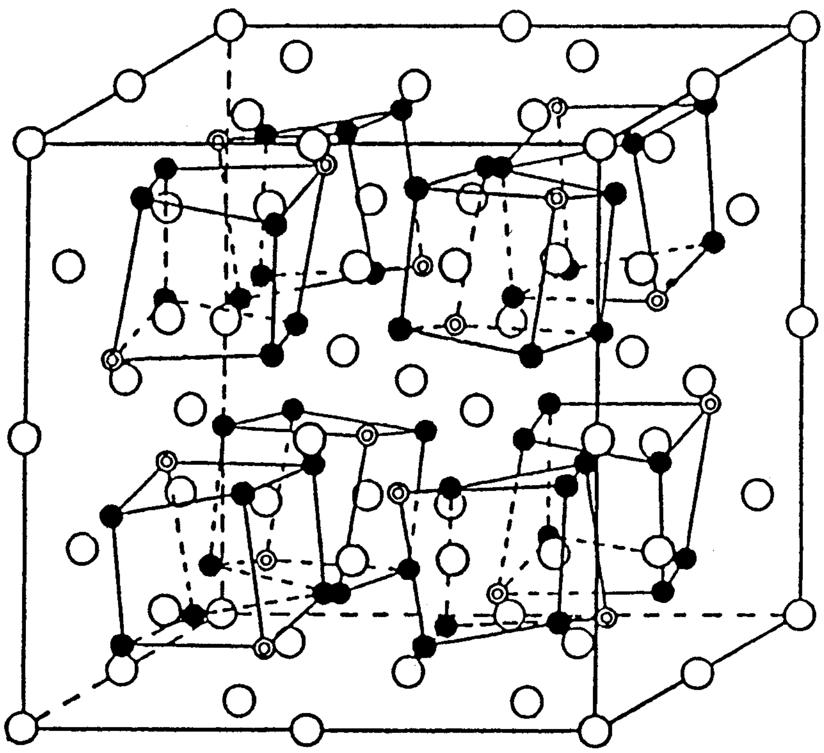

Fig. 4. Crystal structure of Li_3AlN_2. ⊙ Al, ● Li, ○ N.

Table 1. Double metal nitrides containing lithium.

period \ group	I a	I b	II a	II b	III a	III b	IV a	IV b	V a	V b	VI a	VI b	VII a	VII b	VIII
2	Li_3N (b)		LiBeN			Li_3BN_2		Li_2CN_2							
3			$LiMgN$ (a)			Li_3AlN_2 (a)		Li_5SiN_3 (a) $LiSi_2N_3$ (d) Li_2SiN_2 Li_8SiN_4		Li_7PN_4 (a) $LiPN_2$ (e)					
4		$Li_{2.7}Cu_{0.3}N$ (b)	LiCaN	$LiZnN$ (a)		Li_3GaN_2 (a)	Li_5TiN_3 (a)	Li_5GeN_3 (a) $LiGe_2N_3$ (d) Li_2GeN_2 Li_8GeN_4	Li_7VN_4 (a)		Li_9CrN_5 (a)		Li_7MnN_4 (a)		Li_3FeN_2 $Li_{2.5}Co_{0.5}N$ (b) $Li_{2.4}Ni_{0.6}N$ (b)
5							Li_2ZrN_2 (c)		Li_7NbN_4 (a)		Li_9MoN_5 (a)				

(a) Antifluorite-type structure.
(b) Lithium-nitride-type structure.
(c) Anti-Ce_2O_2S structure.
(d) Wurtzite-type structure.
(e) Cristobalite-type structure.

types such as Li_3N, anti-Ce_2O_2S, wurtzite and cristobalite could be observed in the family.

The results of preparation were discrepant between Juza et al. (17) and Lang et al. (18, 19) on the system of Li-Si-N and Li-Ge-N. Lang et al. prepared $LiSi_2N_3$,Li_2SiN_2 and Li_8SiN_4. They could not obtain Li_5SiN_3 reported by Juza et al., which had an antifluorite superstructure. The structure of $LiSi_2N_3$ is derived from wurtzite-type. Lithium is tetrahedraly coordinated in $LiSi_2N_3$ (20). The crystal structures of other phases have not yet been determined.

An existence of Li_3BN_2 was reported by Goubeau et al. (21) and DeVries et al. (22). Its crystal structure has not yet been revealed. DeVries and Fleisher assumed its structure as an antifluorite derivative. Melting points have been reported only for Li_3N (23) and Li_3BN_2 (21, 22), while most of nitrides decompose at high temperature without melting.

Superionic conduction might be expected on the double metal nitrides containing lithium ions in tetrahedral holes of cubic or hexagonal close-packed nitrogen ions. Lithium ions would migrate easily through the adjacent octahedral vacancies. Roth et al. reported appreciable ionic conductivities for Li_3AlN_2 and Li_3BN_2 in their preliminary study. But their sample contained much amount of impurities (24).

It is also interesting and useful to show how to find out new superionic conductor and how to enhance the ionic conductivity. It is obvious that lowering of activation energy in ionic conduction and increasing of a charge carrier number are important for an attainment of the purpose. Open structure and a high lithium content may be favorable factors for lithium superionic conductor. Much ambiguity still remains on preparation, crystal structure and properties of double metal nitrides containing lithium as mentioned above.

The decomposition voltage of Li_3N can be calculated as only 0.4 V using its thermochemical data (23, 25) in spite of its high ionic conductivity. High decomposition voltage is favorable for a long term usage of solid electrolyte in batteries. Formation of compounds by reactions between Li_3N and other materials may increase the decomposition voltage as observed in $Li_9N_2Cl_3$ (26, 27).

The present study attempted to prepare double metal nitrides containing lithium with other metalloids of Mg, Al, Si, P and B, and to examine their electric properties.

The results of preparation and measurements of lithium ion conduction for Li_3AlN_2 are presented in Chapter 2 of the present paper. The products are utilized to a Li-TiS_2 battery as a solid electorlyte. Six compounds prepared in the system of Li_3N-Si_3N_4 are described in Chapter 3. One of them is a new phase having the highest ionic conductivity among the materials under present study. These compounds are characterized by X-ray powder diffraction and chemically analyzed in order to clarify the ambiguity of presence and chemical composition on the phases reported by Juza et al. (17) and Lang et al. (18). Preparation and electic properties of LiMgN and Li_7PN_4 are studied in Chapters 4 and 5 respectively.

Single crystals of α- and β-Li_3BN_2 could be firstly prepared in the present study. The α-Li_3BN_2 is a compound reported by Goubeau and Anselment (21), but its crystal structure has not yet been determined; β-Li_3BN_2 is a new polymorph. In Chapter 6, preparation of these materials and phase relation between α and β-Li_3BN_2 are presented. Their crystal structures were also determined by single-crystal X-ray structural analysis. The structures and phase relation are also discussed in this chapter comparing with each other and other compounds. A general discussion on crystal chemistry of the compounds prepared in the present study is described in Chapter 7. Their ionic conductivities are also compared and discussed in this chapter. Preliminary results of the decomposition voltage study are presented for some products.

Chapter 2

Preparation and Electrical Properties of Li_3AlN_2

2-1. Introduction

Lithium aluminum nitride Li_3AlN_2 was originally prepared by Juza and Hund (15). It crystallizes in a cubic cell with a lattice parameter of a = 9.46 Å. The cell contains 16 formular weights of Li_3AlN_2 distributed in eight fluorite-like units. The 48 lithium and 16 aluminum ions are arranged in an ordered fashison in tetrahedral sites as illustrated in Fig. 4. Its ionic conductvtiy had been very roughly estimated on a mixture with AlN (24). But there has been no further investigation on pure Li_3AlN_2 so far.

In this chapter, the author deals with the preparation of Li_3AlN_2, the examination of its lithium ion conductivity and electrochemical properties in special reference to decomposition voltage. The decompsition voltage of Li_3N was estimated as only 0.4 V from thermochemical data (23, 25), while it has the highest ionic conductivity. This voltage is too low to be used in a lithium battery which can generate high voltage around 3 V.

2-2. Experimental

2-2-1. Preparation

Lithium nitride Li_3N was prepared by a reaction of nitrogen gas (Osaka Oxygen Ind. Ltd., 99.999%) with lithium metal (Wako Pure Chemical Ind. Ltd., 99%) in a temperature range of 375-475 K in a molybdenum boat. It was mixed with AlN having purity of 99.8% purchased from Rare Metallic Co. Ltd. in various molar ratios as shown in Table 2. The starting powder mixtures were pressed as disks of 6.8 mm in diameter and 0.5-3.5 mm in thickness under a pressure of 10 MPa. These operations were carried out in a helium filled grove box. The disks were heated at 875, 1025 and 1175 K in a flow of nitrogen for 20 to 60 min on AlN pellets to prevent an extra reaction with a molybdenum boat.

Single phase of Li_3AlN_2 was obtained above 1025 K from the starting mixture with Li_3N/AlN = 1.2-1.5 in molar ratio as shown in Table 2. The appropriate amount of excess Li_3N was necessary to obtain the single phase without contamination of AlN. The excess Li_3N evapolated during the reaction. The evaporation would be reduced at lower temperature, but the reaction takes longer time as in the case of 875 K.

The fractions of Li_3AlN_2 disks were observed with an scanning electron microscope (JOEL JSM-25S). X-ray powder diffractometry was performed on the samples sealed in glass capillary. Photographs were taken using camera having diameter of 114.59 mm with Ni-filtered Cu-Kα radiation. Silicon was used as an internal standard.

2-2-2. Electrical Measurement

Complex impedance was measured in a range of 5 Hz to 10 MHz using multifrequency LCR meter (YHP 4275A) and vector impedance meter (HP 4800A). Both sides of each sample disk were coated with conductive silver paste or carbon. D.C. conductivity

Table 2. Reaction conditions and products in Li_3N-AlN system.

$\frac{m(Li_3N)^{a)}}{m(AlN)}$	T/K	t/min	products
1.0-1.2	1025	60	Li_3AlN_2, AlN
1.2-1.5	1025	60	Li_3AlN_2
1.5-9.0	1025	60	Li_3AlN_2, Li_3N
1.2-1.5	1175	20	Li_3AlN_2
1.2-1.5	875	60	Li_3AlN_2, Li_3N, AlN

a) Molar ratio in starting mixture.

measurement was carried out with a cell construction of

(-) Li | Li_3AlN_2 | Li (+) : type I.

Electronic contribution was estimated using an arrangement of

(-) Li | Li_3AlN_2 | C or Mo (+) : type II.

The carbon or molybdenum is a blocking electrode. Discharging of a cell: Li | Li_3AlN_2 | TiS_2 and decomposition voltage were studied using a combination of potentio-galvanostat and function generator (Hokuto Denko HA-104 and HB-105).

2-3. Results and Discussion

2-3-1. Pellet Prepartion

X-ray powder diffraction of Li_3AlN_2 shown in Table 3 agreed well with the previous results and all diffraction peaks could be indexed as cubic (15). The lattice parameter was refined as a = 9.470(1) Å. No change was recognized on the parameter of products prepared from starting mixtures having various molar ratios.

Figure 5 shows SEM fracture photographs of the sintered Li_3AlN_2 body. The grains of about 10 μm in diameter are observed on the pellet prepared by heating at 1025 K for 1 hr as represented in Fig. 5 (a). They grew well when the sample was heated at 1175 K for 20 min as shown in Fig. 5 (b). The number of grain boundary was reduced but the bulk density was 60% of the theoretical value. The following measurements were performed on the disks obtained in the latter conditions.

Table 3. X-Ray powder diffraction data of Li_3AlN_2.

h k l	(a) $d_{obs.}$/Å	(a) $d_{cal.}$/Å	(a) I/I_o	(b) d/Å	(b) I/I_o
2 0 0	4.73	4.735	30		
2 1 1	3.87	3.866	100	3.86	100
2 2 2	2.73	2.734	90	2.73	80
3 2 1	2.53	2.531	80	2.53	65
4 0 0	2.37	2.367	40	2.37	20
4 2 0	2.11	2.117	10		
3 3 2	2.02	2.019	70	2.01	55
4 3 1 5 1 0	1.86	1.857	60	1.85	50
5 2 1	1.730	1.729	30		
4 4 0	1.675	1.674	100	1.673	100
5 3 2 6 1 1	1.537	1.536	40	1.534	50
5 4 1	1.460	1.461	30	1.461	20
6 2 2	1.429	1.428	30	1.424	30
6 3 1	1.398	1.396	40	1.391	50
4 4 4	1.367	1.367	30	1.366	20
6 4 0	1.314	1.313	30		
5 5 2 6 3 3 7 2 1	1.288	1.289	40	1.288	50
6 5 1 7 3 2	1.202	1.203	40	1.202	50
8 0 0	1.183	1.184	40	1.183	50
5 5 4 7 4 1 8 1 1	1.166	1.166	30	1.165	20
8 2 0	1.150	1.149	5		
6 5 3	1.132	1.132	20		
7 4 3 7 5 0 8 3 1	1.100	1.101	30	1.100	25
6 6 2	1.087	1.086	20	1.086	20
7 5 2	1.072	1.072	30	1.072	50
8 4 0	1.058	1.059	30	1.058	50
8 3 3 9 1 0	1.045	1.046	30	1.045	40
8 4 2	1.033	1.033	5		
6 5 5 7 6 1 9 2 1	1.022	1.021	30	1.021	60
7 5 4 8 5 1 9 3 0	0.998	0.998	20		
7 6 3 9 3 2	0.972	0.977	40		
8 4 4	0.967	0 967	70		
7 7 0 8 5 3 9 4 1	0.957	0.957	30		
10 0 0 8 6 0	0.947	0.947	20		
10 1 1 7 7 2	0.938	0.938	20		
10 2 0 8 6 2	0.929	0.929	10		

(a) Present work; a = 9.470(1) Å.

(b) Juza and Hund (15).

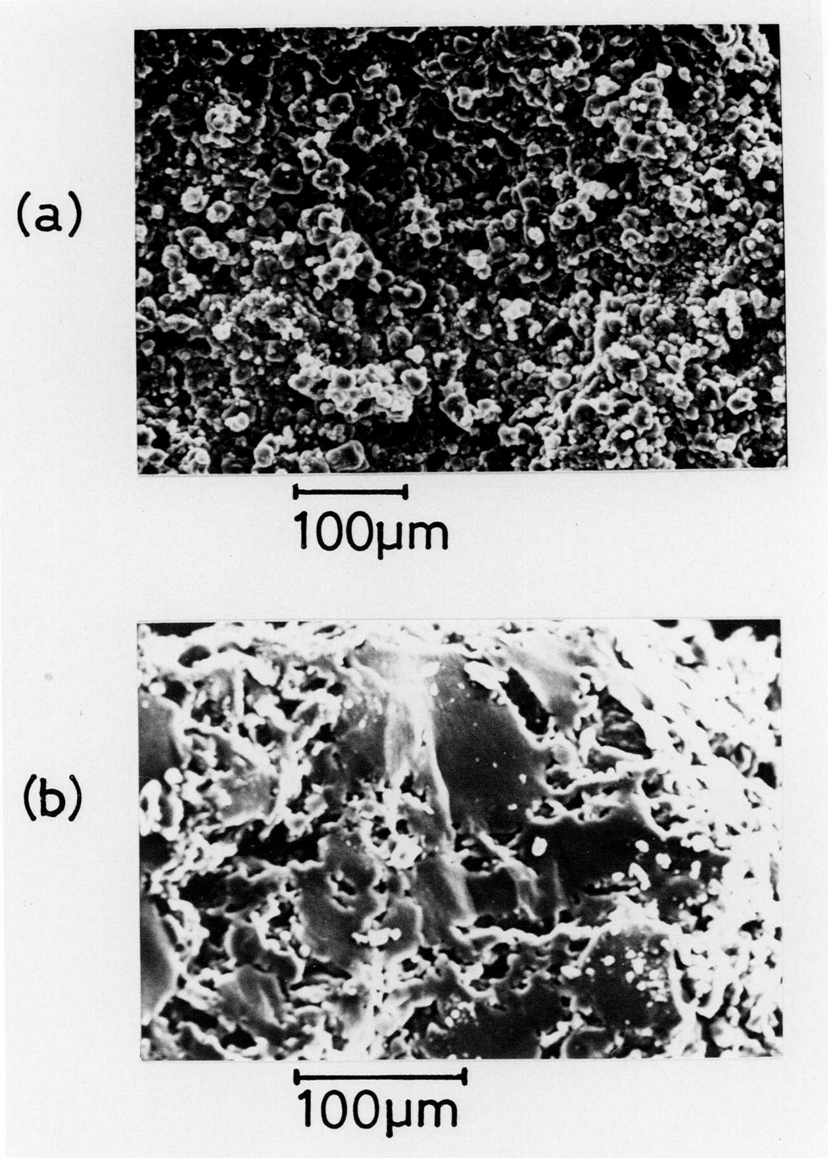

Fig. 5. SEM fracture photographs of sintered Li_3AlN_2 bodies obtained at 1025 K (a) and at 1175 K (b).

2-3-2. Conductivity Measurement

Figure 6 represents the complex impedance diagram observed at 343 K. The diagram consists of a semicircle and a straight line. The semicircle passes through the origin. The gradient of the straight line was about 80 degrees against abscissa and changed with the thickness of silver conductive films. Both the semicircle and the straight line crossed the abscissa almost at the same value. The values of intersections were taken as the total resistance of sample. They were plotted in Fig. 7 in comarison with the values obtained by d.c. method. The conductivity observed using the d.c. measurement was a little lower than those detected by the complex impedance method. This discrepancy was presumably due to the polarization at the interface between the lithium electrode and Li_3AlN_2 electrolyte of the cell type I. The activation energy was 52 kJ/mol (= 0.54 eV) for the ionic conduction as shown in the figure. The conductivity is higher and the activation energy is lower than that of the previous report (24). These discrepancies are obviously due to the presence of AlN in the previous sample. Electronic conductivity was measured using the blocking electrodes of type II cell. It took about a day to attain the equilibrium, when the voltage lower than the decomposition one was applied suddenly to the cell. Electronic contribution was smaller by the three orders of magnitude of total conductivity in the measured temperature range.

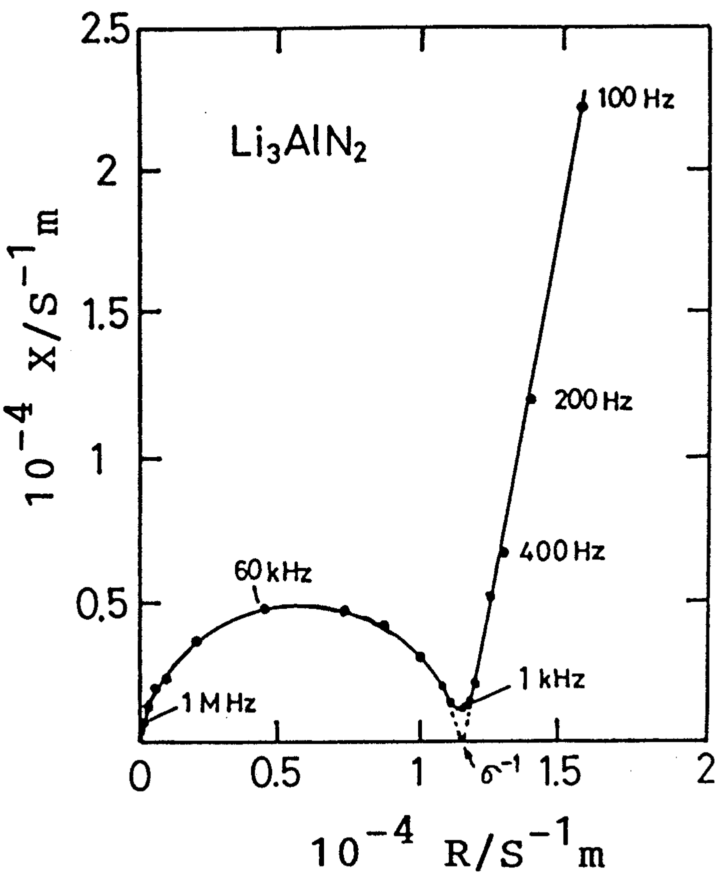

Fig. 6. Complex impedance plot at 343 K for the sintered Li_3AlN_2.

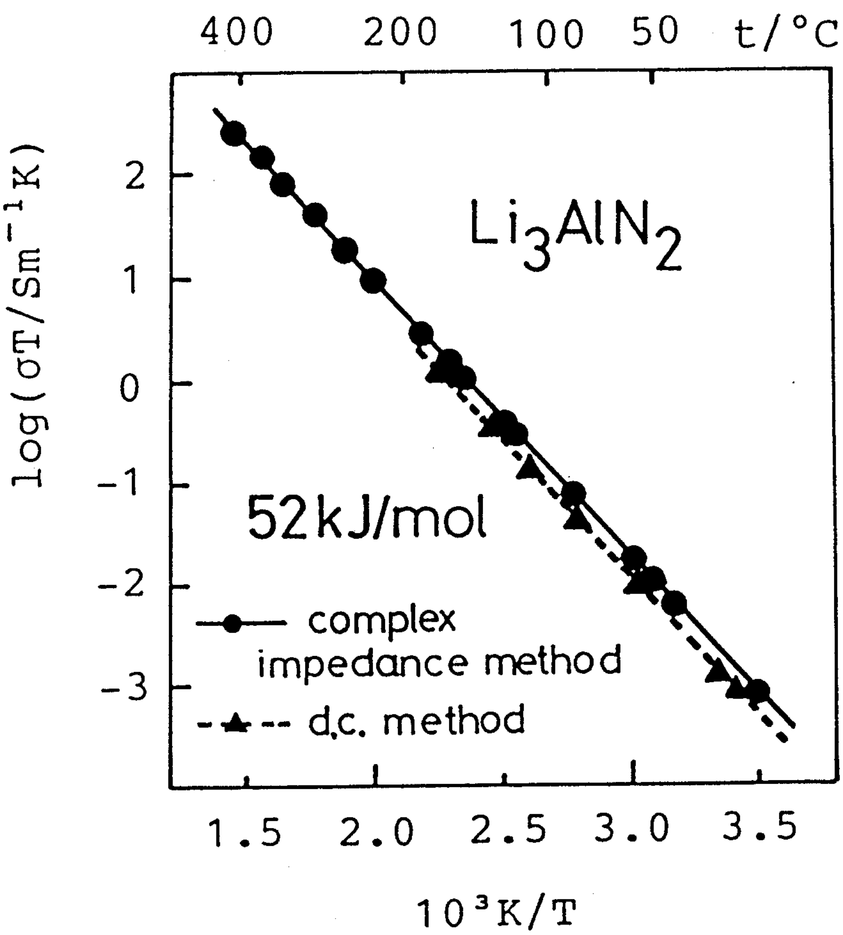

Fig. 7. Semilogarithmic plot of the product of conductivity σ and absolute temperature T against the inverse absolute temperature. The solid and the dotted lines represent the results obtained by complex impedance and by d.c. methods, respectively.

2-3-3. Decompsition Voltage

Decomposition voltage was measured using the cells of types I and II. Figure 8 shows the current against the applied voltage on the type I cell at 337 K. The size of the sample was about 7 mm in thickness. The voltage was changed at a rate of 2 mV/min. The current changed proportionally with the voltage up to 0.85 V. More current was observed than that expected by Ohm's law above 0.85 V. The deviations from Ohm's law above 0.85 V were also observed on the samples having thickness of 0.4 and 3.5 mm. The cell using the very thin sample was easily short-circuited due to the formation of lithium dendrite in the Li_3AlN_2 disk above the decompsition voltage.

An electromotive force of 2.60 V was generated at 381 K when the type II cell using a carbon electrode as a blocking electrode was set up according to Wagner's method (28). An equal amount of voltage was applied in the opposite direction to cancel the EMF. Then the applied voltage was increased at a rate of 2 mV/min. The electronic current linearly increased with the voltage as in the case of type I cell up to 3.45 V. The difference between 3.45 V and the EMF of 2.60 V corresponds to the decomposition voltage of 0.85 V observed on the type I cell. The resistance of the cell increased above the voltage.

Numerical data is not available for the free energy of formation of Li_3AlN_2 at the moment. The following reaction is expected to be exothermic and then its enthalpy change $\Delta H(r)$

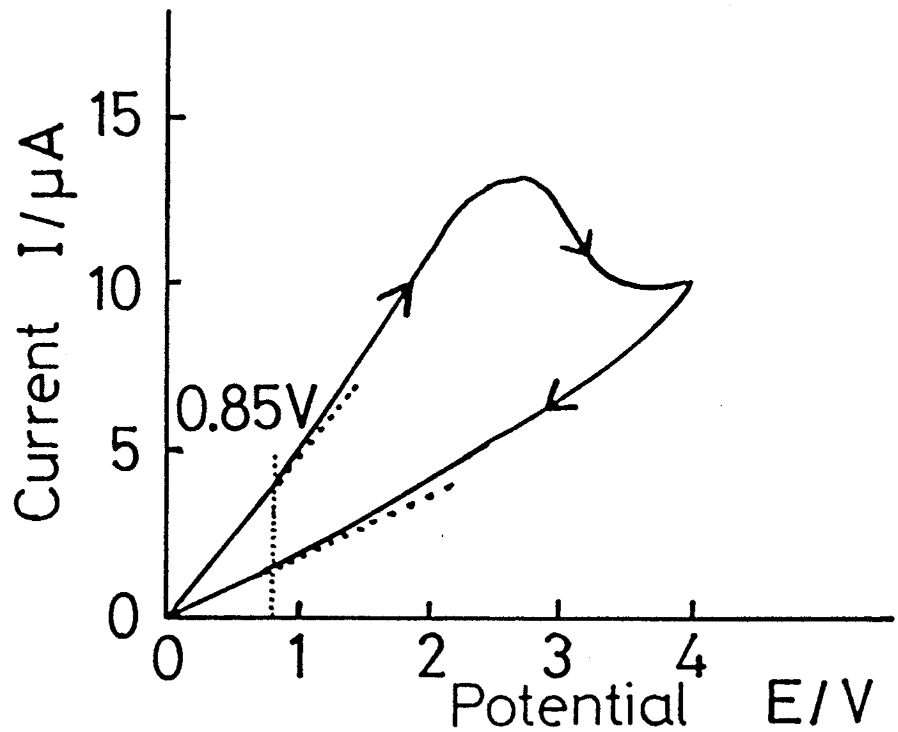

Fig. 8. Current against applied voltage on $Li/Li_3AlN_2/Li$ cell at 377 K.

is negative, because a reaction vessel made of gold melted at the reaction temperature of 1125 K:

$$Li_3N + AlN \xrightarrow[\Delta G(r)]{\Delta H(r)} Li_3AlN_2$$

The melting point of gold is 1336 K. The free energy change $\Delta G(r)$ is also negative, if the term of entropy change $T\Delta S(r)$ is larger than $\Delta H(r)$ at the reaction temperature. The lithium electrolyte Li_3AlN_2 is supposed to decompose into AlN, lithium and nitrogen when the decomposition voltage is applied. In this case, the free energy change of decomposition $\Delta G(d)$ is shown as follows:

$$-\Delta G(d) = \Delta G(r) + \Delta G(Li_3N) < \Delta G(Li_3N)$$

where $\Delta G(Li_3N)$ is the formation free energy of Li_3N. Three electrons are involved in the decomposition of Li_3AlN_2 as in the case of Li_3N. The higher decomposition voltage can be expected for Li_3AlN_2 than that of Li_3N.

2-3-4. Utilization for Lithium Battery

A Li_3AlN_2 sample pellet was sandwiched between lithium metal and TiS_2 disks. Open circuit voltage of 2.5 V was generated. The result agreed with a previous study in which a liquid organic-solvent electrolyte was used (29). Figure 9 shows a discharge curve at a constant current of 45 $\mu A/cm^2$. The initial close circuit voltage was only 1.7 V due to the current-resistance drop of the electrolyte. No remarkable reaction was observed except the formation of

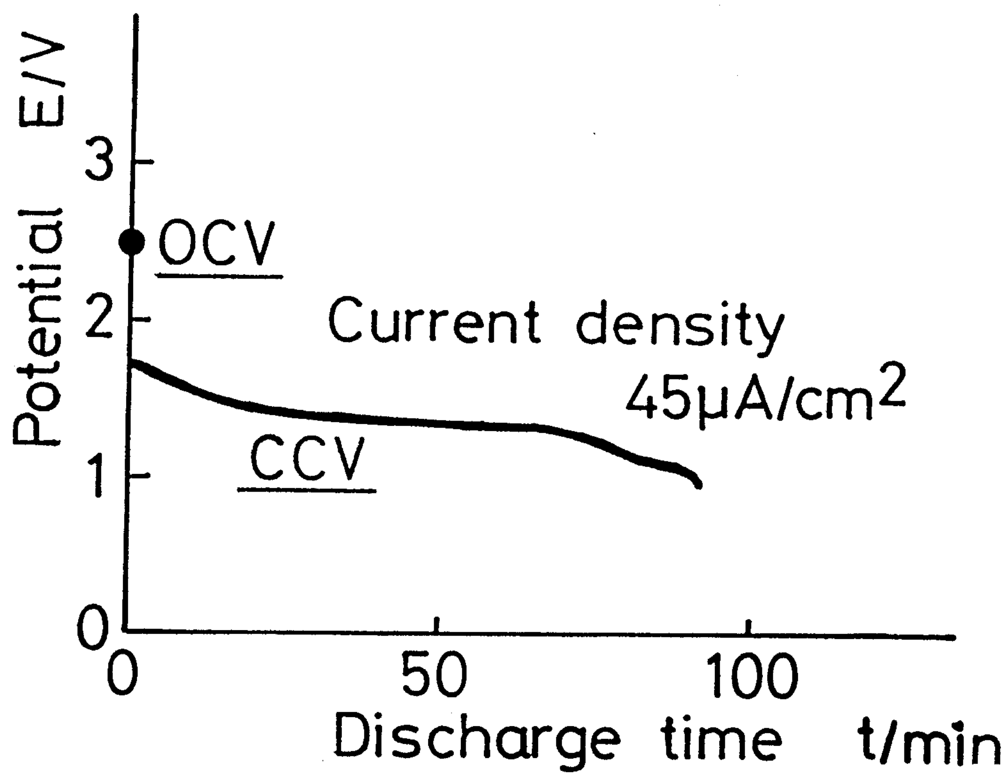

Fig. 9. Discharging of $Li|Li_3AlN_2|TiS_2$ at 377 K.

Li_xTiS_2 at the interface between the electrolyte and TiS_2 electrode. The electrolyte was resistive against the corrosion from lithium even if it was dipped in molten lithium at 425 K for 2 hr.

Chapter 3

Preparation and Properties of Compounds in Li_3N - Si_3N_4 System

3-1. Introduction

Crystal structures of many nitrides are formed by nitrogen close packing in which holes of different types are completely or partially occupied by metalloids. In the ternary metal nitrides containing lithium, there are several kinds of structural types where lithium ions are tetrahedrally coordinated by nitrogen ions. Li_3AlN_2 having antifluorite-type structure is a representative example. It was found to be a lithium ionic conductor as mentioned in Chapter 2. Lithium ionic conduction has been reported for compounds containing lithium in tetrahedral site such as Li_2CdCl_4 and $Li_9N_2Cl_3$ (30, 12).

In Li_3N-Si_3N_4 binary system, Juza et al. (17) firstly described the existence and crystal structure of Li_5SiN_3 which had an antifluorite-type superstructure. Lang and Charlot (18) synthesized three phases of $LiSi_2N_3$, Li_2SiN_2 and Li_8SiN_4 in this system. They could not prepare Li_5SiN_3. The structure of $LiSi_2N_3$ was determined as wurtzite-type by David et al. (20). Crystal structures of other phases were not clarified. These compounds may be lithium ionic conductors. A compound containing a large number of lithium such as Li_8SiN_4 possesses a possibility to have superionic conduction from a viewpoint of charge carrier number.

The previous studies on Li_3N-Si_3N_4 compounds encountered the difficulties of lithium content control because of the reaction of lithium with iron or stainless steel containers and also the violent vaporization of lithium at high temperature. Chemical compositions would be derived from those of starting materials, especially in the case of larger lithium contents. The chemical analysis was not carried out for most of the products prepared in the previous studies.

In the present study, tantalum foils were used as containers, which are relatively stable to lithium at high temperature as tested by DeVries and Fleisher (22). The duration of heating was also shortened in order to minimize lithium vaporization. The heating time in previous studies was longer than 24 h above 1075 K. Homogeneous samples were however obtained by heating for 10-20 min at 1075 K in the present study. Chemical compositions were determined for some single phase products by chemical analyses of lithium, silicon and nitrogen.

Six kinds of phases could be obtained from various mixtures of Li_3N and Si_3N_4. X-ray diffraction patterns of phases I, II and IV agreed with those of $LiSi_2N_3$, Li_2SiN_2 and Li_8SiN_4 presented by Lang and Charlot (18). Phase III was Li_5SiN_3 having an antifluorite-type structure. The superstructure described by Juza et al. (17) could not be systhesized in the present study. Its X-ray powder diffraction pattern rather agreed with that of phase V whose chemical formula is $Li_{21}Si_3N_{11}$ in the present study. Phase VI did not correspond to any ternary compounds reported previously in this system.

The present chapter will describe the results of preparations, chemical analysis and lithium ionic conductivity of the phases in lithium silicon nitrides.

3-2. Experimental

3-2-1. Preparation

Starting materials were lithium nitride prepared in the way as mentioned in Chapter 2 and silicon nitride (UBE-SN-E10, Ube Industries, Ltd.) containing 2 wt% of oxygen. They were mixed in various molar ratios as shown in Tabel 4. The starting mixtures were compressed to pellets and enclosed in tantalum foils. These operations were carried out in helium-filled glove box. The mixtures were heated under flowing nitrogen and reacted under the conditions described in Table 4. All products were characterized by X-ray powder diffraction methods.

3-2-2. Chemical Analysis

Chemical analysis was carried out by atomic absorption spectroscopy for lithium and silicon. Approximately 0.05 g of samples was weighed into polyethylene beaker and about 10 ml water was added. If the sample was not dissolved in

Table 4. Reaction conditions and products in Li_3N-Si_3N_4 system.

$\frac{m(Li_3N)}{m(Si_3N_4)}$ a)	T/K	t/min	products
1.6	1075	10-20	α-Si_3N_4, Li_2SiN_2
1.6	1475	60	$LiSi_2N_3$
2.0	1075	10-20	Li_2SiN_2
3.9	1075	10-20	Li_2SiN_2, Li_5SiN_3
4.9	1075	40	Li_5SiN_3, Li_2SiN_2
5.1	1075	10-20	Li_5SiN_3
5.5	1075	10-20	Li_5SiN_3, $Li_{18}Si_3N_{10}$
6.0	1075	10-20	$Li_{18}Si_3N_{10}$
6.6	1075	10-20	$Li_{21}Si_3N_{11}$, $Li_{18}Si_3N_{10}$
7.1	1075	10-20	$Li_{21}Si_3N_{11}$
8.0	1075	10-20	Li_8SiN_4, $Li_{21}Si_3N_{11}$
8.2	1075	10-20	Li_8SiN_4
10.2	1075	10-20	Li_8SiN_4, Li_3N
17.0	1075	10-20	Li_3N, Li_8SiN_4

a) Molar ratio in the starting mixture.

water, 3 ml of HF and 0.5 ml of aqua regia were added. The solution was transfered into volumetric 250 ml polyethylene flask, diluted to the volume with 5 ml of 0.4 N Na_2CO_3 aqueous solution and water for silicon determination. For lithium determination, 10 ml of this solution was dilute to 100 or 250 ml with 10ml of 0.5 N HCl and water in a polyethylene volumetric flask.

Silicon 1000 ppm in 0.4 N Na_2CO_3 aqueous solution and 1000 ppm lithium in 0.01 N HCl aqueous solution (Wako Pure Chemical Ind. Ltd.) were used as standards (correction factor 1.01 and 1.00 respectively). The silicon standard solution was diluted to 25, 40, 50, 60 and 80 ppm, adding appropriate amounts of Li_3N and occasionally HF and aqua regia in order to make the similar condition with solution of samples. The lithium standard solution was diluted to 1, 2, 3, 4, 5 and 10 ppm with water, adding adequate amounts of NH_4Cl and silicon standard solution for the same purpose. Blank test did not show detectable reagent contaminations. The following instrumental settings were used;

	Si	Li
Analytical line	2516 Å	6708 Å
Slit	3-4	2-3
Source: Hollow Cathode	10 mA	10 mA
Fuel :	Acetylene	Acetylene
Oxidizer:	N_2O	Air

The sensitvity of silicon analysis was strongly influenced by flow rates of acetylene and N_2O gases and also by the position of burner.

Nitrogen content was determined by modified Kjeldahl method as follows (31, 32). Approximately 0.05-0.10 g sample was weighed into a flask and 10 ml water was added. The solution was heated on a hot plate at about 400 K. Undissolved samples in water were decomposed with 0.5 g sodium hydroxide at about 650 K in nickel crucible. The resulting ammonia was collected in 1% boric acid solution with the aid of steam as a carrier. The collected solution was titrated with a standard acid solution (0.1 N H_2SO_4) using methyl red as an indicator.

3-3. Results and Discussion

3-3-1. Phases in Li_3N - Si_3N_4

The preparations are summarized in Table 4. No reaction was observed between sample pellets and tantalum foils, while the surface of the foils was slightly reacted with vaporized lithium.

There were six kinds of lithium silicon nitrides in the preparations. Table 5 shows the results of chemical analyses for the single phase products. The residual amounts of less

Table 5. Chemical analysis of the compounds in Li_3N-Si_3N_4 system.

		Li	Si	N	O[a)]	Total	(+)	(-)[b)]
Phase VI Li_8SiN_4	wt%	39.4	19.5	37.0		95.9		
	mol%	61.2	7.4	28.5	2.8	99.9	90.8	91.1
Phase V $Li_{21}Si_3N_{11}$	wt%	37.7	21.3	37.1		96.1		
	mol%	59.8	8.4	29.2	2.6	100.0	93.4	92.8
Phase IV $Li_{18}Si_3N_{10}$	wt%	35.2	24.1	37.1		96.8		
	mol%	57.5	9.8	30.4	2.3	100.0	96.7	95.8
Phase III Li_5SiN_3	wt%	33.1	25.7	37.1		95.9		
	mol%	55.5	10.7	30.8	3.0	100.0	98.3	98.4
Phase II Li_2SiN_2	wt%	19.5	39.8	38.5		97.8		
	mol%	39.5	19.9	38.6	2.0	100.0	119.1	119.8

a) Residual was calculated as oxygen in mol%.

b) Sum of the positive(+) and negative(-) charge.

than 5 wt% was probably oxygen contained in the starting material and introduced during handlings of samples. The electrical neutrality of the products is almost satisfied by taking into account the residual content as oxygen. No oxide was detected by X-ray powder diffraction method. The oxygen may be present statistically in nitrogen sites due to their similar ionic radii (O^{2-} 1.28 and N^{3-} 1.32 Å after Shannon and Prewitt (33)).

Phase I, $LiSi_2N_3$, was synthesized from the mixture of of X = 1.6 at 1475 K. Hereafter X represents a molar ratio of Li_3N/Si_3N_4. Heating at 1075 K, the products were mixtures of Li_2SiN_2 and Si_3N_4. The reactions are described as follows:

$$2\ Li_3N + Si_3N_4 \xrightarrow{1075\ K} 3\ Li_2SiN_2 \qquad (1)$$

$$Li_2SiN_2 + Si_3N_4 \xrightarrow{1475\ K} 2\ LiSi_2N_3 \qquad (2)$$

$LiSi_2N_3$ was white color, relatively stable in air. X-ray diffraction data is compared with that of David et al. (20) in Table 6. Crystal structure is derived from that of wurtzite-type as illustrated in Fig. 10. $LiSi_2N_3$ crystallizes in the orthorhombic system and its space group is $Cmc2_1$. The unit cell contains four formula units. Nitrogen atoms build a slightly distorted hexagonal close-packing. Lithium and silicon atoms are ordered in a half of the tetrahedral sites of structure.

Phase II, Li_2SiN_2, was prepared from the mixture of x

Table 6. X-Ray powder diffraction data for $LiSi_2N_3$.

hkl	(a) $d_{obs.}$/Å	(a) $d_{calc.}$/Å	(a) I/Io	(b) $d_{obs.}$/Å	(b) I/Io
200	4.594	4.599	81	4.59	73
110		4.597			
111	3.308	3.313	87	3.30	76
310	2.656	2.655	100	2.65	100
020		2.654			
002	2.388	2.390	58	2.39	64
311	2.321	2.320	80	2.32	72
021		2.320			
202	2.120	2.120	6	2.12	6
112		2.120			
221	2.072	2.071	6	2.07	7
022	1.777	1.776	25	1.773	27
312		1.776			
130		1.738			
510	1.738	1.738	9	1.738	10
420		1.738			
402	1.658	1.657	4	1.714	4
222		1.657			
511		1.633			
131	1.632	1.633	15	1.631	16
421		1.633			
600	1.533	1.532	43	1.531	44
330		1.532			
113	1.504	1.505	5	1.504	7
512		1.406			
422	1.406	1.405	5	1.403	5
132		1.405			
023	1.367	1.366	33	1.365	39
313		1.366			

(a) Present study. Orthorhombic a = 9.198(3), b = 5.307(2), c = 4.779(2) Å.

(b) After David et al.(20).

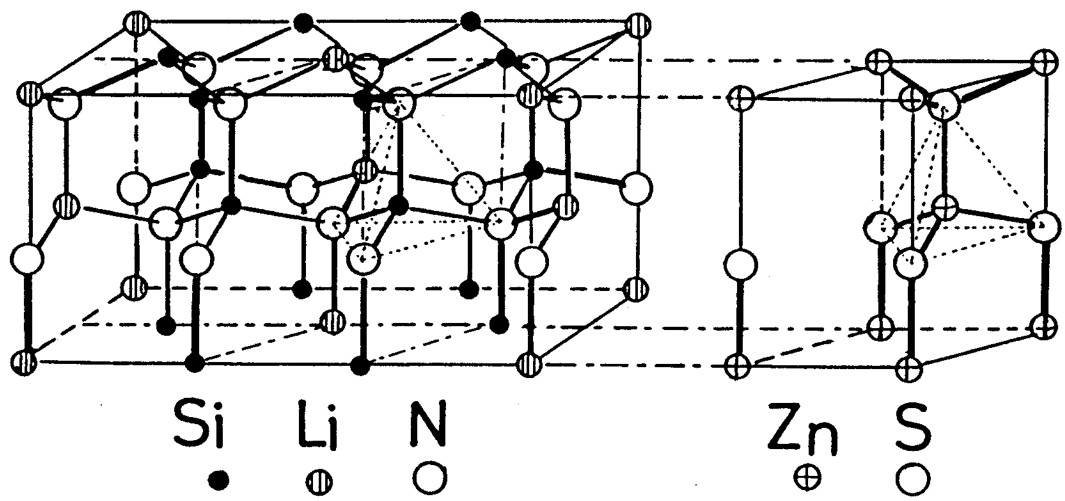

Fig. 10. Crystal structure of $LiSi_2N_3$ compared with that of wurtzite.

= 2.0 at 1075 K, following the equation (1). It was white color and relatively stable in air. Chemical analysis showed its composition as $Li_{0.95}Si_{0.98}N_{1.90}O_{0.10}$. X-ray powder diffraction data are listed in Table 7 with those by Lang and Charlot (18). They infered the formula of Li_2SiN_2 from the similarity of $CaSiN_2$ (34), $MgSiN_2$ (35) and $BeSiN_2$ (36). Crystal structures of $MgSiN_2$ and $BeSiN_2$ were derived from wurtzite-type (16, 37). The structure of Li_2SiN_2 could not be determined. It might be related to the anti-La_2O_3 or anti-Ce_2O_2S structure such as Li_2ZrN_2 (38) and Li_2CeP_2 (39). In the structure of these compounds, nitrogen ions build a hexagonal close-packing. Zirconium ion is in the octahedral site due to a larger ionic radius and lithium ion is in the tetrahedral site. The structure of Li_2ZrN_2 are illustrated in Fig. 11.

Phase III, Li_5SiN_3, was obtained from the mixture of x = 5.1 at 1075 K. It was grayish white color and soluble in water. It crystallizes in cubic system (a = 4.724 Å) as shown in Table 8. Juza et al. (17) reported an existance of cubic phase having a = 4.71 Å in the preparation of their Li_5SiN_3 phase. They obtained the former phase by heating a mixture of x = 5.15 at 1475 K for 2hr and estimated a chemical composition as $Li_{4.98}Si_{1.0}N_{2.66}O_{0.4}$ having 4.5 wt% Fe impurity by chemical analysis. This phase probably corresponds to the phase III of the present study. Chemical formula of the present product could be estimated as $Li_{4.92}Si_{0.95}N_{2.73}O_{0.27}$. The Li_5SiN_3 reported by Juza et al. had an

Table 7. X-Ray powder diffraction data for Li_2SiN_2.

(a) $d_{obs.}$/Å	(a) I/I_o	(b) $d_{obs.}$/Å	(b) I/I_o
6.34	1	6.36	4
5.12	100	5.14	100
4.96	26	4.97	25
		4.62	4
4.25	33	4.27	35
4.12	12	4.15	18
3.88	2		
3.83	2	3.82	4
3.53	2		
3.32	84	3.32	80
2.98	5		
2.89	45	2.90	40
2.80	1		
2.71	1		
2.67	5		
2.56	46	2.57	50
2.48	6	2.48	10
2.41	29	2.42	35
2.35	12	2.36	18
2.31	3	2.32	8
2.23	8	2.24	10
2.17	9	2.17	18
2.13	8	2.13	20
2.08	1	2.05	35
2.03	59	2.03	95
1.97	19	1.97	18

(a) Present study.

(b) After Lang and Charlot(18).

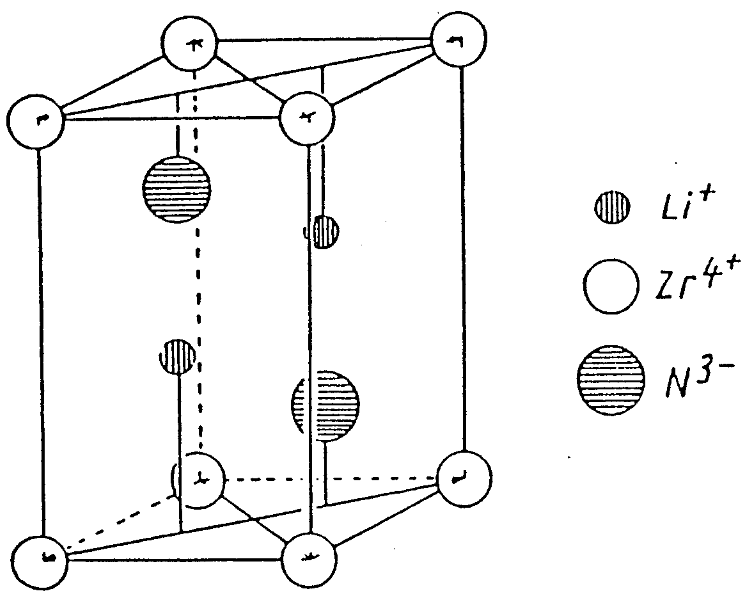

Fig. 11. Crystal structure of Li_2ZrN_2.

Table 8. X-Ray powder diffraction data for Li_5SiN_3.

hkl	$d_{obs.}$/Å	$d_{calc.}$/Å	I/I_o
111	2.729	2.727	100
200	2.361	2.362	6
220	1.6701	1.6701	84
311	1.4244	1.4244	4
222	1.3434	1.3637	3
400	1.1810	1.1810	5
420	1.0562	1.0562	3
422	0.9643	0.9643	8

Cubic a = 4.7240(3) Å.

antifluorite superstructure belonging to cubic system (a = 9.436 Å). They prepared this compounds by heating the mixture of x = 10.1 at 1475 K for 1 h and then at 1075 K for 24 h in a sealed iron tube. An awkward crystal structure was determined from X-ray powder diffraction data as an analogue of Li_3AlN_2 structure. But the chemical analysis was not performed probably because the product was contaminated with the iron reaction vessel. The unit cell of the nominal Li_5SiN_3 phase described by Juza et al. contained 32/3 formula units. The calculated and observed densities were 2.21 and 2.23 Mgm^{-3}, respectively. Nitrogen ions are in 8a and 24d, lithium ions in 48e site of the space group Ia3. Other 16/3 of lithium and 32/3 silicon ions statistically occupy 16c site. If this site is occupied by aluminum ion, the structure is identical to that of Li_3AlN_2. X-ray powder diffraction pattern of Li_5SiN_3 superstructure phase was relatively comparable with that of phase V as shown in Table 10, which was prepared from the mixture of x = 7.

Phase III may have the antifluorite structure in which 4/3 formula unit of Li_5SiN_3 is contained, since the lattice parameter of 4.724 Å is about a half value of the nominal Li_5SiN_3 superstructure. While the configuration of Li and Si was not confirmed, 20/3 Li and 4/3 Si might be statistically distributed in 8c cation site of space group Fm3m. The oxynitride $Li_5SiN_3{:}2Li_2O$ crystallizes in the same space group (17). This structure is antifluorite-type (cubic a = 4.676 Å). The anions of 12/5 N and 8/5 O are statistically occupy 8c site of space group Fm3m. Another example is Li_5SnP_3 which also has the antifluorite structure containing 4/3 formula unit (39). Lithium and tin occupy statistically in the tetrahedral site.

Phase IV was represented as $Li_{18}Si_3N_{10}$ in Table 4. The color of powdered sample was greenish blue-gray. It was unstable against moisture and soluble in water. The molar ratio of the lithium and silicon was 5.9:1 calculated from the chemical analylsis. X-ray powder diffraction data shown in Table 9 almost agreed with that of Li_8SiN_4 reported by Lang and Charlot (18). All reflections could be tentatively indexed with the tetragonal lattice: a = 14.17, c = 14.35 Å. They prepared this phase by heating the mixture of x = 6.7-13.3 at 1075 K for 24 h in sealed stainless tube. They recognized a reaction of the tube with lithium.

Phase V represented as $Li_{21}Si_3N_{11}$ was also unstable against moisture and soluble in water. The powdered sample was greenish light blue-gray color. Table 10 shows X-ray powder diffraction data of phase V. It could be indexed as tetragonal lattice with a = 9.470 and c = 9.530 Å. Judging from the agreement of diffraction line positions and their intensities, the structure of phase V is related to the superstructure of antifluorite-type proposed for Li_5SiN_3 by Juza et al.(17), where the cubic lattice had a parameter of a = 9.436 Å. The molar ratio of Li/Si was 7.1, however. Excess lithium ions might be in the octahedral site of nitrogen cubic close-packing.

Table 9. X-Ray powder diffraction data.

hkl	(a) $d_{obs.}$/Å	(a) $d_{calc.}$/Å	(a) I/I_o	(b) $d_{obs.}$/Å	(b) I/I_o
002	7.14	7.177	2	7.13	30
200	7.10	7.084	8		
212	4.76	4.750	59		
221	4.74	4.729		4.73	14
222	4.10	4.108	100	4.11	55
302	3.94	3.945	4	3.94	16
400	3.54	3.542	7	3.53	10
403	2.84	2.846	1		
430	2.83	2.834	2	2.829	4
115	2.76	2.760	30		
333	2.74	2.739	67	2.735	100
512	2.59	2.588	11	2.590	12
315	2.41	2.417	1		
513	2.40	2.403	2		
442	2.36	2.365	34	2.360	18
600	2.36	2.361			
206	2.27	2.266	2	2.266	4
533	2.16	2.166	1		
622	2.14	2.138	7	2.138	4
316	2.11	2.110	2		
640	1.96	1.965	1		
217	1.95	1.951	4		
336	1.94	1.945	4		
525	1.94	1.940			
633	1.93	1.932	10		
552 712	1.93	1.930			
721	1.93	1.929		1.926	16
553 713	1.85	1.848	3		
463 506	1.83	1.828	2	1.839	6
605	1.82	1.824	1	1.829	6
228	1.68	1.689	90	1.682	70
606	1.68	1.681			
822	1.67	1.671	30	1.671	50
660	1.67	1.670			

(a) Present study of $Li_{18}Si_3N_{10}$. Tetragonal a = 14.168(4), c = 14.353(8) Å.

(b) Li_8SiN_4 reported by Lang and Charlot(18).

Table 10. X-Ray powder diffraction data.

(a) hkl	$d_{obs.}$/Å	$d_{calc.}$/Å	I/I_o	(b) hkl	$d_{obs.}$/Å	I/I_o
101	6.68	6.717	37			
002	4.75	4.765	47	200	4.73	50
112	3.87	3.882	100	211	3.82	80
				220	3.34	40
301	2.99	2.997	5			
222	2.74	2.740	72	222	2.73	100
213	2.54	2.541	7			
321	2.53	2.532	9	321	2.52	40
400	2.36	2.368	2	400	2.37	10
303	2.24	2.239	3	411	2.24	5
420	2.12	2.118	4	420	2.11	40
332	2.02	2.021	11	332	2.01	50
224	1.94	1.941	3	422	1.932	10
413	1.86	1.861	2			
501 510 431	1.86	1.857	5	431	1.844	30
				521	1.733	10
404	1.68	1.679	21	440	1.669	100
440	1.674	1.674	29	433	1.624	10
424	1.584	1.583	1			
600	1.577	1.578	3	600 442	1.575	20
523	1.541	1.536	2			
532	1.539	1.537	3			
				611 532	1.531	30

(a) Present atudy of $Li_{21}Si_3N_{11}$. Tetragoanl
a = 9.470(3), c = 9.530(8) Å.

(b) Li_5SiN_3 reported by Juza et al. (17). Cubic
a = 9.436 Å.

Phase VI, Li_8SiN_4, was prepared from the mixture of x = 8.2 at 1075 K. The powdered sample was greenish gray color, and unstable against moisture and soluble in water. X-ray diffraction pattern was explained with tetragonal lattice as shown in Table 11: a = 10.217 and c = 9.536 Å. The diffraction pattern did not agree with that of Li_8SiN_4 reported by Lang and Charlot (18). The latter agreed well with that of phase IV as described above.

3-3-2. Structural Relations

The structures of four phases III, IV, V and VI are probably related to antifluorite-type. All of their X-ray powder diffraction patterns have large peaks around 2Θ = 31-32° and 53-55°(CuKα) as illustrated in Fig.12. These phases have basically the same structural unit. The phase III, Li_5SiN_3, is assumed to have the antiflorite structure with a cubic symmetry (a = 4.724 Å). Table 12 shows the comparision of lattice dimensions. The reduced lattice constants of phases IV, V and VI are also arround 4.7-4.8 Å. Figure 13 illustrates relations between the unit cells. These phases are considered to have superstructures or derivatives of the antifluorite structure. Nitrogen ions are in cubic packing, forming face-centered lattice.

In the case of Li_5SiN_3, 20/3 of lithium and 4/3 of silicon ions might be distributed statistically at all tetrahedral sites of the nitrogen closest packing as

Table 11. X-Ray powder diffraction data for Li_8SiN_4.

hkl	$d_{obs.}$/Å	$d_{cal.}$/Å	I/I_o
110	7.23	7.224	3
200	5.11	5.108	14
002	4.77	4.768	27
211	4.12	4.120	87
202	3.49	3.486	11
310	3.23	3.231	4
222	2.88	2.879	1
302	2.77	2.771	100
312	2.67	2.675	3
213	2.61	2.609	7
400	2.55	2.554	2
411	2.40	2.398	9
402	2.25	2.251	2
204	2.16	2.160	2
332	2.15	2.150	6
304	1.954	1.953	19
502	1.878	1.878	1
423	1.855	1.855	7
324	1.824	1.824	2
522	1.762	1.763	1
404	1.743	1.743	1
600	1.704	1.703	22
513	1.695	1.695	34
334	1.693	1.694	29
442	1.690	1.689	4
523	1.629	1.629	7

Tetragonal a = 10.217(2), c = 9.536(3) Å.

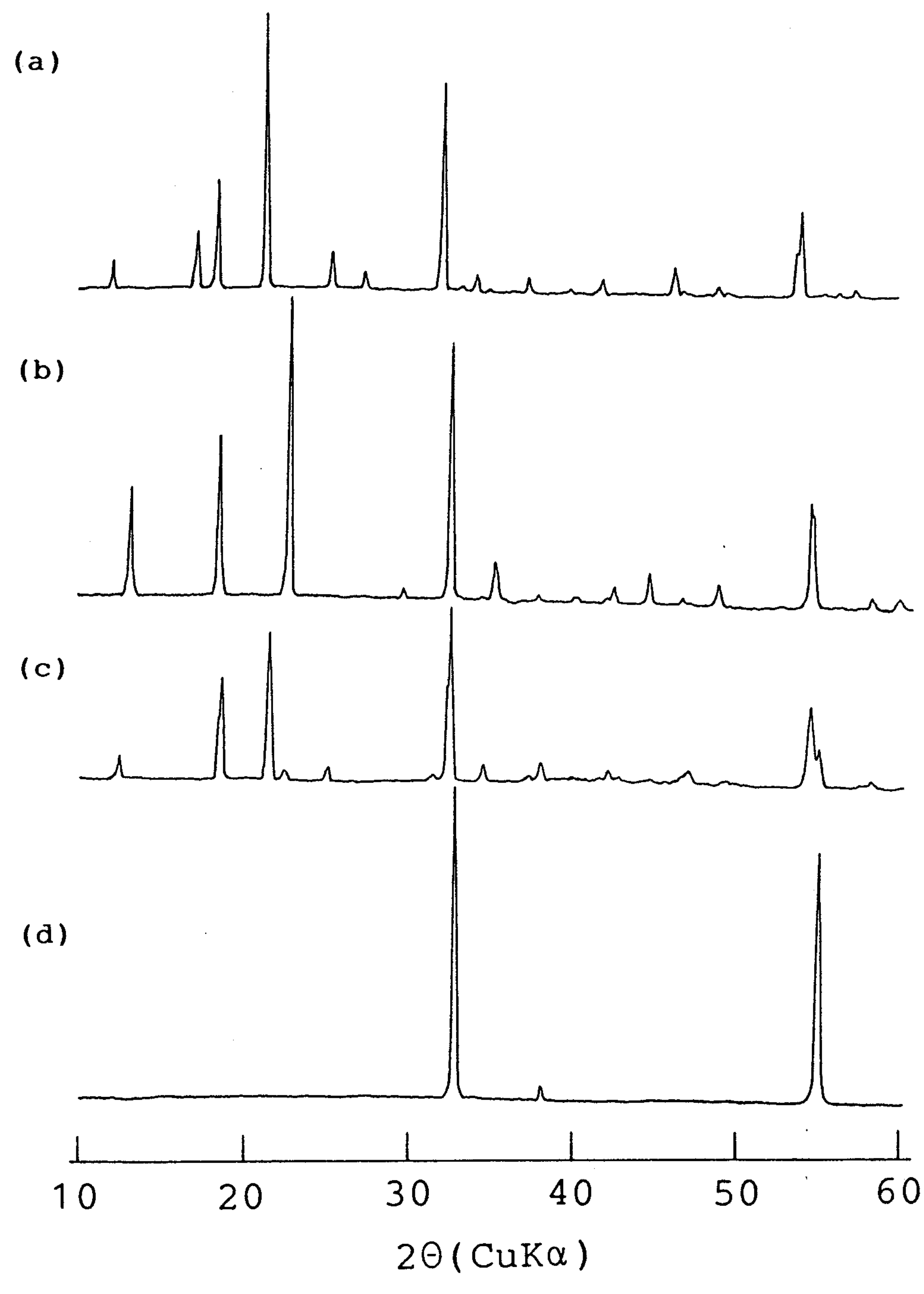

Fig. 12. X-Ray powder diffraction patterns of (a) Li_8SiN_4, (b) $Li_{21}Si_3N_{11}$, (c) $Li_{18}Si_3N_{10}$, (d) Li_5SiN_3.

Table 12. Relationship of the lattice dimensions of Li_3N-Si_3N_4 compounds.

Phases	Phase III	Phase IV	Phase V	Phase VI
Chemical Formula[a)]	Li_5SiN_3 $(Li_{6.56}Si_{1.26}N_{3.64}O_{0.36})$	$Li_{18}Si_3N_{10}$ $(Li_{7.04}Si_{1.20}N_{3.72}O_{0.28})$	$Li_{21}Si_3N_{11}$ $(Li_{7.52}Si_{1.06}N_{3.68}O_{0.32})$	Li_8SiN_4 $(Li_{7.82}Si_{0.94}N_{3.64}O_{0.36})$
M : X[b)]	7.82 : 4	8.24 : 4	8.58 : 4	8.76 : 4
Lattice Constants(Å)	a = 4.724	a = 14.158 c = 14.349	a = 9.470 c = 9.530	a = 10.217 c = 9.536
Reduced Lattice Constants(Å)		a/3 = 4.719 c/3 = 4.783	a/2 = 4.735 c/2 = 4.765	$\sqrt{2}a/3$ = 4.816 c/2 = 4.768
Cell Volume(Å³)	V = 105.4	V = 2876.2	V = 854.7	V = 995.4
Reduced Cell Volume(Å³)		V/27 = 106.5	V/8 = 106.8	2V/18 = 110.6

a) The total amount of anion in each formular is four.

b) Molar ratio of tatal cation to anion.

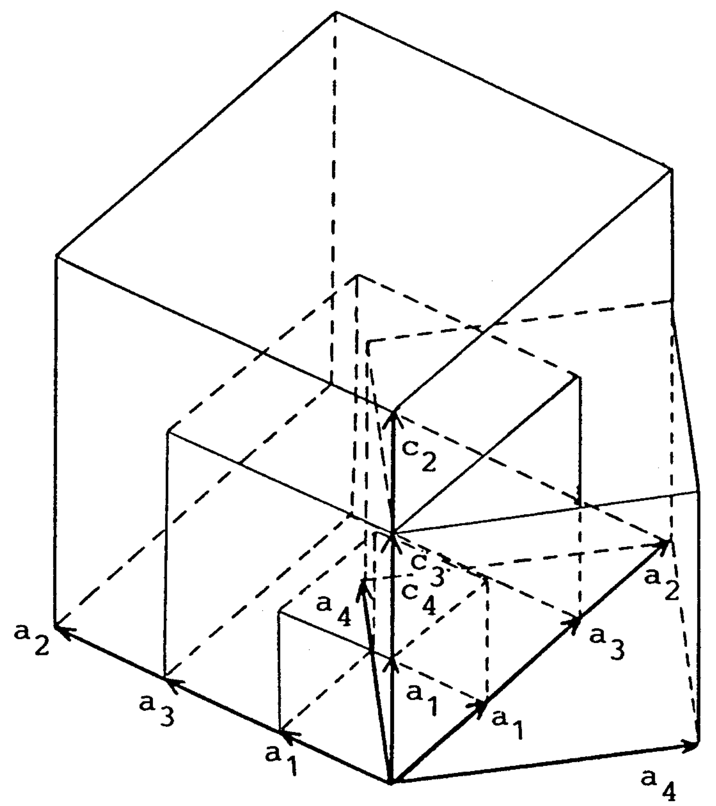

Fig. 13 Relationship of the unit cells;

a_1, a_1, a_1, : Li_5SiN_3 ,

a_2, a_2, c_2 : $Li_{18}Si_3N_{10}$,

a_3, a_3, c_3 : $Li_{21}Si_3N_{11}$,

a_4, a_4, c_4 : Li_8SiN_4 .

$(a_1 \doteqdot 1/3a_2 \doteqdot 1/2a_3 \doteqdot 1/3c_2 \doteqdot 1/2c_2 \doteqdot 1/2c_4 \doteqdot 3/\sqrt{2a_4})$

discussed before. There are excess amounts of cations in the phases IV, V and VI from the viewpoint of antifluorite structure as shown in Table 12. They may be placed in octahedral site of the cubic-close packing. Lithium and silicon ions of these phases would be in long range ordered fashion like the superstructure of Li_5SiN_3 described by Juza et al. (17). The elemental antifluorite cell contains four anions. The phase V has lithium ions more than phase IV in amount, while both phases have almost the same reduced elemental cell volume. This matter might be caused by the ordering and degrees of statistical mixing of lithium and silicon ions whose ionic radii are 0.73 and 0.40 Å after Shannon and Prewitt (33). But it is uncertain in the present study because the crystal structure is not determined.

Figure 14 indicates the abrupt increase in reduced cell volume at Li_8SiN_4. This may suggest the fundamental change of cation arrangements; for example, most of the lithium ions are in the octahedral site, and silicon and other lithium ions occupy the tetrahedral position in ordered fashion. The direction of the unit cell axis is along the diagonal line of other three phases as illustrated in Fig. 13.

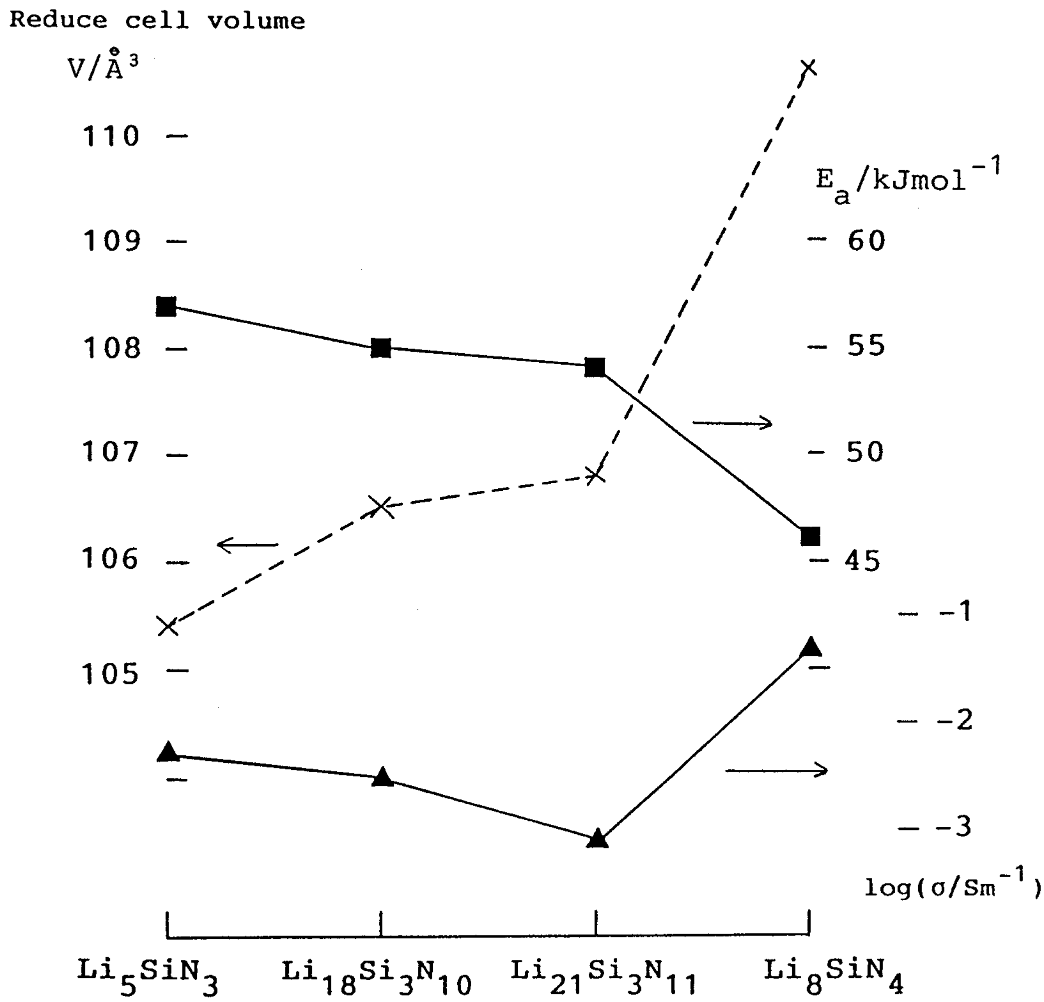

Fig. 14. Compositional dependence of reduced cell volume, activation energy of ionic conduction and ionic conductivity at 400 K among the lithium silicon nitrides.

3-4. Ionic Conductivity

Total conductivities of the products were measured by complex impedance method described in Chapter 2. Most of the conductions are caused by migration of lithium ions. The electronic conductivities of these materials were less than 1% of the total conductivities. Figures 15 and 16 show the temperature dependence of ionic conductivity for the phases I and II, and phases III, IV, V and VI, respectively. Table 13 summarizes the conductivities at 400 K and activation energies of the conduction.

The Phase I, $LiSi_2N_3$, has the smallest conductivity and the highest activation energy in the Li_3N-Si_3N_4 system probably because of the lowest content of lithium ion in the structure.

Li_2SiN_2 has fairly higher conductivity than that of $LiSi_2N_3$. The structure of Li_2SiN_2 has not yet been determined. If the structure is based on the hexagonal colse-packed nitrogen ions such as Li_2ZrN_2, some lithium ions may preferentially occupy the octahedral site due to its larger ionic radius than that of silicon. The presence of the lithium ions in the octahedrons might contribute to the ionic conduction.

As mentioned in the previous section, phases III, IV, V and VI may have the crystal structure related to antifluorite. Nitrogen ions construct a cubic or a distored cubic close-packing. The conductivity of $Li_{21}Si_3N_{11}$ was the lowest among these compounds at 400 K as shown in Fig. 14, 16 and Table 13. Phase V, $Li_{18}Si_3N_{10}$, had also lower conductivity

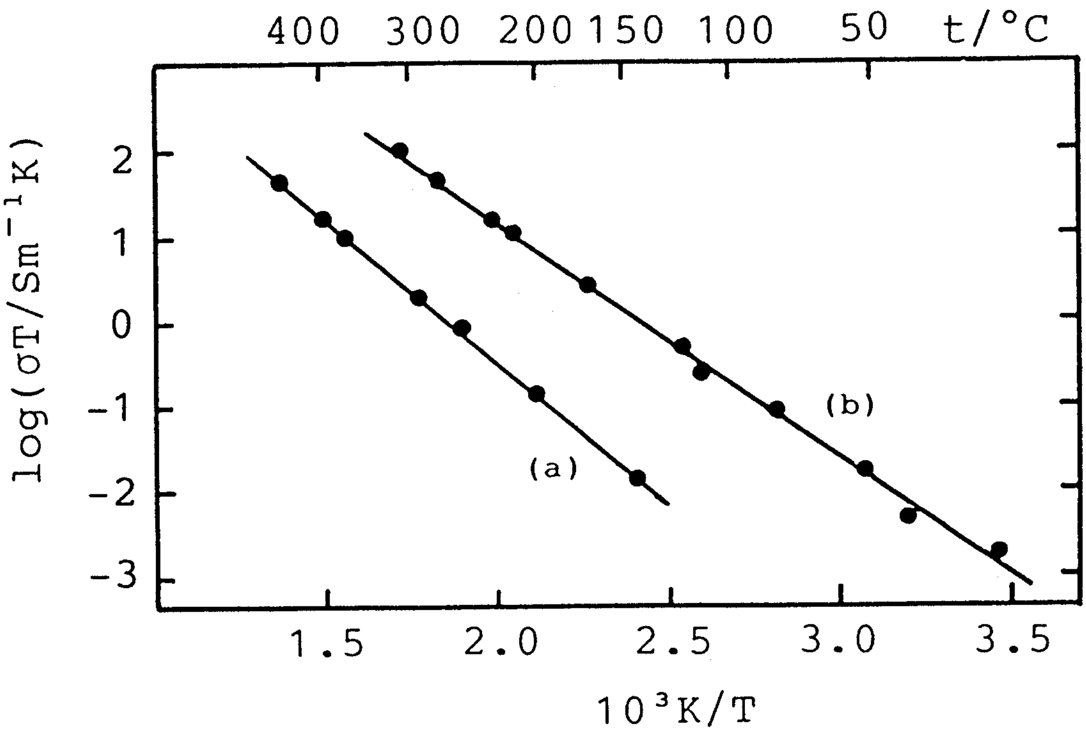

Fig. 15. Semilogarithmic plot of the conductivity σ times the absolute temperature T against the inverse absulte temperature: (a) $LiSi_2N_3$ and (b) Li_2SiN_2.

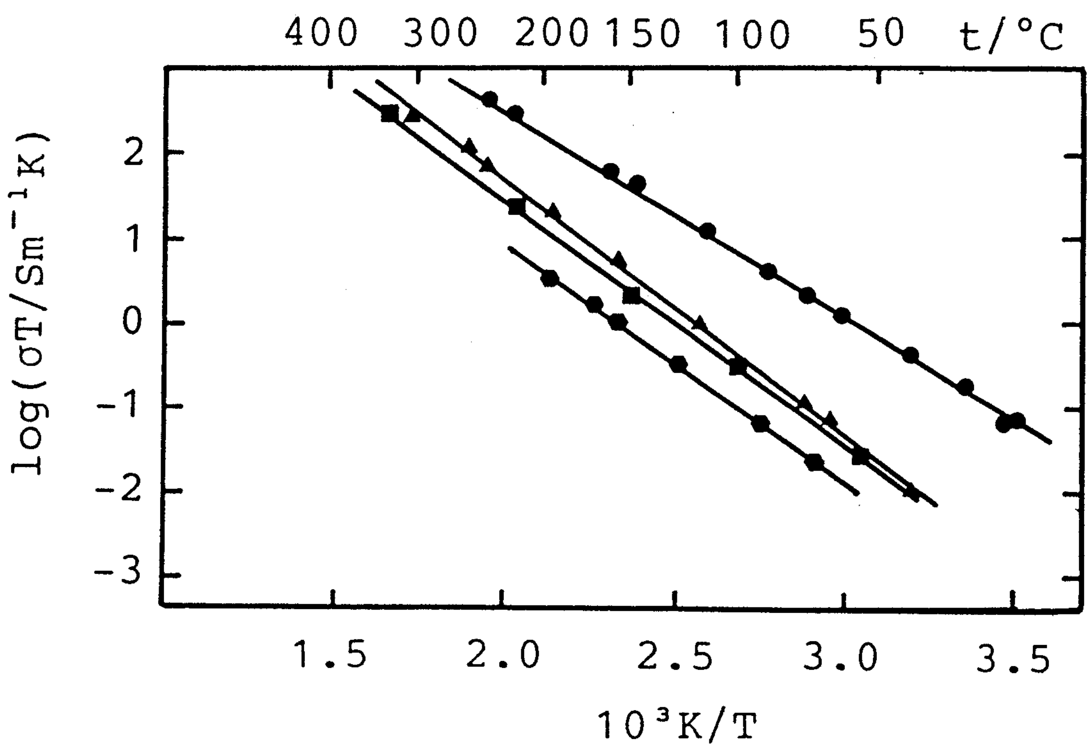

Fig. 16. Semilogarithmic plot of the conductivity σ times the absolute temperature T against the inverse abolute temperature: (●) Li_8SiN_4, (▲) Li_5SiN_3, (■) $Li_{18}Si_3N_{10}$ and (⬢) $Li_{21}Si_3N_{21}$.

Table 13. Ionic conductivity and activation energy of lithium silicon nitrides.

	σ/Sm^{-1} at 400 K	$Ea/kJmol^{-1}$
Li_8SiN_4	$5.0x10^{-2}$	46
$Li_{21}Si_3N_{11}$	$8.6x10^{-4}$	54
$Li_{18}Si_3N_{10}$	$2.9x10^{-3}$	55
Li_5SiN_3	$4.7x10^{-3}$	57
Li_2SiN_2	$1.1x10^{-3}$	53
$LiSi_2N_3$	$1.9x10^{-5}$	64

than that of Li_5SiN_3, while the former lithium content was larger than that of the latter. A reason for these facts could not be clarified, since the structures of these phases, especially configurations of lithium and silicon, have not been determined.

The reduced cell volumes of phases III to V slightly increased with lithium content as indicated in Fig. 14. The activation energy of ionic conduction slightly decreased among the three phases with increase in lithium content and in elemental cell volume. Phase VI, Li_8SiN_4, showed the smallest activation energy in accordance with the largest reduced cell volume. The ionic conductivity was one order of magnitude higher than others below 525 K. The high ionic conduction may be caused by the large amount of lithium ions as carriers and the low activation energy. Details of the ionic conduction cannot be discussed, since the structure of Li_8SiN_4 also has not yet been determined.

Chapter 4

Preparation and Electrical Properties of LiMgN

4-1. Introduction

Juza and Hund (14) prepared a compound of LiMgN in the preliminary studies of ternary nitride involving lithium. This phase has the antifluorite structure. Lithium and magnesium ions are statistcally placed in cation sites as shown in Fig. 3. This chapter describes the preparation of Li_3N-Mg_3N_2 compounds and the results of conductivity measurement.

4-2. Preparation

Magnesium nitride was prepared by reaction of granular magnesium (Mistuwa Pure Chemicals, 99%) with nitrogen gas (Osaka Oxygen Ind. Ltd., 99.999%) at 1175 K for one hour in a molybdenum boat. It was yellow brown color and unstable against moisture. Its X-ray powder diffraction data are listed in Table 14. Pulverized Li_3N and Mg_3N_2 were mixted in various molar ratios as shown in Table 15. The starting mixtures were compressed to pellet and enclosed in tantalum foil. These operations were carried out in a helium filled glove box. The pellets were heated under flowing nitrogen on the reaction conditions given in Table 15. The phases in the products were identified by X-ray powder diffractometry.

Table 14. X-Ray powder diffraction data for Mg_3N_2.

	(a)		(b)	
hkl	d/Å	I/I_o	d/Å	I/I_o
211	4.06	8	4.08	13
222	2.88	18	2.87	20
321	2.66	29	2.66	27
400	2.49	23	2.49	20
332	2.125	37	2.12	42
431,510	1.955	6	1.95	3
521	1.821	5	1.81	1
440	1.765	100	1.76	100
611,532	1.619	4	1.61	3
620	1.574	1		
541	1.538	5	1.53	3
622	1.504	3	1.50	2
631	1.470	6	1.47	3
444	1.439	5	1.44	2
543,550 710	1.409	2		
640	1.382	1		
633,552 721	1.356	23	1.36	20
651,732	1.265	18	1.27	12
800	1.246	5	1.24	1
811,741 554	1.227	2		

(a) Present study, Cubic a_o= 9.968(2) Å.

(b) Data from JCPDS. Cubic a_o= 9.95 Å.

Table 15. Reaction conditions and products in Li_3N-Mg_3N_2.

No.	$\frac{m(Li_3N)}{m(Mg_3N_2)}$ [a]	T/K	t/min	Products
1	1.5	1275	10	LiMgN, Li_3N
2	1.2	1275	10	LiMgN
3	1.2	1275	30	Li-Mg-N [b]
4	1.5	975	10	LiMgN, Li_3N
5	1.1	975	10	LiMgN, Li_3N
6	1.0	975	10	Li-Mg-N
7	0.9	975	10	Li-Mg-N
8	0.5	975	10	Li-Mg-N

a) Molar ratio in the starting mixture.
b) See in the text.

4-3. Results and Discussion

4-3-1. Phases in Li_3N - Mg_3N_2 System

Table 15 shows the phases obtained in the present studies in Li_3N-Mg_3N_2 binary system. LiMgN was synthesized at 1275 K for 10 min from the mixture of Li_3N/Mg_3N_2 = 1.2 in molar ratio. The excess Li_3N evaporated at this temperature. The product was reddish brown. Its X-ray powder diffraction data are listed in Table 16. Cell paramter of a = 4.9883(1) Å was determined by the least-squares method. The peaks of (111) and (311) reflections had broad tails on both sides as indicated in Fig. 17. These tails might be caused by some long range modurations of the structure. The further evaporation of Li_3N changed LiMgN into another phase represented as "Li-Mg-N". This phase was also prepared from the mixture of $Li_3N/Mg_3N_2 \leqq 1$ at 970 K. The color of this product was brownish white. X-ray diffraction patterns of this phase are illustrated in Fig. 18 (b) and (c). The structure of this phase is considered to be related to Mg_3N_2 structure from the correspondence of main peak positions, while we could not index all the reflections. Mg_3N_2 has the anti-C-rare earth structure (c-M_3O_2) which is derived by removing one-quarter of cations from that of antifluorite-type and the followed slight rearrangment of the atoms. The cubic lattice constant a = 9.968 Å for Mg_3N_2 well agreed with 2 x 4.988 Å of LiMgN which has the antifluorite structure. The structure of Li-Mg-N is probably a hybridization of LiMgN and Mg_3N_2 structures.

Table 16. X-Ray powder diffraction data for LiMgN.

	(a)		(b)	
hkl	d/Å	I/I_o	d/Å	I/I_o
111	2.88	95	2.89	80
200	2.49	20	2.50	60
220	1.764	100	1.760	100
311	1.504	12	1.503	45
222	1.440	8	1.438	40
400	1.247	8	1.244	60
331	1.145	2	1.141	10
420	1.115	9	1.114	30
422	1.018	18	1.014	70
333,511	0.959	1	0.960	10
440	0.882	5	0.880	50

(a) Present study. Cubic a = 4.9883(1) Å.

(b) Juza and Hund (14). Cubic a = 4.890 Å.

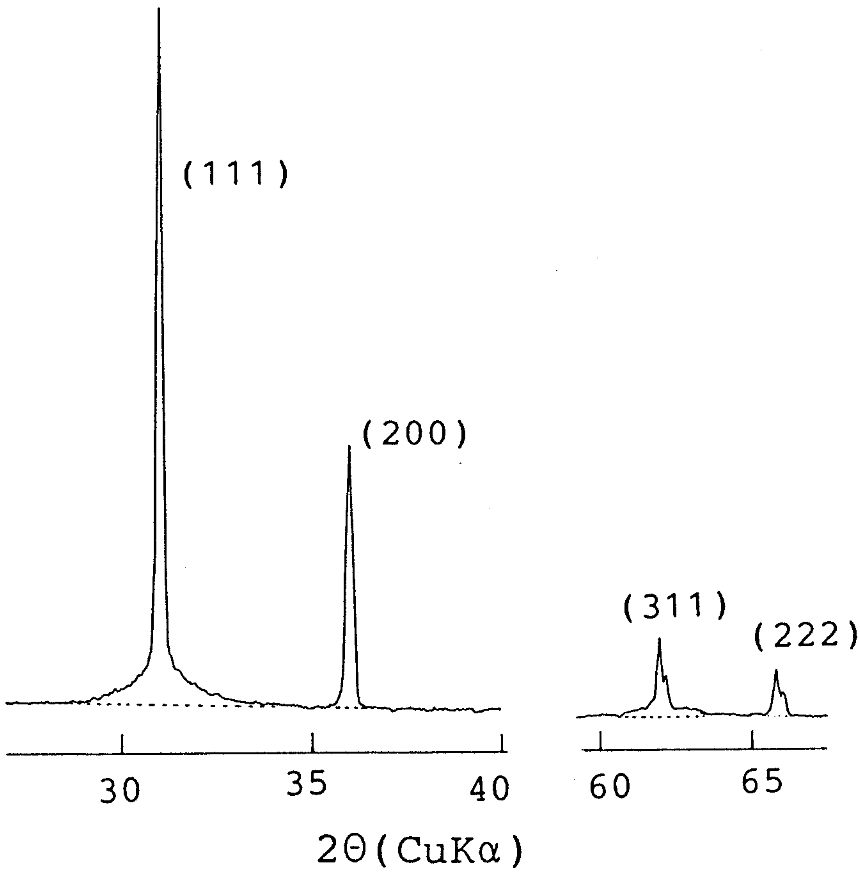

Fig. 17. X-ray powder diffracion pattern of LiMgN.

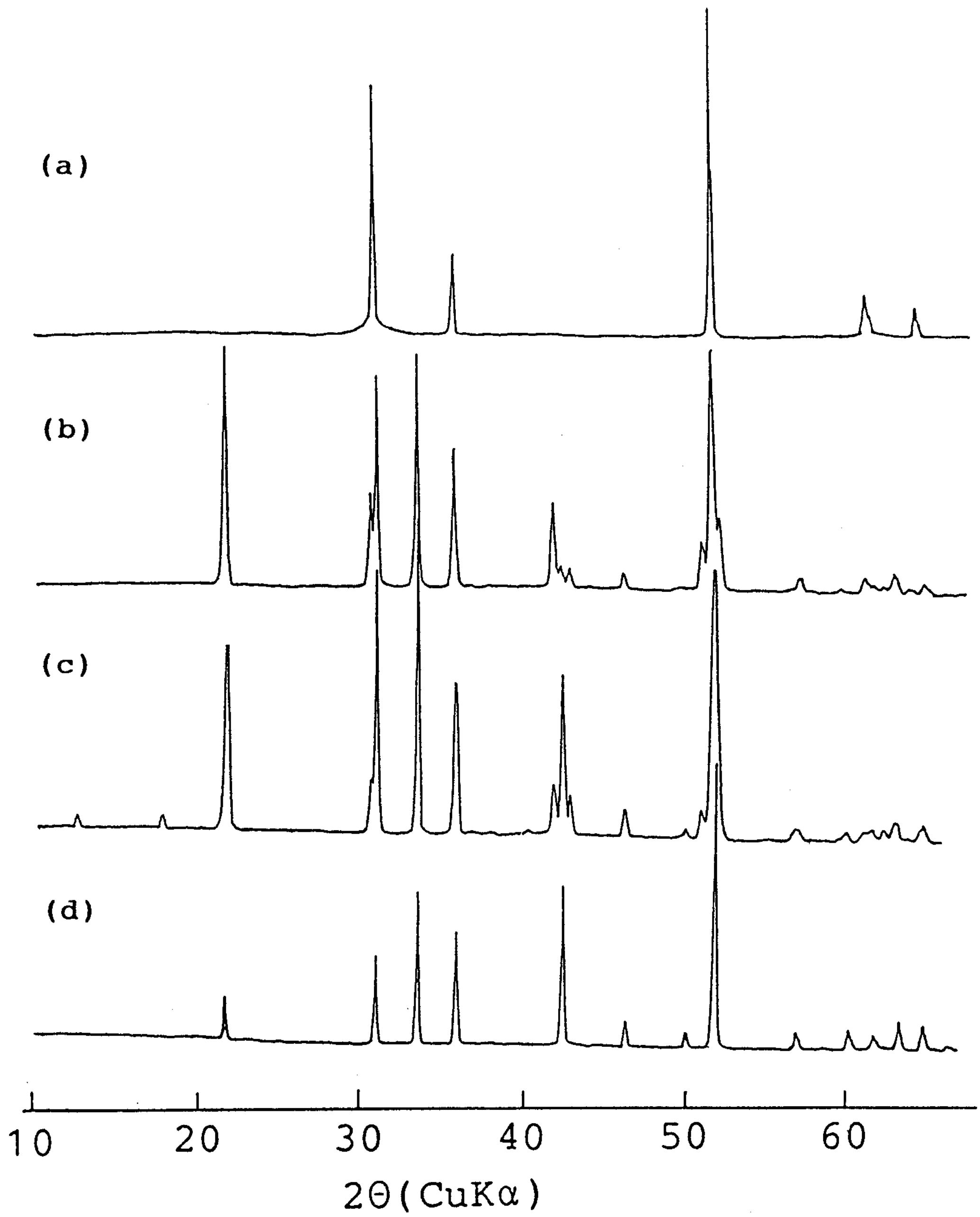

Fig. 18. X-Ray powder diffraction patterns of (a) LiMgN, (b) Li-Mg-N of No. 7 and (c) that of No. 8 in Table 15 and (d) Mg_3N_2.

4-3-2. Conductivity Measurement

Figure 19 shows the temperature dependence of the conductivity measured by complex impedance method for LiMgN. Direct current measurements with carbon electrodes indicated that electron and/or hole migrations contribute to the total conduction in less than 80%. The electronic contribution might be comparable to that of other ternary nitrides which exhibit lithium ionic conductions. A reason for low conduction will be discussed in Chapter 7 comparing with the case of Li_5SiN_3.

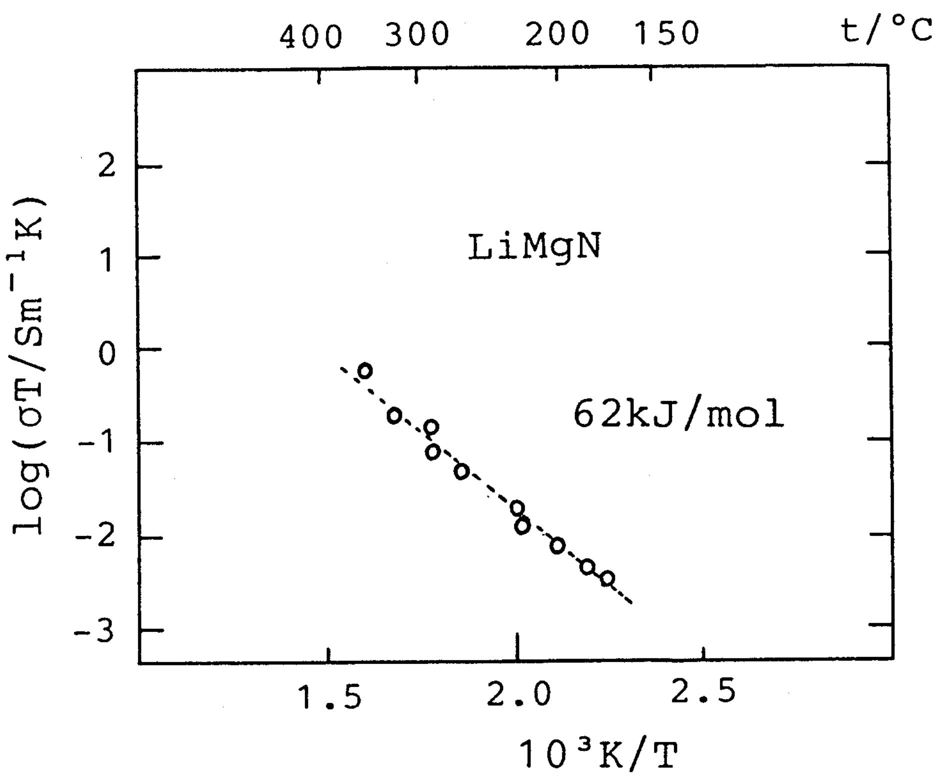

Fig. 19. Temperature dependence of the conductivity for LiMgN.

Chapter 5

Preparaiton and Electrical Properties of Li_7PN_4

5-1. Introduction

Lithium phosphorus nitride, Li_7PN_4 was firstly synthesized by Brice et al. (40). They obtained this material under nitrogen atmosphere by two methods: (i) the reaction of Li_3N, Li_3P and nitrogen, (ii) the reaction of Li_3N, red phosphorus and nitrogen. They assumed the crystal structure of Li_7PN_4 to be isostructural with Li_7VN_4 from the analogy of X-ray powder diffraction patterns. The structure of Li_7VN_4 reported by Juza et al. (41) is an antifluorite superstructure in which vanadium and lithium are distributed orderly as shown in Fig. 20. In the case of Li_7PN_4, vanadium is replaced by phosphorus. The 7/8 of cation sites is occupied by lithium ions.

The present chapter deals with preparations and electric conductivity measurements for Li_7PN_4.

5-2. Experimental

Prepartion was carried out by the second method of Brice et al. The starting materials were lithium nitride and red phosphorus (Nakarai Chemicals, Ltd., 99.999%). They were mixed in various molar ratios as shown in Table 17 and placed in tantalum boat. These operations were carried out in a helium-filled glove box. The mixtures were reacted under nitrogen atmosphere on the conditions described in Table 17. All products were characterized by X-ray powder diffraction method.

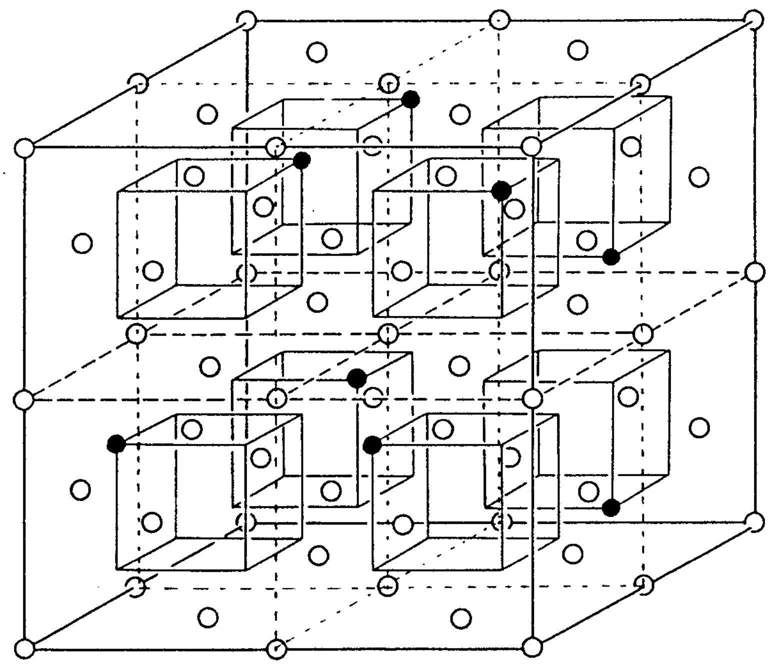

Fig. 20. Crystal structure of Li_7VN_4 and Li_7PN_4;

● vanadium or phosphorus,

⊣ lithium, ○ nitrogen.

Table 17. Reaction conditions and products in Li_3N-P system.

No.	$\frac{m(7/3 x Li_3N)}{m(P)}$ [a]	T/K	t/h	Products
1	1.0	1275	24	Li_3P
2	1.0	1075	24	X[b], Li_3P
3	1.0	875	72	X, Li_7PN_4[c]
4	1.0	875	24	X, Li_7PN_4[c]
5	1.0	875	1/6	X, Li_7PN_4[c], Li_3P
6	1.0	675	24	Li_3N, Li_3P
7	3.2	875	24	Li_3N, X
8	1.6	875	24	X, Li_7PN_4[c], Li_3N
9	1.2	875	24	X, Li_7PN_4[c]
10	1.1	875	24	X, Li_7PN_4[c]
11	0.9	875	24	X, Li_7PN_4[c], Li_3P
12	0.7	875	24	X, Li_7PN_4[c], Li_3P
13	0.6	875	24	Li_3P, X

a) Molar ration in starting mixture.

b) Unidentified phase.

c) The phase of Li_7PN_4 was occasionally prepared.

Electric conductivity measrements were performed by complex impedance and d.c. methods with lithium metal or silver conductive paste as electrodes under inert gas atmosphere.

5-3. Results and Discussion

5-3-1. Preparation

Preparations are summarized in Table 17. Li_7PN_4 was prepared as a mixture with unknown phase X at 875 K from the starting mixture of $7/3Li_3N:P$ = 1:1 in molar ratio. It was not stable above 1075 K and the product was Li_3P. The excess lithium was evaporated. Li_3P was also obtained with Li_3N at 675 K in spite of heating under nitrogen atmosphere. Lithium phosphate was considered to be more stable than Li_7PN_4 at these temperatures. During the preparations, some amounts of phosphorus sublimed and deposited on the cooler part of reaction tube. Single phase of Li_7PN_4 could not be prepared by heating the mixtures of Li_3N and P at 875 K. Li_7PN_4 was always accompanied by the unidentified phase X. The mixing ratios of these phases varied occasionally and could not be controlled. Sometimes the phase X could be obtained by itself. Table 18 shows X-ray diffraction data of the product containig Li_7PN_4 and X-phase whose content was the lowest in the present study comparing with that of X-phase. There might be some relationship between

Table 18. X-Ray powder diffraction data.

hkl	(a) d/Å	(a) I/I₀	(b) d/Å	(b) I/I₀	(c) d/Å	(c) I/I₀
			5.01	2	5.00	20
200	4.67	50	4.68	25	4.67	45
210	4.19	85	4.19	72		
			4.02	9	4.03	65
			3.87	3	3.88	30
211	3.82	85	3.82	81		
			3.41	3	3.41	10
			3.18	5	3.18	40
			2.95	5	2.94	20
222	2.700	100	2.70	100	2.71	100
320	2.593	10	2.60	5		
					2.55	5
321	2.500	15	2.50	11		
400	2.336	5	2.34	3	2.35	5
420	2.092	5	2.10	2	2.10	5
421	2.040	10	2.04	3		
332	1.995	10	1.999	4		
					1.938	10
422	1.909	5	1.910	3	1.911	10
431,510	1.836	15	1.837	7	1.835	5
					1.800	10
520,432	1.739	15	1.739	7	1.741	1
521	1.704	5				
440	1.655	95	1.655	55	1.656	70
442,600	1.560	10	1.561	3		
532,611	1.519	10	1.519	4		

(a) Li_7PN_4 after Brice et al. (40). Cubic a = 9.363 Å.

(b) Mixture of Li_7PN_4 and unidentified phase X given No. 10 of Table 17.

(c) Unidentified phase X.

Li_7PN_4 and X-phase structures from the correspondance of d-spacing and intensities of main reflections above θ = 33^{o}(CuKα). But the reflections of X-phase could not be indexed. Phosphorus can take oxidation states between +5 and -3, and relatively stable as a form $Li^{+}{}_{3}P^{3-}$ observed above. It might be difficult to fully oxidize phosphorus to the highest oxidation state +5 in nitrogen atmosphere. The phase X might be a lithium phosphorus nitride containing phosphorus in lower oxidation state.

5-3-2. Electric Conductivity

Figure 21 shows the conductivity of Li_7PN_4 containing some amount of X-phase. The values measured by complex impedance method agreed with those by d.c. method using lithium metal electrodes. They also agreed with those measured by d.c. method with Ag paste as ion blocking electrodes. The most part of conduction can be attributed to electron or hole migrations. The conductivity of X-phase had the same value with that of the mixture. The conduction behavior is not clear for Li_7PN_4 itself in the present study. The electornic conduction observed in the present study might be due to a mixed valence state of phosphorus in the structure as assumed in the structural discussion.

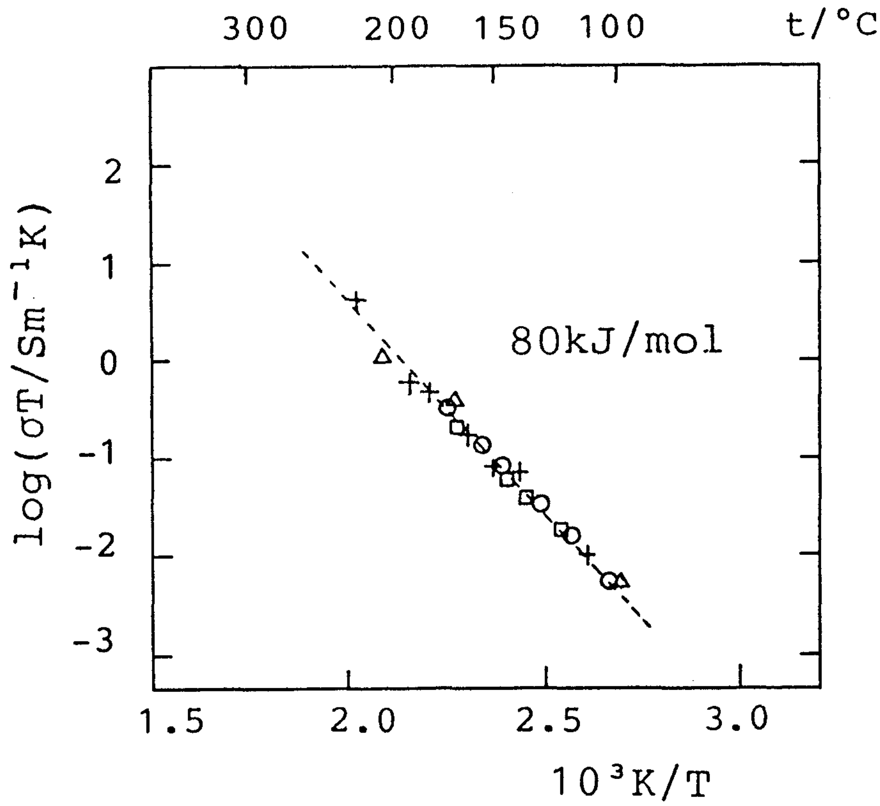

Fig. 21. Temperature dependence of electric conductivity. Li_7PN_4 containing X-phase:
+, complex impedance method,
□ and △, d.c. method with lithium and Ag conductive paste as electrodes, respectively.
X-phase: ○, d.c. method with lithium electrode.

Chapter 6

High(β) and Low(α) Temperature Phases of Li_3BN_2

6-1. Introduction

The binary system of Li_3N-BN was firstly studied by Goubeau and Anselment (21). They claimed the presence of $(NBN)^{3-}$ ion in the ternary metal-boron nitride using infrared spectroscopy. DeVries and Fleisher (22) synthesized a high pressure phase of Li_3BN_2, and reported a pressure-temperature formation diagram for these phases. They presumed that the structre of high and low pressure phases could be related to the antifluorite structure such as Li_3AlN_2, but the structures themselves had not yet been solved.

Another new polymorph was found out in the present study by slow cooling of the melt under flowing nitrogen. The known and newly discovered polymorphs of Li_3BN_2 are denoted as α- and β-phases respectively in the present paper.

In this chapter, we report the preparations of Li_3N-BN binary compounds. Crystal structures of α- and β-Li_3BN_2 are also studied by single crystal X-ray diffractometry. Ionic conductivity of the two phases is measured on the the polycrystalline samples.

6-2. Preparation and Phase Relation

6-2-1. Experimental

Pulverized Li_3N was mixed with boron nitride powder

(Showa Denko Co., 99.8%) in various molar ratios as shown in Table 19. The starting mixtures were compressed to a pellet and enclosed in tantalum foils. These operations were performed in a hellium filled gove box. The pellets were heated in a stream of nitrogen on the desired reaction conditions as shown in Table 19, and then quenched in a furnace to room temperature. The estimated rate of temperature decrease was about 100 K/min above 800 K. Phases in the products were identified by X-ray powder diffractometry. X-ray powder diffraction data were obtained by means of a goniometer (r = 185 mm) using CuKα (1.5418 Å) radiation monochromatized with a pyrolytic graphite.

Differential thermal analysis was carried out using an alumel-chromel thermocouple under nitrogen atmosphere. A heating rate was 20 K/min and α-Al_2O_3 was used as a reference. Samples of 3-5 mg and the reference were encapsuled in tantalum foil.

6-2-2. Results and Discussion

A. Phases in Li_3N-BN System

Table 19 shows the phases observed in the present preparations in Li_3N-BN binary system. Most of the products showed the existence of α-Li_3BN_2 which could be obtained without other kinds of nitrides from the mixture of Li_3N/BN = 1.0-1.1 in molar ratio at 1070 and 1270 K. The product

Table 19. Reaction conditions and products in Li_3N-BN system.

No.	$\frac{m(Li_3N)}{m(BN)}$ [a]	t/min	T/K	Products
1	2.0	10	1070	Li_3N, α-Li_3BN_2, (Li_2O)
2	1.5	60	1070	Li_3N, α-Li_3BN_2, (Li_2O)
3	1.1	60	1070	α-Li_3BN_2, (Li_2O)
4	0.7	80	1070	α-Li_3BN_2, Li-BN, (Li_2O)
5	0.3	150	1340	Li-BN, α-Li_3BN_2
6	0.2	60	1220	BN, Li-BN, α-Li_3BN_2
7	1.1-1.0	10	1270	α-Li_3BN_2, (Li_2O)
8	1.1-1.0	10	1170	β-Li_3BN_2, (Li_2O)
9	1.1-1.0	10	1070	α-Li_3BN_2, (Li_2O)
10	1.1-1.0	10	970	α-Li_3BN_2, Li_3N, BN, (Li_3N)

a) Molar ratio in the starting mixture.

heated up to 1270 K had a glassy white surface and did not hold a shape of the initial pellet of starting mixture. Other products were white polycrystalline pellets. β-Li_3BN_2 could be prepared only in the case of heating at 1170 K. X-ray powder diffraction data are shown in Table 20 (c) for the product of No. 3 in Table 19, comparing with the values in the previous studies (21, 22).

Table 20 (d) lists the values calculated from single-crystal data of α-Li_3BN_2 shown later in 6-3 of this chapter. The calculated intensities were obtained from I (calc.) = F^2m/L where F is the single-crystal structure factor, m is the multiplicty of crystal planes of a set of hkl values, and L is the combined Lorentz and polarization factor. The observed data agreed well with the calculated results except the reflection at 2.67 Å. Intensity of this reflection was much smaller than those reported by DeVries and Fleisher (22). The d-value corresesponds to that of (111) plane of Li_2O listed in Table 2 (e). The Li_2O content was estimated as 0.5-1.0 wt% using the method of standard addition on X-ray diffractometry.

Another compound represented as Li-BN in Table 19 was synthesized from the mixtures in the compositional range of $Li_3N/BN < 1.0$. Its single phase, however, could not be obtained in the present study. Its X-ray powder diffraction data are given in Table 20 (f). These diffraction lines were relatively broad in comparison with those of the coexisting phases in the products. They could not be indexed at the moment. The reflections at 3.81, 2.24 Å in Table 20

Table 20. X-Ray powder diffraction data.

(a)		(b)		(c)		(d)			(e)			(f)	
d/Å	I	d/Å	I/I_o	d/Å	I/I_o	hkl	d/Å	I/I_o	hkl	d/Å	I/I_o	d/Å	I
3.81	m	3.73	10									3.75	vs
3.50	s	3.47	50	3.48	47	101	3.481	45					
		3.27	10	3.29	4	110	3.283	4					
2.82	vs	2.78	100	2.78	100	111	2.785	100					
		2.67	20	2.67	5				111	2.664	100	2.65	vw
2.63	s	2.63	30	2.63	24	002	2.630	29	200	2.306	8	2.23	w
2.24	w	2.22	5									2.21	w
2.07	vs	2.07	15	2.08	8	210	2.077	11				2.07	vw
		2.05	25	2.05	32	112	2.053	34				2.06	w
1.93	w	1.91	5	1.93	1	211	1.932	1				1.91	w
1.83	w												
1.74	vw	1.74	10	1.74	8	202	1.740	11					
		1.69	5										
1.64	vs	1.64	20	1.64	16	220	1.641	19				1.64	vw
						103	1.640	2					
		1.63	10	1.63	9	212	1.630	4	222	1.631	40		
				1.567	1	221	1.567	1					
1.55	m	1.55	10	1.546	5	113	1.546	9					
1.48	w			1.486	2	301	1.485	3					
						310	1.468	0.2					
1.42	w			1.415	3	311	1.414	5					
1.40	w			1.392	3	222	1.393	3	311	1.391	16		
1.32	w			1.316	2	004	1.315	5					
						320	1.288	0.5					
1.29	w			1.283	2	312	1.284	6					
1.25	w			1.252	2	321	1.251	5					

(a) Li_3BN_2 Goubeau and Anselment (1961).

(b) Li_3BN_2 DeVries and Fleischer (1969).

(c) $Li_3BN_2(\alpha)$ + (Li_2O 1wt%) prepared at 1070K in the present study.

(d) $Li_3BN_2(\alpha)$ calculated from the result of single-crystal study.

(e) Li_2O from JCPDS card.

(f) Li-BN prepared at 1340K in the present study.

(a) and 3.73, 2.22 Å in (b) may correspond to those at 3.75, 2.23 and 2.21 Å of Li-BN compound.

Boron nitride has a layered structure analogous to graphite. The interlayer distances are 3.33 and 3.348 Å, respectively in BN (42) and in graphite (JCPDS 26-1029). The spacing of 3.75 Å in Li-BN is comparable to the interlayer distance of 3.70 Å in lithium intercalated graphite, C_6Li (43). The structural similarity between graphite and boron nitride led Croft to attempt the preparation of boron nitride intercalation compounds (44). Catalytic activity was examined on additional compounds of boron nitride with K, Rb and Cs (45). However, there still remains some ambiguity about the presence of boron nitride intercalation compounds because of the diffculty of preparation and identification.

B. Phase Relation beteen α- and β-Li_3BN_2

Single crystals of β-Li_3BN_2 were picked up from the inside of the product obtained by slow-cooling of a melt at a rate of 1.5-3.0 K/h from 1200 to 1000 K. Its DTA traces are shown in Fig. 22. No thermal event appeared below 1100 K in the case of raising temperature at a rate of 20 K/min. An endotherm started at 1189 K was probably due to a melt. A very sharp exothermic peak was observed between 1136 and 1144 K on cooling the melt at a rate of 20 K/min. The exotherm began at 1160 K at the cooling speed

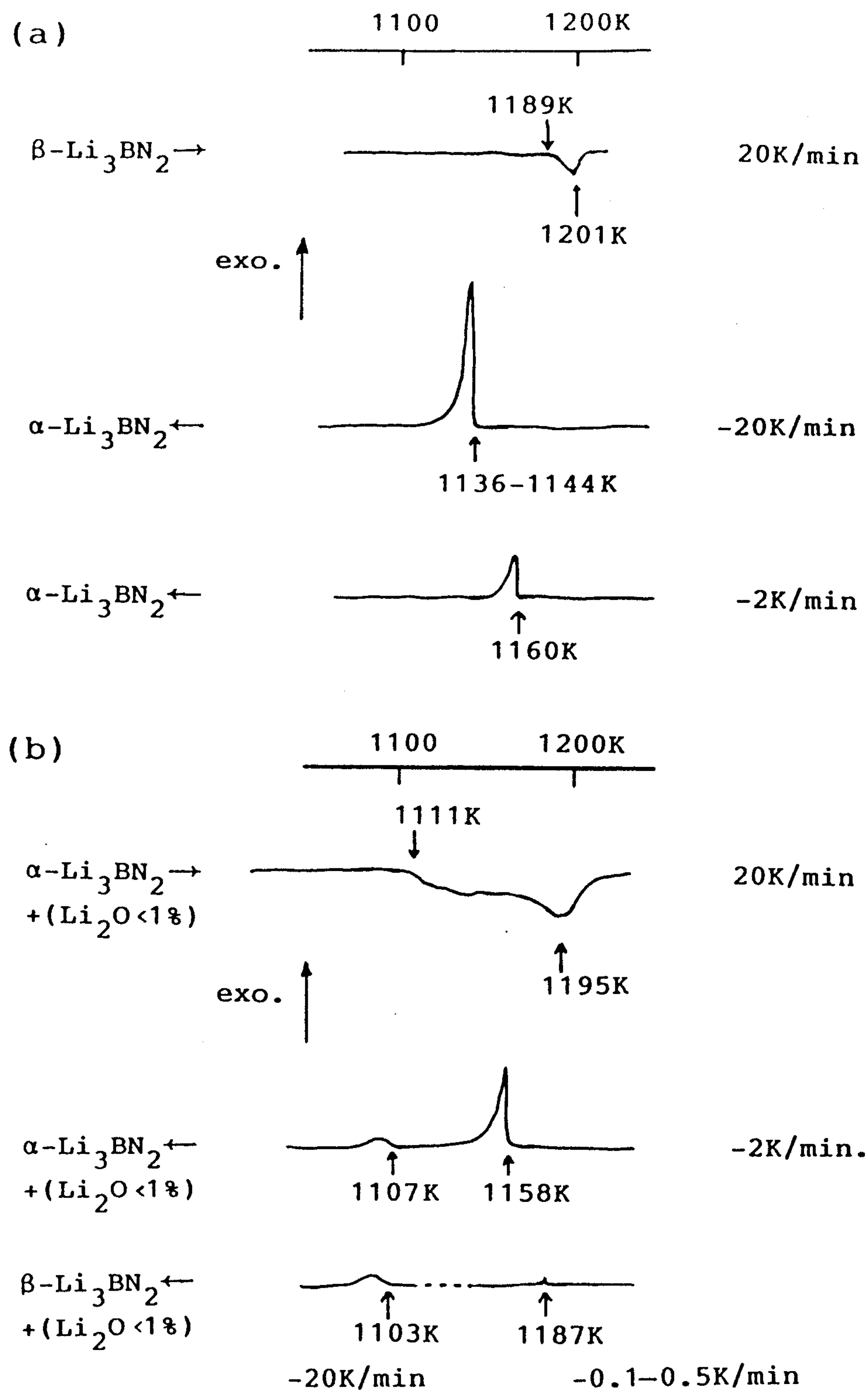

Fig. 22. Differential thermal analyses of (a) β-Li_3BN_2 single crystals (0.3-1.0 mm) and (b) α-Li_3BN_2 polycrystalline containing Li_2O<1 wt%.

of 2 K/min. The samples had changed to polycrystalline α-Li_3BN_2 after the DTA experiments.

Figure 22 (b) shows the DTA curves of α-Li_3BN_2 containing less than 1 wt% Li_2O as an impurity. During the heating at a rate of 20 K/min, endothermic change started at 1111 K and its maximum was at 1195 K. On cooling the melt at a rate of 2 K/min, a sharp exotherm at 1158 K was followed by a small exothermic peak at 1107 K. The product remained a mixture of α-Li_3BN_2 and a small amount of Li_2O. β-Li_3BN_2 was obtained by an extremely slow-cooling at a rate of 0.1-0.5 K/min to 1150 K and successive cooling at a rate of 20 K/min to room temperature. A very small exothermic peak was detected at 1187 K. It corresponds to the melting point of β-Li_3BN_2 single crystal shown in Fig. 22 (a). Another small exotherm also appeared at 1103 K. These DTA results lead to the conclusion that α-Li_3BN_2 crystallizes below 1160 K and β-Li_3BN_2 has a melting point around 1189 K. The small exothermic peak appeared around 1107 K is considered as an eutectic temperature in Li_3BN_2-Li_2O binary system.

Both α- and β-Li_3BN_2 were annealed on the desired conditions shown in Table 21 and quenched to room temperature in order to study the phase relation. Compressed pellets of β-Li_3BN_2 powder transformed completely to α-Li_3BN_2 maintaining the external shape of initial pellet at the temperature range from 973 to 1088 K, while no transition occured in the case of β-Li_3BN_2 single crystal. The velocity of transformation probably depends on the crystal size. The phase transition of α- to β-Li_3BN_2 was caused by heating above 1140 K. The

Table 21. Heat treatments of α- and β-Li_3BN_2.

	T/K	t/min	Product
β-Li_3BN_2 a)	1173	10	β-Li_3BN_2
	1023-1093	300	β-Li_3BN_2
β-Li_3BN_2 b)	1088	60	α-Li_3BN_2
	973	60	α-Li_3BN_2
α-Li_3BN_2	1160	10	β-Li_3BN_2
	1150	10	β-Li_3BN_2
	1140	10	β-Li_3BN_2, α-Li_3BN_2
	1130	10	α-Li_3BN_2
	1073	70	α-Li_3BN_2

a) single crystal(0.3-1.0 mm)
b) powder

initial form of α-Li_3BN_2 pellet was also maintained in all the runs shown in Table 21. The reversible transition temperature between α- and β-phases can be estimated at around 1135 K. This phase transition could not be detected clearly by DTA. The transformation may partly contribute to the broad endothermic signal between 1111 and 1195 K shown in Fig. 22 (b), but the peak of phase transition itself could not be resolved.

Figure 23 illustrates schematic free energy curves for the Li_3BN_2 phases against temperature. The high temperature phase, β-Li_3BN_2, is obtained by slow-cooling of liquid. On a rapid cooling, the liquid is supercooled along the the dotted line. The α-phase, which is low-temperature phase, is directly crystallizid at 1160 K from the super-cooled liquid.

6-3. Crystal Structre of β-Li_3BN_2

6-3-1. Experimental

Mixtures having molar ratio Li_3N/BN = 1.0-1.2 were heated above a melting temperature of the product at 1200 K, kept at this temperature for 7 hr and cooled to 1000 K at a rate of 1.5-3.0 K/h under a flow of nitrogen. Prismatic crystals with a size of 3.0 x 1.5 x 1.5 mm were taken out from the product. They were colorless, transparent, unstable against moisture and soluble in water.

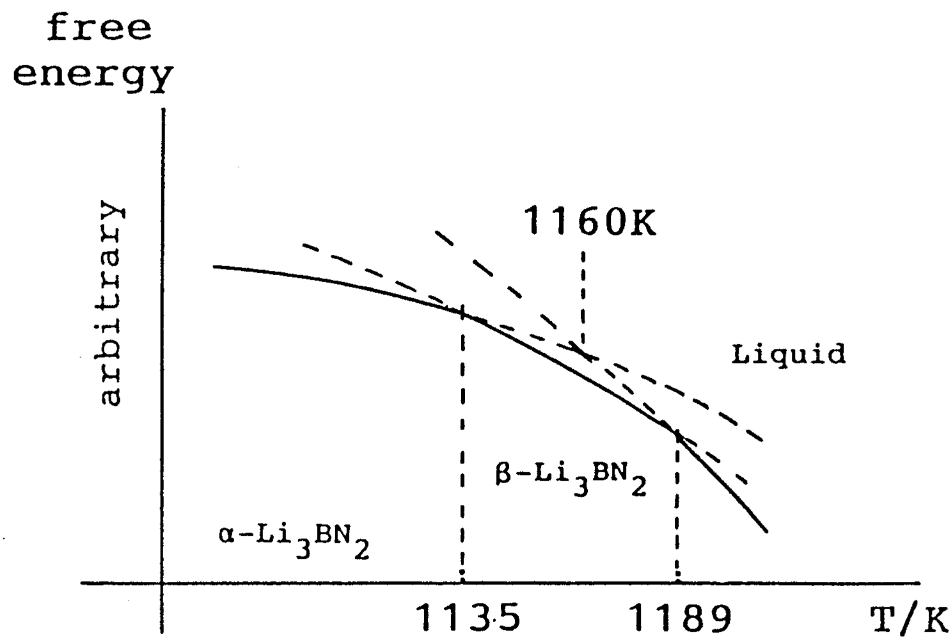

Fig. 23. Schematic free energy curves of Li_3BN_2 against temperature.

The amounts of lithium, boron and nitrogen were determined by atomic absorption and Kjeldahl methods as presented in Chapter 3. Boron standard solution (Wako Pure Chemical Ind. Ltd., 1000ppm) was diluted to 4, 5 and 10 ppm. The following instrumental setting were used;

	B
Analytical line	2498 Å
Slit	3-4
Source: Hollow Carthode	10 mA
Fuel:	Acetylene
Oxidzer:	N_2O

The sensitivity of boron analysis was also strongly influenced by the flow rate of acetylene and N_2O gas. The results are shown in Table 22. Denstiy measured by flotation method was 1.74 Mgm^{-3}.

Weissenberg and precession photographs taken with CuKα and MoKα radiations, respectively, indicated systematic absence of reflections, with $l = 2n + 1$ for h0l and $k = 2n + 1$ for 0k0, which are consistent with the space group $P2_1/c$ of monoclinic system.

A single crystal used for intensity collection was ground to an ellipsoid having dimension of 0.8 x 0.5 x 0.5 mm in argon atmosphere. It was sealed with argon gas in a glass capillary of 0.5 mm in diameter.

Cell parameters were determined by the least-squares method using 36 reflections ($2\Theta = 23\text{-}29^{o}$, MoK$\alpha$ $\lambda = 0.71069$ Å) measured with a four-circle diffractometer. Crystallographic data are summarized in Table 23.

Table 22. Analytical results of β-Li_3BN_2 for lithium, boron and nitrogen.

	1	2	3	av.	ideal
Li%	35.0	34.2	34.8	34.7	34.9
B	18.5	17.3	18.3	18.0	18.1
N	44.5	47.0	--	45.8	47.0
total				98.5	100.0

Table 23. Crystallographic data.

	α-Li_3BN_2	β-Li_3BN_2
	tetragonal	monoclinic
space group	$P4_22_12$	$P2_1/c$
a =	4.6435(2)Å	5.1502(2)Å
b =	4.6435(2)Å	7.0824(2)Å
c =	5.2592(5)Å	6.7908(2)Å
		β = 112.956(2)°
V =	113.40 $Å^3$	228.08 $Å^3$
$D_{obs.}$ =	1.75 Mgm^{-3}	1.74 Mgm^{-3}
$D_{calc.}$ =	1.747 Mgm^{-3}	1.737 Mgm^{-3}
μ =	0.082 mm^{-1}	0.082 mm^{-1}
Z =	2	4

MoKα radiation monochromatized by pyrolytic graphite was used for intensity measurements. The intensities of 2773 reflections including crystallographically equivalent reflections within the range of $0<2\Theta<80^{\circ}$ were obtained at 293 K by $2\Theta - \Theta$ scan techique on a four-circle diffractometer (RIGAKU AFC-5 FOS). Three standard reflections measured after every 55 reflections showed no evidence of crystal deterioration and no instability of the detection system. All the observed reflections were summarized in 1425 unique reflections. Sixty-three reflections having high standard deviations ($3\sigma_{hkl}(F_o) > F_o$) or unobservable intensities were eliminated from the least-squares refinement procedure, where $\sigma_{hkl}(F_o)$ is a standard deviation of each reflection obtained from counting statistics. Conventional Lorentz and polarization corrections were carried out in the process of data collection. No absorption correction was made because of the small value of $\mu r(0.04)$.

An appropriate structure model was obtained from Patterson synthesis diagrams. Full-matrix least-squares refinement with anisotropic temperature factors for all atoms gave final agreement factors of R = 0.023

$$R = \frac{\Sigma||Fo|-|Fc||}{\Sigma|Fo|}$$

$$R_w = \frac{\Sigma w(|Fc| - |Fo|)^2}{\Sigma w|Fo|^2}$$

,

where $w = 1/\sigma^2_{hkl}(F_o)$. Ratio of maximum least-squres shift to error in final refinement cycle was 0.00. Maximum and minimum residual electron densities in final difference-

Fourier synthesis diagrams were +0.5 $eÅ^{-3}$ and -0.1 $eÅ^{-3}$. Atomic scattering factors for Li, B and N were taken from International Tables for X-ray Crystallography, Vol. IV (46). Final positional and thermal parameters are given in Table 24.

All computations for the least-squares refinements of lattice constants and structure parameters, interatomic distances and angles, Patterson, Fourier and diffrernce-Fourier syntheses, and crystal structure drawing, were carried out using the program LCLSQ (47), RFINE (48), UMBADTEA (49), 3DFR (50) and ORTEP-II (51), respectively, at the Crystallographic Research Center, Institute for Protein Research, Osaka University (ACOS-700).

6-3-2. Results and Discussion

Stereoscopic illustrations of the structure are shown in Fig. 24. The structure of β-Li_3BN_2 can be explained by alternations of two kinds of layers; one is composed of only N atoms and the other includes Li and B atoms. These layers are parallel to (100). Nitrogen atom layers are located at around x = 0 and x = 1/2, and layers including lithium and boron atoms are at around x = 1/4 and x = 3/4.

Interatomic distances and angles are given in Table 25. Figure 26 shows the environments around N(1) and Li(2). Li(1), Li(2) and Li(3) are tetrahedraly coordinated by 2N(1) and 2N(2), and the tetrahedra are fairly distorted. The

Table 24. Refined results of atomic coordinates and thermal parameters of β-Li_3BN_2. Anisotropic temperature factors are in the form, $\exp[-(\beta_{11}h^2+\beta_{22}k^2+\beta_{33}l^2+2\beta_{12}hk+2\beta_{13}hl+2\beta_{23}kl)]$. Estimated standard errors are given in parentheses.

	x	y	z
Li(1)	24995(17)	48518(12)	49811(12)
Li(2)	25228(18)	1212(13)	37502(13)
Li(3)	74360(16)	20714(11)	31402(12)
B	21509(7)	31982(5)	17648(5)
N(1)	43403(6)	43735(4)	21904(5)
N(2)	99439(6)	20472(5)	13461(5)

	β_{11}	β_{22}	β_{33}	β_{12}	β_{13}	β_{23}
Li(1)	1267(27)	610(13)	713(15)	150(14)	179(16)	-8(10)
Li(2)	1288(27)	876(15)	671(15)	223(15)	339(16)	18(11)
Li(3)	1159(25)	466(11)	763(14)	4(13)	316(15)	14(10)
B	712(11)	332(5)	406(6)	18(5)	188(7)	-9(4)
N(1)	760(10)	335(4)	627(6)	-53(4)	171(6)	-1(3)
N(2)	817(10)	511(5)	538(6)	-160(5)	195(6)	39(4)

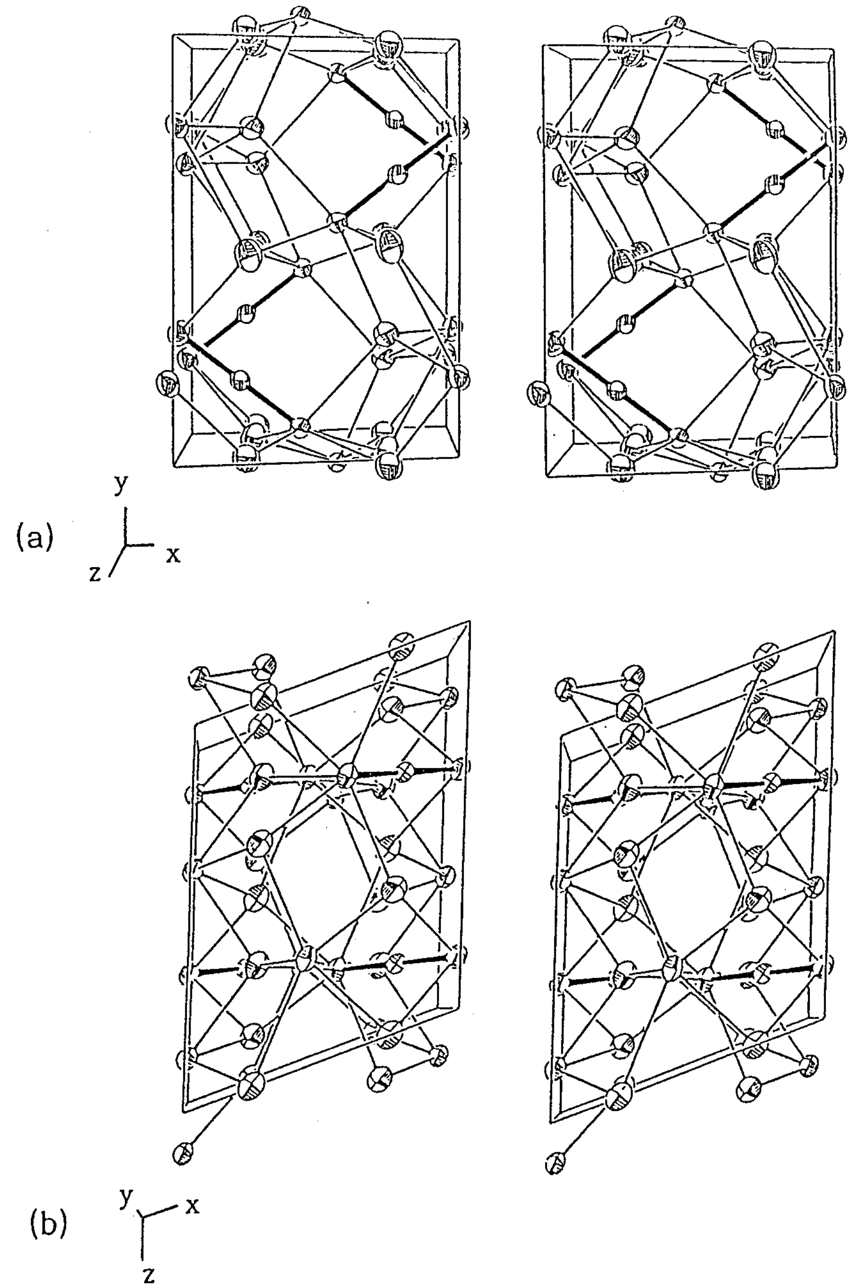

Fig. 24. Stereoscopic views down [001] (a) and [010] (b) of the β-Li_3BN_2 structure. The 70% probability thermal ellipsoids for all atoms are shown. No atoms are labeled, but straight N-B-N bonds are obvious because of their thicker bonds which denote covalent B-N bonds. Larger ellipsoids are Li(1) and Li(2).

Table 25. Interatomic distances (Å) and angles (°) with estimated standard errors given in parentheses.

Li(1)-N(1)	2.4508(11)
$-N(1)^{vii}$	2.0497(9)
$-N(2)^{vi}$	2.3134(10)
$-N(2)^{ix}$	1.9821(9)
$Li(2)-N(1)^{i}$	2.1809(9)
$-N(1)^{ix}$	2.0256(11)
$-N(2)^{v}$	2.1444(9)
$-N(2)^{x}$	2.5087(10)
Li(3)-N(1)	2.1941(8)
$-N(1)^{ix}$	2.0924(8)
-N(2)	2.0930(11)
$-N(2)^{i}$	2.1457(9)
N(1)-B	1.3393(5)
$N(2)-B^{iii}$	1.3361(5)
$N(1)-N(2)^{v}$	2.6753(5)

N(1)	$-Li(1)-N(1)^{vii}$	110.88(4)
N(1)	$-Li(1)-N(2)^{ix}$	97.20(4)
N(1)	$-Li(1)-N(2)^{vi}$	132.97(2)
$N(1)^{vii}$	$-Li(1)-N(2)^{vi}$	98.51(4)
$N(1)^{vii}$	$-Li(1)-N(2)^{ix}$	110.33(4)
$N(2)^{ix}$	$-Li(1)-N(2)^{vi}$	98.41(3)
$N(1)^{i}$	$-Li(2)-N(1)^{ix}$	108.58(4)
$N(1)^{i}$	$-Li(2)-N(2)^{v}$	126.21(5)
$N(1)^{i}$	$-Li(2)-N(2)^{x}$	99.89(4)
$N(1)^{ix}$	$-Li(2)-N(2)^{v}$	105.05(5)
$N(1)^{ix}$	$-Li(2)-N(2)^{x}$	102.88(4)
$N(2)^{v}$	$-Li(2)-N(2)^{x}$	112.03(4)
N(1)	$-Li(3)-N(1)^{ix}$	114.20(4)
N(1)	-Li(3)-N(2)	112.18(4)
N(1)	$-Li(3)-N(2)^{i}$	119.43(4)
$N(1)^{ix}$	-Li(3)-N(2)	105.86(4)
$N(1)^{ix}$	$-Li(3)-N(2)^{i}$	116.07(4)
N(2)	$-Li(3)-N(2)^{i}$	109.21(4)

$N(1)-B-N(2)^{v}$ $N(2)-B^{iii}-N(1)^{iii}$
179.12(4)

Li(1)	$-N(1)-Li(1)^{vi}$	69.12(4)
Li(1)	$-N(1)-Li(2)^{ii}$	132.20(3)
Li(1)	$-N(1)-Li(2)^{viii}$	143.54(3)
Li(1)	-N(1)-Li(3)	109.34(3)
Li(1)	$-N(1)-Li(3)^{viii}$	70.85(3)
Li(1)	-N(1)-B	72.89(3)
$Li(1)^{vi}$	$-N(1)-Li(2)^{ii}$	144.31(4)
$Li(1)^{vi}$	$-N(1)-Li(2)^{viii}$	77.64(4)
$Li(1)^{vi}$	-N(1)-Li(3)	72.72(4)
$Li(1)^{vi}$	$-N(1)-Li(3)^{viii}$	90.59(3)
$Li(1)^{vi}$	-N(1)-B	131.50(4)
$Li(2)^{ii}$	$-N(1)-Li(2)^{viii}$	71.42(4)
$Li(2)^{ii}$	-N(1)-Li(3)	113.33(4)
$Li(2)^{ii}$	$-N(1)-Li(3)^{viii}$	75.41(4)
$Li(2)^{ii}$	-N(1)-B	84.10(4)
$Li(2)^{viii}$	-N(1)-Li(3)	73.11(4)
$Li(2)^{viii}$	$-N(1)-Li(3)^{viii}$	95.54(4)
$Li(2)^{viii}$	-N(1)-B	143.36(4)
Li(3)	$-N(1)-Li(3)^{viii}$	161.31(3)
Li(3)	-N(1)-B	93.19(3)
$Li(3)^{viii}$	-N(1)-B	104.38(3)
$Li(1)^{iii}$	$-N(2)-Li(1)^{iv}$	73.82(4)
$Li(1)^{iii}$	$-N(2)-Li(2)^{iii}$	86.86(4)
$Li(1)^{iii}$	$-N(2)-Li(2)^{viii}$	116.34(3)
$Li(1)^{iii}$	-N(2)-Li(3)	81.06(4)
$Li(1)^{iii}$	$-N(2)-Li(3)^{ii}$	75.09(4)
$Li(1)^{iii}$	-N(2)-B	155.77(4)
$Li(1)^{iv}$	$-N(2)-Li(2)^{iii}$	69.82(3)
$Li(1)^{iv}$	$-N(2)-Li(2)^{viii}$	148.82(3)
$Li(1)^{iv}$	-N(2)-Li(3)	144.56(3)
$Li(1)^{iv}$	$-N(2)-Li(3)^{ii}$	88.51(3)
$Li(1)^{iv}$	-N(2)-B	82.55(3)
$Li(2)^{iii}$	$-N(2)-Li(2)^{viii}$	136.79(2)
$Li(2)^{iii}$	-N(2)-Li(3)	84.36(4)
$Li(2)^{iii}$	$-N(2)-Li(3)^{ii}$	155.02(4)
$Li(2)^{iii}$	-N(2)-B	90.18(3)
$Li(2)^{viii}$	-N(2)-Li(3)	65.60(3)
$Li(2)^{viii}$	$-N(2)-Li(3)^{ii}$	67.83(3)
$Li(2)^{viii}$	-N(2)-B	81.73(3)
Li(3)	$-N(2)-Li(3)^{ii}$	108.92(4)
Li(3)	-N(2)-B	122.55(3)
$Li(3)^{ii}$	-N(2)-B	99.44(4)

Symmetry code

(i)	x	$\frac{1}{2}-y$	$z+\frac{1}{2}$	(vi)	x-1	$\frac{1}{2}-y$	$z-\frac{1}{2}$
(ii)	x	$\frac{1}{2}-y$	$z-\frac{1}{2}$	(vii)	1-x	1-y	1-z
(iii)	x-1	y	z	(viii)	1-x	$y+\frac{1}{2}$	$\frac{1}{2}-z$
(iv)	x+1	$\frac{1}{2}-y$	$z-\frac{1}{2}$	(ix)	1-x	$y-\frac{1}{2}$	$\frac{1}{2}-z$
(v)	x+1	y	z	(x)	1-x	$y-\frac{1}{2}$	$z+\frac{1}{2}$

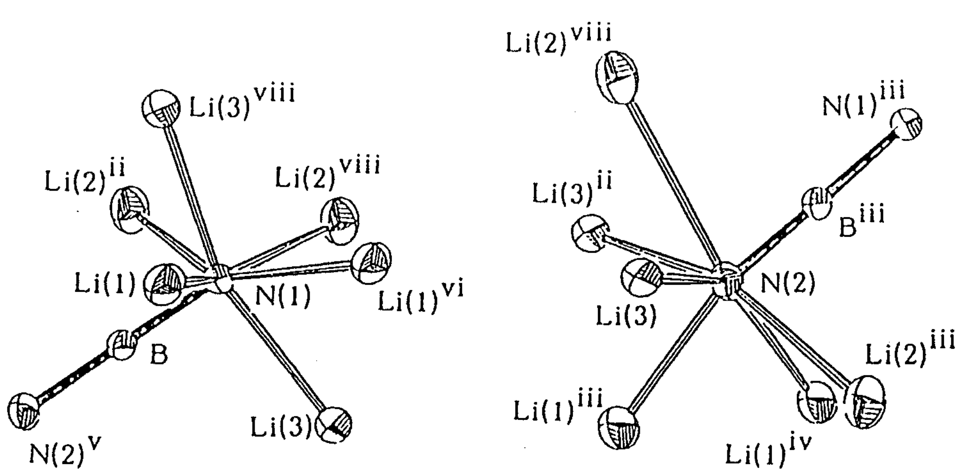

Fig. 25. Environments around N(1) and N(2) in β-Li_3BN_2.

distances between lithium and nitrogen atoms are in a wide range from 1.9 to 2.5 Å for Li(1) and Li(2) tetrahedra, while those of Li(3)-N are in a narrow range of 2.09-2.19 Å. A Li-N distance is 2.10 Å in the tetrahedral coordination of $LiSi_2N_3$ (20). Bond angles are largely deviated from the tetrahedral values. Both coordination numbers around N(1) and N(2) are seven. The nitrogen atoms are coordinated by 2Li(1), 2Li(2), 2Li(3) and B.

Lithium aluminum nitride Li_3AlN_2 has a crystal structure derived from antifluorite (15). Nitrogen atoms are in cubic closest packing and surrounded by six lithium and two aluminum atoms. Lithium and aluminum atoms are coordinated by four nitrogen atoms. DeVries and Fleicher (22) presumed that the structure of Li_3BN_2 was related to that of Li_3AlN_2. But the crystal structure of the present β-Li_3BN_2 cannot be directly related to that of Li_3AlN_2 because of the linear N(1)-B-N(2) bond.

In hexagonal and cubic boron nitrides, the lengths of B-N bonds are 1.45 and 1.57 Å (42, 52). Those of B-N single bonds are in a range of 1.58-1.64 Å in $(CH_3)_3N\text{-}BX_3$ (X = F, Cl and I) molecules (53, 54). The distance of B-N bond is 1.45 Å in triangular coordination observed in $Ce_{15}B_8N_{25}$ structure (55).

The reported lengths for B=N double bonds are 1.379 Å in $(CH_3)_2N\text{=}BCl_2$ and 1.42 Å in $(CH_3)_2N\text{=}B(CH_3)_2$ (56, 57). The B-N bond lengths in Li_3BN_2 are about 1.34 Å as shown in Table 25. The values are a little shorter than those for the above mentioned B=N double bond and comparable to 1.333 Å for

C=C double bond (58).

Figure 26 shows residual electron densities observed between nitrogen and boron atoms. We carried out difference-Fourier systhesis with coefficients $F_{obs}-F_{calc}$, where F_{calc} is a calculated structure factor with atomic parameters of Table 24. The densities are around 0.5 $eÅ^{-3}$. These values are equivalent to that of C=C double bond (59).

The outer part of the density distribution between N(1)-B is elongated toward lithium ions as depicted in Fig. 26. B and N(1) are situated at X = 0.22 and x = 0.43, respectively. N(1)-B bond transverses a lithium atoms plane of x = 0.25 parallel to (100). The elongations of bonding electron distributions between N(1) and B are due to electrostatic contributions of positive charge of lithium ions. This fact suggests that lithium atoms are present as cations in the crystal structure. The N(1)-B-N(2) unit might be regarded as $[N=B=N]^{-3}$ molecular ion as expected in another low-pressure phase of Li_3BN_2.

6-4. Crystal Structure of α-Li_3BN_2

6-4-1. Experimental

Single crystals of α-Li_3BN_2 for structural analysis were prepared from the starting mixture having molar ratio Li_3N/BN = 1.0-1.2. The mixture was heated at 1300 K for

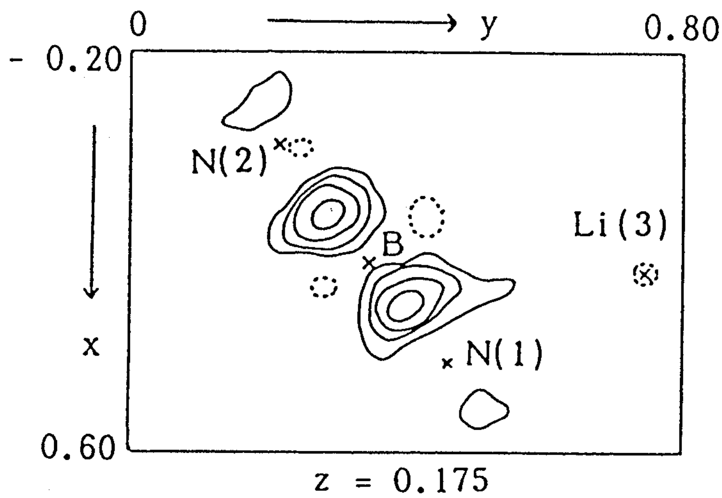

Fig. 26. Section at Z = 0.175 of the difference electron density in β-Li_3BN_2 synthesized using F_{obs}-F_{calc} as coefficients, where F_{calc} is a structure factor computed with the coordinates shown in Table 24. Contours begin at 1 e/$Å^{-3}$; intervals of 1 e/$Å^{-3}$; negative contours are shown as broken lines; zero contours are omitted.

20 min and cooled to 1000 K at a rate of about 2 K/min. A single-crystal with a size of 0.15 x 0.1 x 0.1 mm was obtained by crushing the massive product. The crystal had an irregular and angular shape with white surface . It was sealed with argon gas in glass capillary because of its unstability against moisture.

Oscillation and Weissenberg photographs taken with CuK_α radiation and intensity measurements with a four-circle diffractometer (RIGAKU AFC-5 FOS) indicated systematic absence of reflections with l = 2n + 1 for 00l and h = 2n + 1 for h00, which are consistent with space group $P4_22_12$ of tetragonal system. The cell parameters were determined by the least-squares method using 36 reflections (2Θ 20 - 28°, MoK_α, λ = 0.71069 Å) measured with a four-circle diffractometer.

MoK_α radiation monochromatized by pyrolytic graphite was used for intensity measurements. The intensities of reflections including crystallographically equivalent reflections within the range of $0<2\Theta<90^\circ$ (+h, +k, +l) were obtained at room temperature by 2Θ - Θ scan technique on a four-circle diffractometer. All the observed reflections were summarized in 317 unique reflections. Ninety-nine reflections having high standard deviations ($3\sigma_{hkl}(F_o) > F_o$) or unobservable intensities were eliminated from the least-squrares refinement procedure, where $\sigma_{hkl}(F_o)$ is a standard deviation of each reflection obtained from counting statistics. Conventional Lorentz and polarization correction was made because of the small value of μr (<0.02).

All computations in the present study were carried out using the programs referred in Section 6-3. Atomic scattering factors for Li, B and N were taken from International Tables for X-ray Crystallography, Vol. IV (46).

6-4-2. Results and Discussion

Crystallographic data are compared betweem α- and β-Li_3BN_2 in Table 23. Low-temperature phase, α-Li_3BN_2, has a higher symmetry and a little higher density than those of β-phase. A model of structure for α-Li_3BN_2 was obtained directly by placing all atoms in special positions of $P4_22_12$ space group. The initial value for parameter x in 4f site was estimated by considering the bond lengths of B-N observed in β-Li_3BN_2 shown in Section 6-4. The final full-matrix least-square refinement gave agreement factors of R = 0.042 and R_w = 0.037; representations of R and R_w were given in sub-Section 6-3-1. The final positional and thermal parameters are presented in Table 26.

A stereoscopic view of the structure is shown in Fig. 27. The structure contains $(NBN)^{3-}$ ions as expected by Goubeau and Anselment (21). Boron atoms construct an elongated body-centered lattice. Each boron atom is straightly coordinated by two nitrogen atoms. The B-N bond length is 1.339 Å as shown in Fig. 28. The value agrees well with 1.339 and 1.336 Å in β-Li_3BN_2. A maximum residual electron density of 0.4 $eÅ^{-3}$ appeared along the B-N bond like

Table 26. Refined results of atomic coordinates and thermal parameters of α-Li_3BN_2. Anisotropic temperature factors are in the form, $\exp[-(\beta_{11}h^2+\beta_{22}k^2+\beta_{33}l^2+2\beta_{12}hk+2\beta_{13}hl+2\beta_{23}kl)]$. Estimated standard errors are given in parentheses.

Atom	Position	x	y	z
Li(1)	2b	0	0	1/2
Li(2)	4d	0	1/2	1/4
B	2a	0	0	0
N	4f	0.2962(3)	0.2962(3)	1/2

β_{11}	β_{22}	β_{33}	β_{12}	β_{13}	β_{23}
0.0229(25)	0.0229(25)	0.0524(28)	-0.0155(17)	0	0
0.0183(53)	0.0092(42)	0.0118(7)	0.0032(55)	0	0
0.0070(6)	0.0070(6)	0.0080(5)	-0.0015(5)	0	0
0.0075(3)	0.0075(3)	0.0119(3)	-0.0004(3)	0.0029(19)	-0.0029(19)

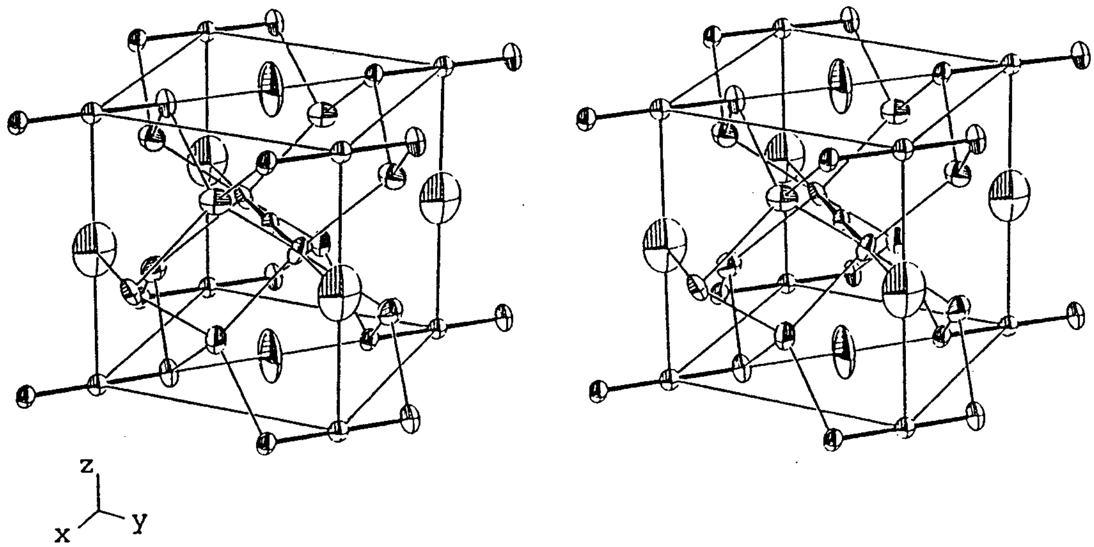

Fig. 27. Stereoscopic view of α-Li_3BN_2 structure. Probability thermal ellipsoids of 70% for all atoms are shown. The straight N-B-N bonds are represented by thicker lines which denote covalent B-N bonds.

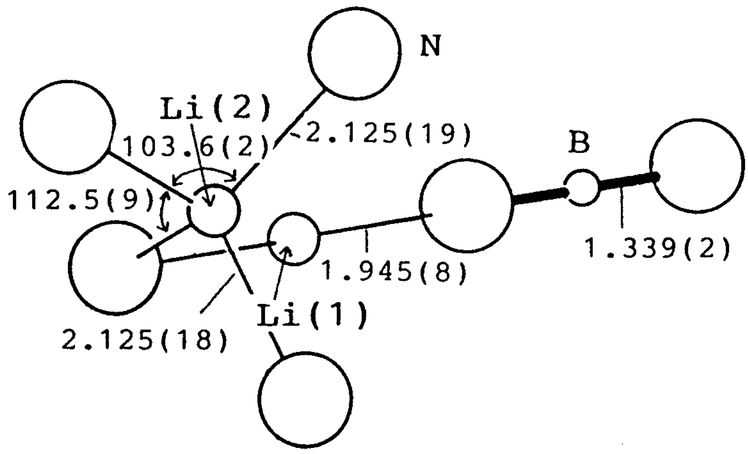

Fig. 28. Interatomic distances (Å) and angles (degrees) with estimated standard errors in parentheses.

the case of β-Li_3BN_2. It suggests the covalency of B-N bond. Figure 29 (a) illustrates the packing of $(NBN)^{3-}$ ions on the x-y plane at z = 0 and 1/2. The direction of $(NBN)^{3-}$ ions in z = 0 plane is orthogonal to that in z = 1/2.

There are two sites of lithium ion. Lithium(1) is coordinated linearly by two nitrogen atoms of two neighboring $(NBN)^{3-}$ ions in the same x-y plane as shown in Fig. 27 and 29 (a). $Li^+(2)$ is situated between the $Li^+(1)$-$(NBN)^{3-}$ layers and is tetrahedrally coordinated by 4N atoms. The tetrahedron is elongated to the direction of z-axis. Lithium nitride Li_3N has some similarities to α-Li_3BN_2 in the circumstance of lithium ions. It has 2-coordinated lithium ions between $(Li_2N)^-$ layers as shown in Fig. 30. A half of the interlayer distance of 1.94 Å in Li_3N (60), which corresponds to Li-N distance, coincides with the observed value 1.945 Å for Li(1)-N distance in α-Li_3BN_2 indicated in Fig. 28. The Li(2)-N distance of 2.125 Å is comparable with the Li-N distance of 2.13 Å within $(Li_2N)^-$ layer of Li_3N.

6-5. Relation of Crystal Structure

6-5-1. α- and β-Li_3BN_2

The crystal structure of α-Li_3BN_2 is compared with that of β-Li_3BN_2 as illustrated in Fig. 31. The plane containing

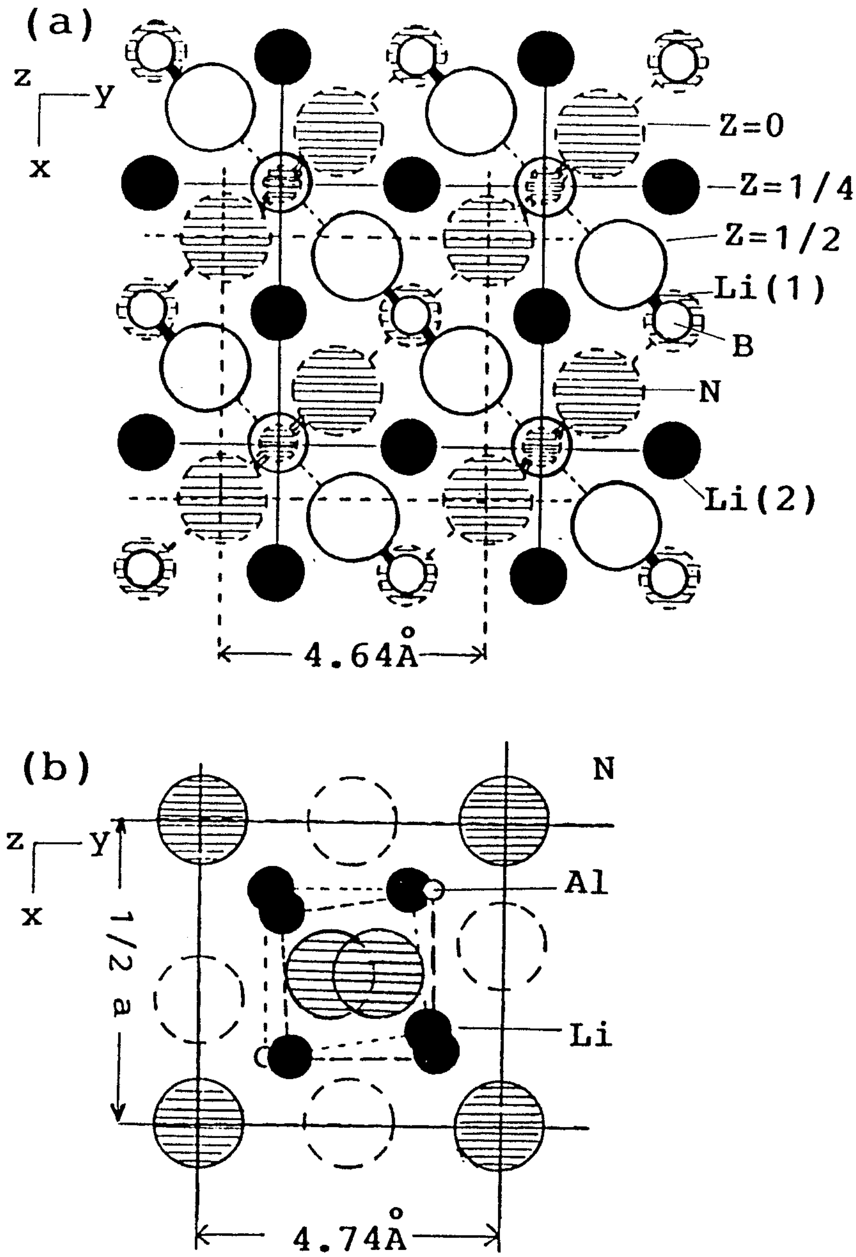

Fig. 29. Comparison of the structure: (a) projection of α-Li_3BN_2 structure along Z axis, (b) projection of antifluorite structure unit of Li_3AlN_2.

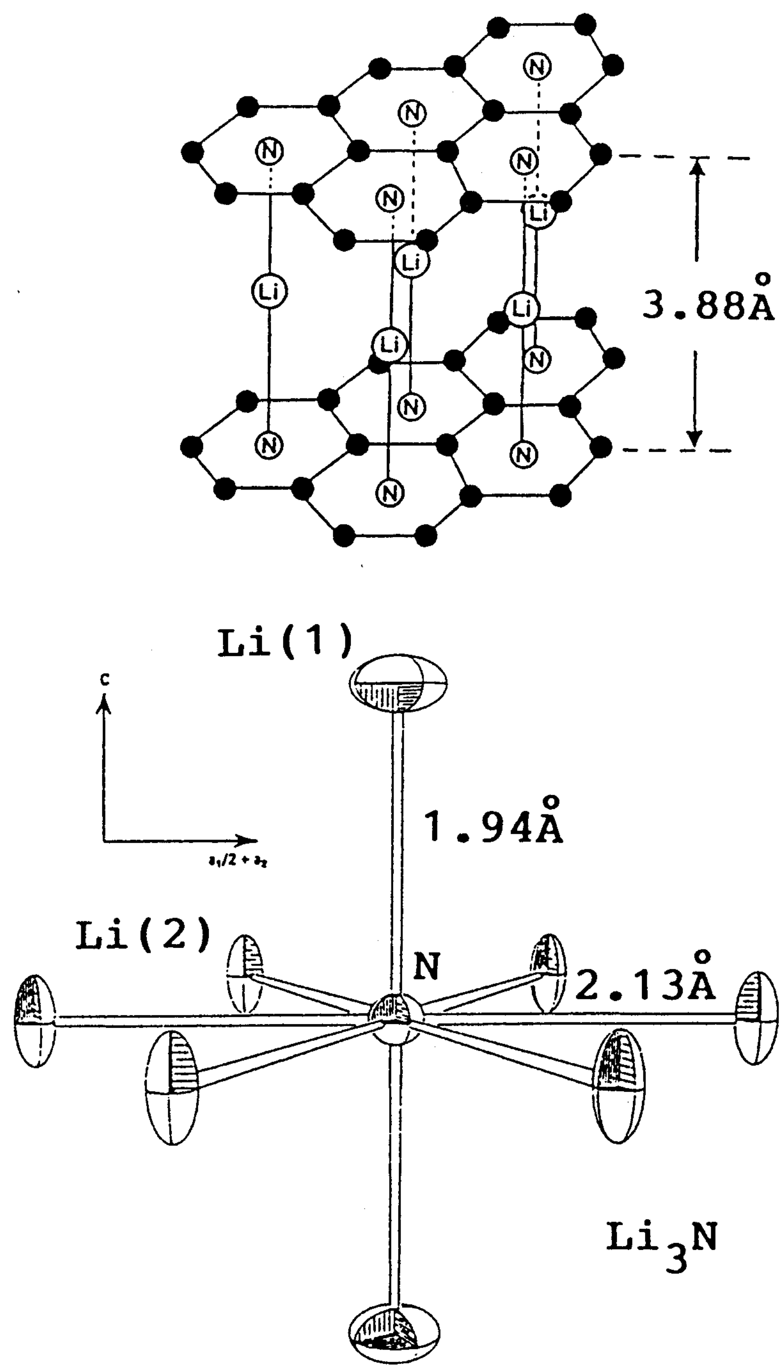

Fig. 30. Crystal structure of Li_3N.

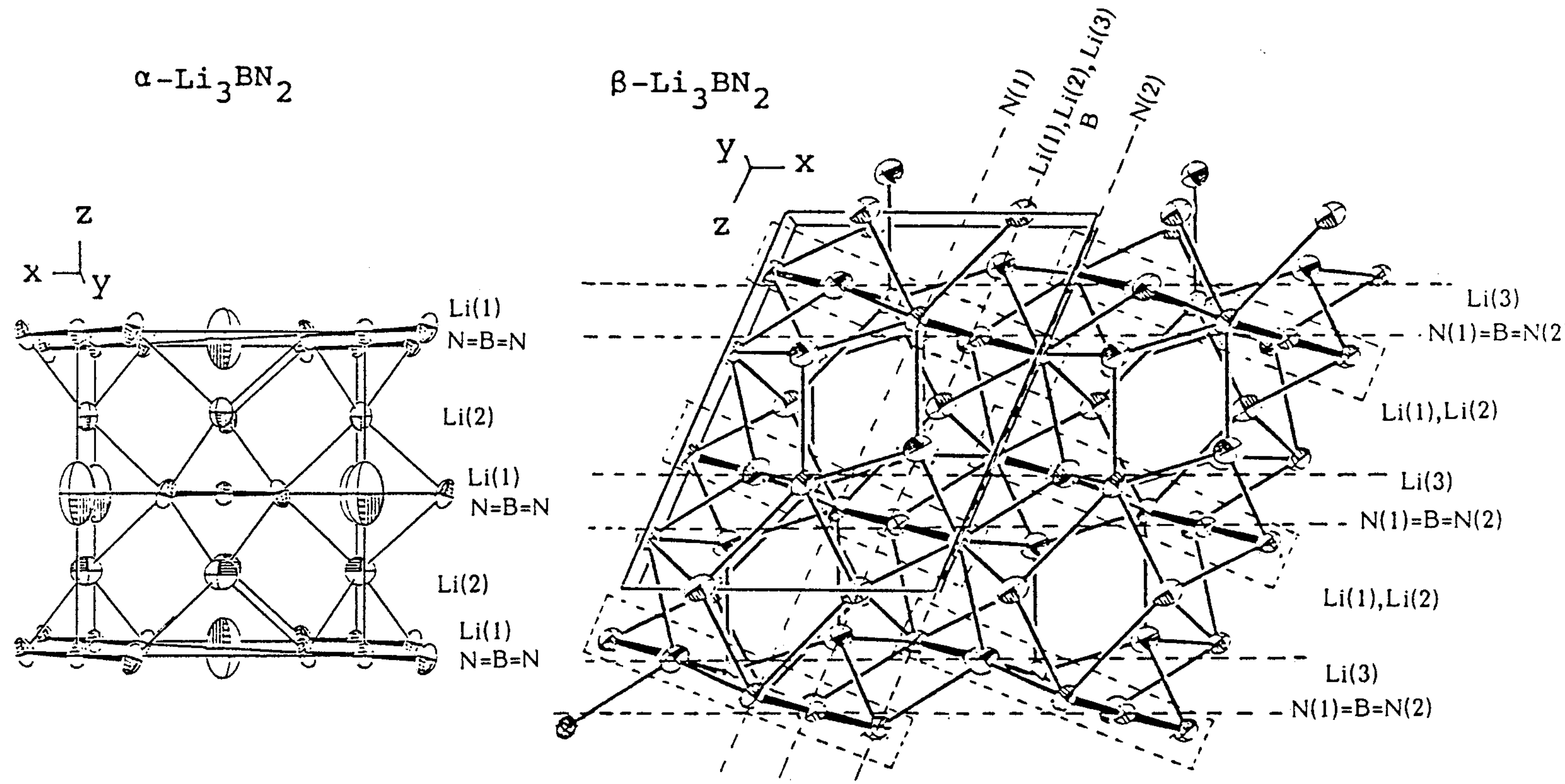

Fig. 31. Perspective views along [010] of the structure of α- and β-Li_3BN_2.

N=B=N and Li(1) of α-phase corresponds to the array of N(1)=B=N(2) and Li(3) parallel to X-Y plane of β-phase. The interlayered Li(2) of α-phase is related to Li(1) and Li(2) of β-phase. The flat layer of N=B=N in α-Li_3BN_2 is due to the presence of 2-coordinated lithium ion. The layer in the β-phase is relatively puckered. All lithium ions are tetrahedrally coordinated with nitrogen ions in β-Li_3BN_2. The tetrahedrons around Li(1) and Li(2) are fairly distorted as represented previously (sub-Section 6-3-2).

The $(NBN)^{3-}$ units are closely packed in low temperature phase, α-Li_3BN_2, as illustrated in Fig. 29 (a). The packing seems to require the 2-coordinated lithium ion to link the units. The $(NBN)^{3-}$ ions reorient at the phase transition from α to β. The rotation causes a change of coordination number around the 2-coordinated Li(1) in α-phase, which corresponds to the tetrahedrally surrounded Li(3) in β-Li_3BN_2. As far as the interlayered lithium ions are concerned, their coordinations are always tetrahedral in both α- and β-phases. But the tetrahedrons in β-phase are squashed. The $(NBN)^{3-}$ packing is looser in high temperature phase, β-Li_3BN_2, than in α-phase probably because $(NBN)^{3-}$ ions reorient for all lithium ions to take tetrahedral coordination. The low temperature phase, β-Li_3BN_2, has a little higher density than that of high temperature phase.

6-5-2. α-Li_3BN_2 and Li_3AlN_2

The structure of Li_3AlN_2 is a superstructure of distorted antifluorite. Figrue 29 (b) schematically shows 1/8 of the cubic unit cell, which is closely related to an elemental unit cell of antifluorite type. Anions basically pack in a face-centered cubic lattice. Cations are in tetrahedral sites. The tetrahedra are distorted because of the size difference between Li^+ and Al^{3+}. Nitrogen ions are at the levels of z = 0, 1/4, 1/2, 3/4 and 1 of the 1/8 cell. Nitrogen ions on the corner of elemental cell superimpose each other along z-axis in Fig 29 (b). But the positions of nitrogen, which should be located at the face center, shift to off-center.

The square enclosed by dotted line in Fig. 29 (a) represents the face-centered arrangement of nitrogen ions in α-Li_3BN_2. From the viewpoint of nitrogen packing, the α-phase can be related to Li_3AlN_2 of antifluorite structure. The Li(2) ion is tetrahedrally surrounded by N ions like the case of Li_3AlN_2. Both B and Li(1) ions are linearly coordinated by two N ions and situated on the edges of nitrogen tetrahedra. On the other hand, Al and Li ions in Li_3AlN_2 are at the centers of nitrogen tetrahedra. A half of the tetrahedral sites is vacant in α-Li_3BN_2.

6-5-3. β-Li_3BN_2 and Li_3AlN_2

Projections shown in Fig. 32 reveal the contrast of structures between β-Li_3BN_2 and Li_3AlN_2. The distance

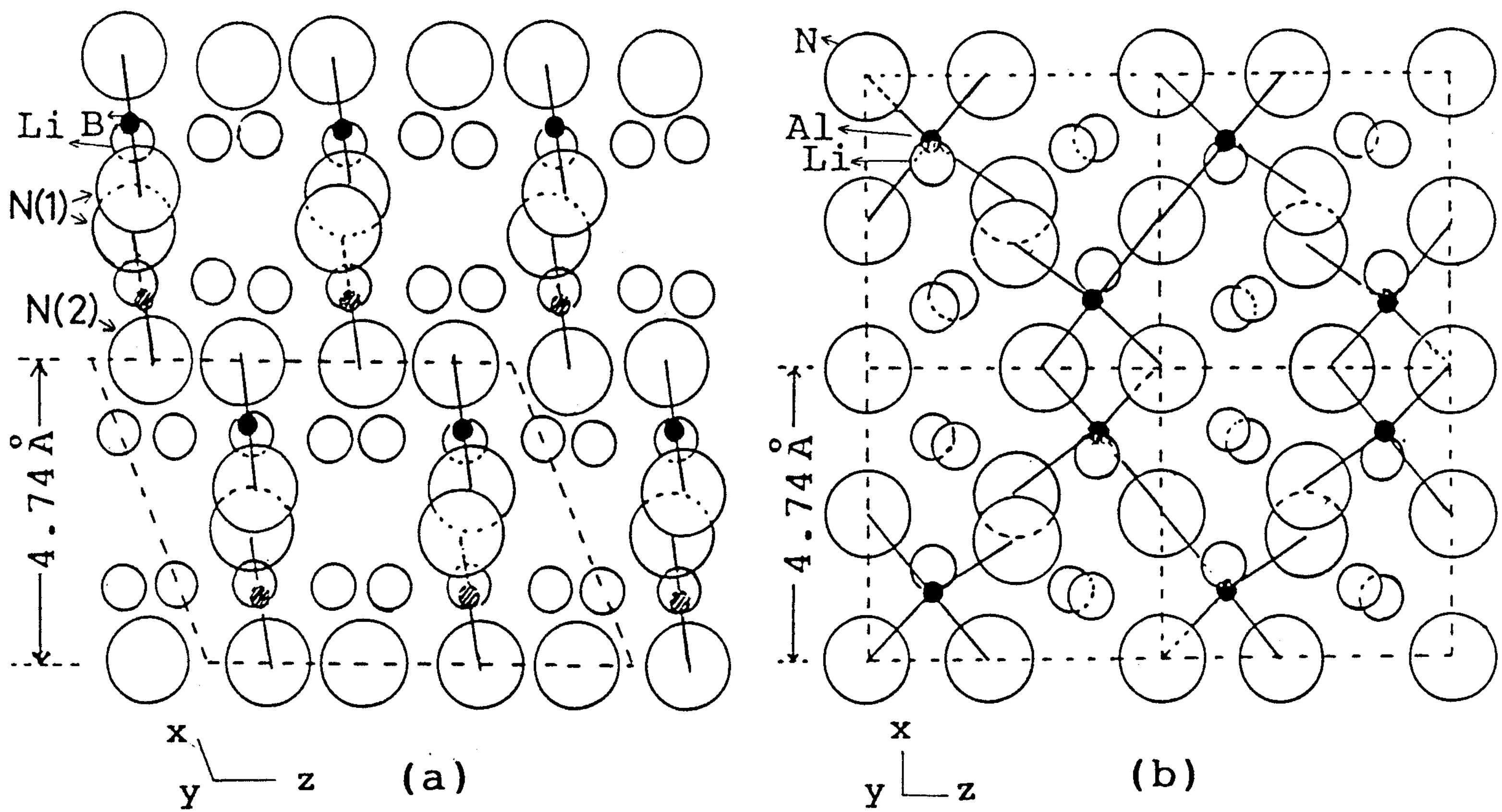

Fig. 32. Comparison of the structure: (a) projection of β-Li_3BN_2 structure along y axis, (b) projection of Li_3AlN_2 structure along y axis.

between the N(2) layers in β-Li_3BN_2 is 4.74 Å which agrees with a half of lattice constant of Li_3AlN_2 (a = 9.470 Å). Arrays of Li, B and N(2) ions in β-Li_3BN_2 correspond to those of Li, Al and N ions in Li_3AlN_2. The nitrogen ions in β-Li_3BN_2, however, cannot keep the face-centered cubic packing as revealed in Li_3AlN_2 due to the presence of linear N-B-N unit. The tetrahedra around lithium are also fairly distorted in β-Li_3BN_2. The structure of β-Li_3BN_2 is opener than that of Li_3AlN_2.

6-5-4. Li_2CN_2 and Li_3BN_2

We have considered the structures of α- and β-Li_3BN_2 comparing with the antiflurite structure of Li_3AlN_2. Li_3BN_2 can also be related to that of Li_2CN_2 which is composed of Li^+ and $(NCN)^{2-}$ ions as shown in Fig. 33 (61). Carbon atom is linearly coordinated by two nitrogen atoms. The $(NCN)^{2-}$ ion is centrosymmetric and the N-C bond length is 1.23 Å. The $(NCN)^{2-}$ ions are located at the corners and at the body-center of tetragonal lattice. Each Li^+ ion is at the center of a squashed tetrahedron of N atoms.

Ternary lithium nitrides containing the elements belonging to the third line of periodic table (Mg, Al, Si and P) crystallize in antifluorite-type crystal structure. The third line elements are tetrahedrally coordinated by nitrogen. In the case of the second line elements such as B and C, the structure is characterized by the presence of linear $(NBN)^{3-}$

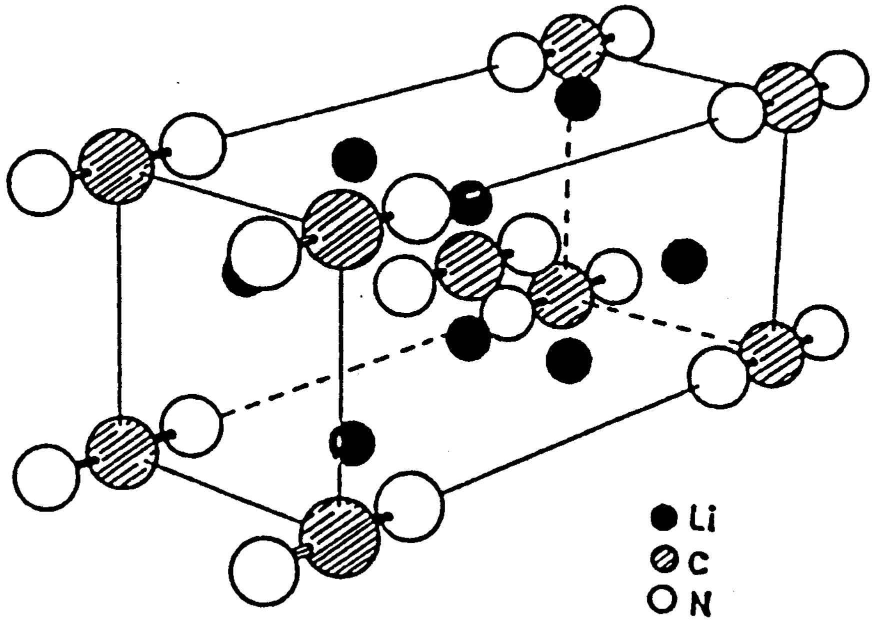

Fig. 33. Crystal structure of Li_2CN_2.

and $(NCN)^{2-}$ anion groups. High covalencies are expected for the bondings in the groups from the residual electron densities of difference-Fourier synthesis and also from the short bond lengths.

6-6. Ionic Conductivity

6-6-1. Experimental

Complex impedance of the sintered polycrystalline samples were measured in the range 5 Hz to 500kHz using vector impedance meter (HP 4800A). Carbon or Ag conductive paste were used as electrodes. Specimens were placed under vacuum or Ar atmosphere.

6-6-2. Results and Discussion

Figure 34 illustrates examples of complex impedance diagrams for polycrystalline sintered samples of α- and β-Li_3BN_2. Conductivity was estimated from the values of intersections of extraporated semicircle and real axis. They were plotted in Fig. 35. The conductivity of low temperature phase, α-Li_3BN_2, was a little lower than that of high temperature one, β-Li_3BN_2, at 400 K. Electronic conductivity was measured by d.c. method using carbon as ion blocking electrodes. The contributions were less than

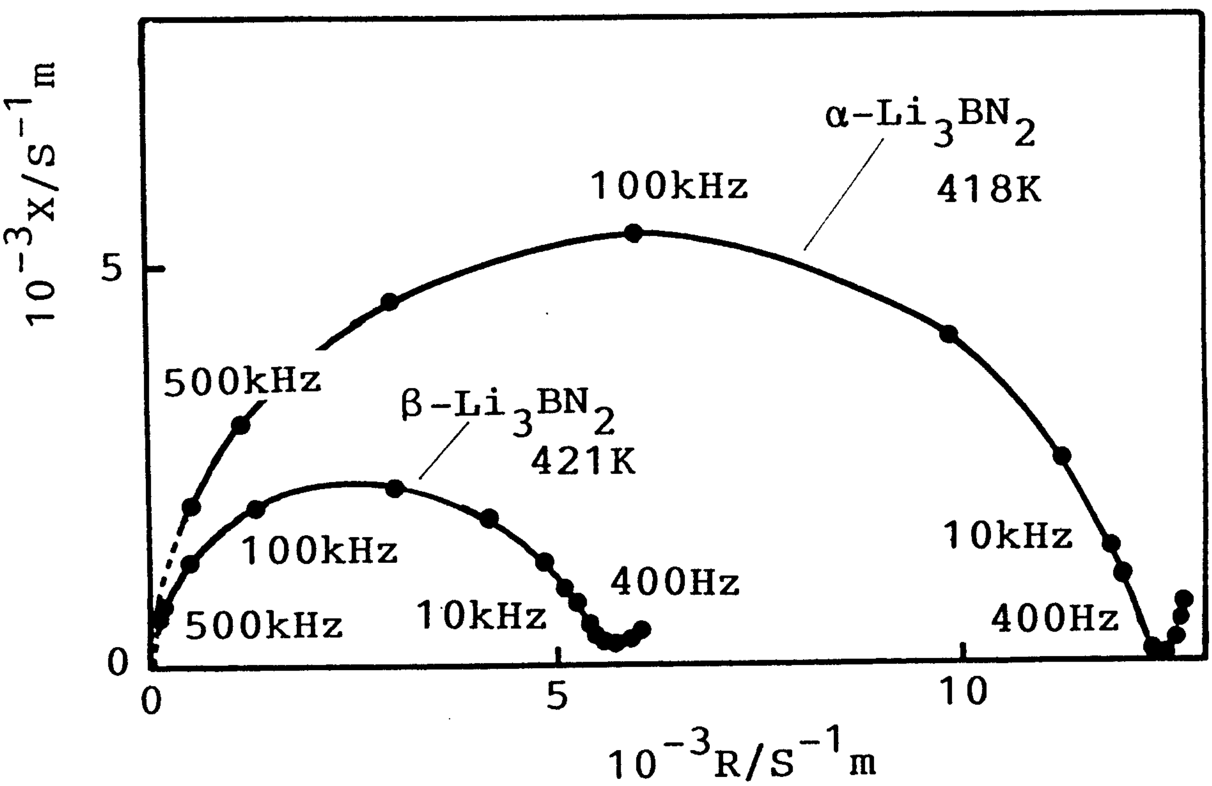

Fig. 34. Complex impedance plots for the polycrystalline α-Li_3BN_2 at 418 K and β-Li_3BN_2 at 421 K.

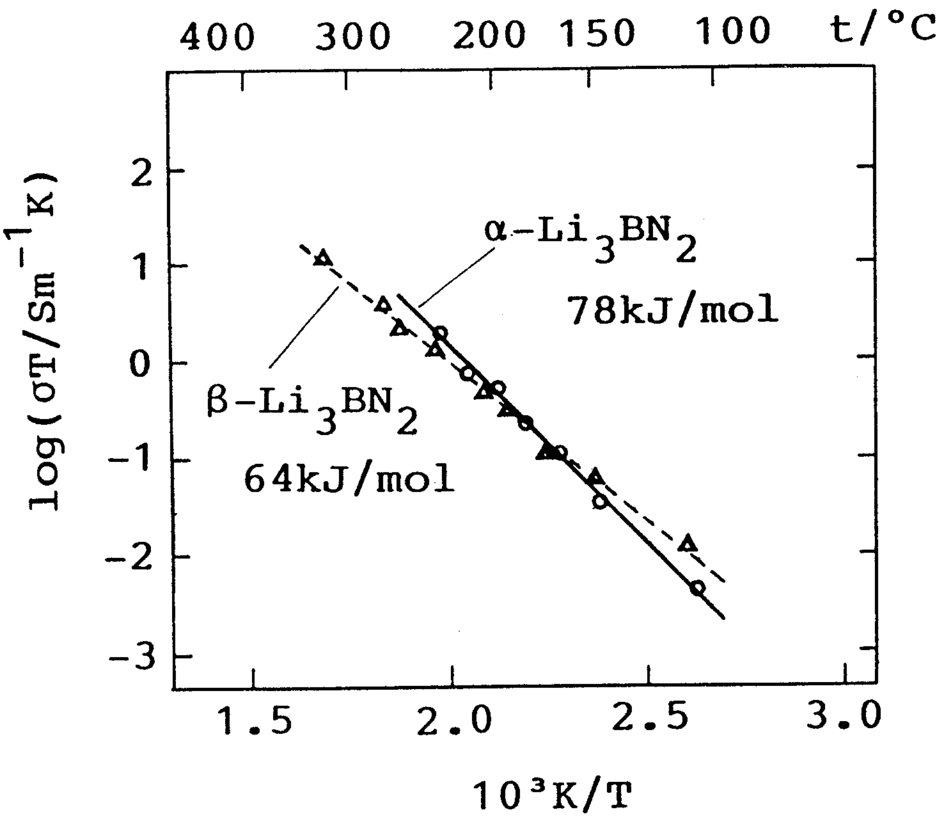

Fig. 35. Semilogarithmic plot of the conductivity σ times the absolute temperature T against the inverse absolute temperature.

1% of total conductivity around 500 K for both samples.

The activation energy of β-Li_3BN_2 (64 kJ/mol) was smaller than that of α-Li_3BN_2 (78 kJ/mol). The difference in activation energy should be discussed in relation to the crystal structure, especially the coordination number, the configuration around lithium ions, the size of bottleneck for ionic conduction and so on. α-Li_3BN_2 has 1/3 of Li in two-coordination site and 2/3 of Li in tetrahedral site. β-Li_3BN_2 has all lithium ions in tetrahedral site. We have no information about the diffusion or migration paths of lithium ions in the crystal structure. Thus it is quite difficult to estimate the size of bottleneck for the ionic conduction.

Anisotropies of ionic conduction should be expected from consideration of the crystal structures. It might contribute to the elongation of the semicircle along real axis as shown in Fig. 34, while we could not obtain single crystals with an adequate size for conductivity measurements.

Chapter 7

General Discussion

7-1. Structural Chemistry

Table 27 summarizes materials synthesized in the present study. Compounds which crystallized in the cubic system are LiMgN, Li_3AlN_2, Li_5SiN_3 and Li_7PN_4. LiMgN and Li_5SiN_3 have the antifluorite structure in which lithium and other metalloids are distributed disorderly in tetrahedra of nitrogen cubic close-packing. Lithium and aluminum or phosphorus are arranged orderly in the tetrahedral sites of Li_3AlN_2 or Li_7PN_4 having antifluorite superstructures.

Lattice constants of elemental cell for these materials are plotted against ionic radii of metalloids presented by Shannon and Prewitt (33) in Fig. 36. The lattice constants for the superstructure compounds are reduced to that of elemental cell having antifluorite structure, which contains four nitrogen ions. The cell dimension slightly decreases with decrease of the ionic radius from Al^{3+} to P^{5+}. Lithium content is different between these compounds. Compounds, (LiAlN), (LiSiN) and (LiPN) are supposed in order to compare the influence of each metalloid at the same lithium content with LiMgN. These compounds cannot exist actually, since they do not keep electroneutralities. Lattice constants for the imaginary compounds (LiMN), where M = Al, Si and P, were estimated under the following assumption: (i) the imaginary compounds of (Li_2N) has the same lattice constant as LiMgN, since lithium and magnesium ions have the ionic radii of almost the same size (0.71-0.73 Å), (ii) the changes of lattice constants obey Vegard's Law on the substitution of

Table 27. Products prepared in the present study.

IIa	IIIb	VIb	Vb
LiMgN	α-Li_3BN_2 β-Li_3BN_2 Li_3AlN_2	$LiSi_2N_3$ Li_2SiN_3 Li_5SiN_3 $Li_{18}Si_3N_{10}$ $Li_{21}Si_3N_{11}$ Li_8SiN_4	Li_7PN_4

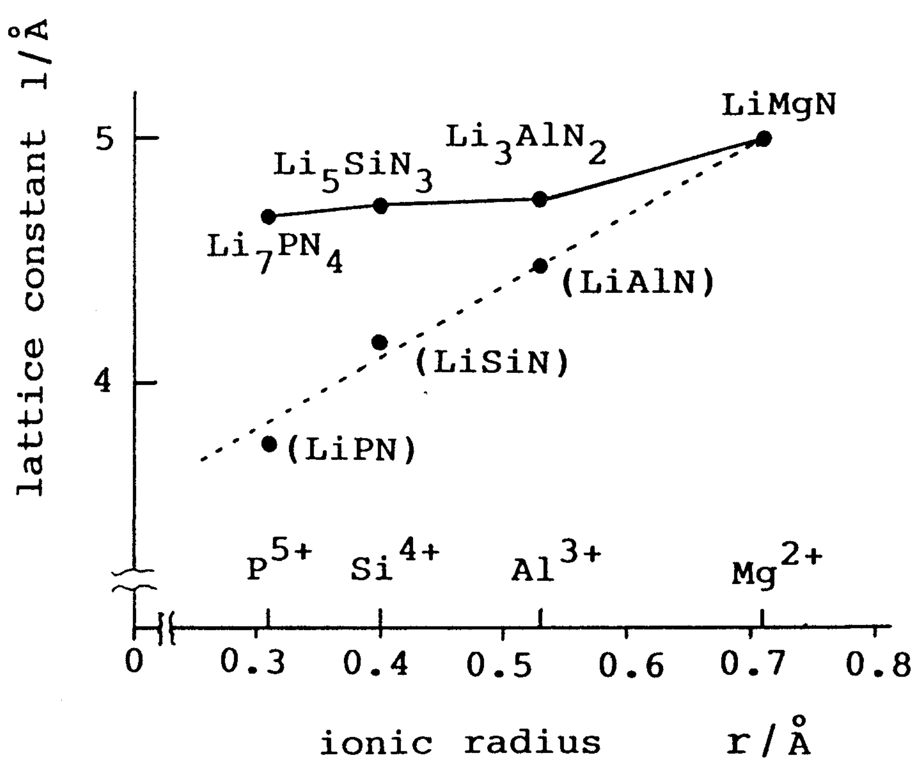

Fig. 36. Lattice constants of elemental cell versus ionic radii. The value of imaginary compounds (LiAlN), (LiSiN) and (LiPN) are obtained from Fig. 35.

lithium to other metalloids as shown in Fig. 37. The values of these lattice constants almost linearly increase with the ionic radii as indicated by a broken line in Fig. 36. These linear plots suggest that the metalloids are present mostly as ionic in the double metal nitrides. If a covalency of some compound was higher than others, the hypothetical lattice constants would not increase liearly.

Crystal structures and crystal systems could not be determined for Li-Mg-N presented in Chapter 4 and for X-phase in Li-P-N system. These structure would be related to anti-fluorite-type as described in Chapters 4 and 5. Lithium silicon nitrides, $Li_{18}Si_3N_{10}$, $Li_{21}Si_3N_{11}$ and Li_8SiN_4 probably crystallize in structures related to that of Li_5SiN_3 considering the similarity of main peak position at high Bragg angle and the relation of cell dimensions as presented in Chapter 3. All of the above mentioned structure may have the antifluorite structural unit.

$LiSi_2N_3$ has a wurzite-type structure, in which nitrogen is in hexagonal close-packing. Crystal structure of Li_2SiN_2 is still unknown. It might be related to the anti-La_2O_3 or anti-Ce_2O_2S structures. Li_2ZrN_2 has an anti-Ce_2O_2S-type structure, in which nitrogen ions are hexagonally close-packed (38).

Elements belonging to the third row of periodic table such as Mg, Al, Si and P are in nitrogen tetrahedra of cubic or hexagonal close-packing with lithium in the case of double metal nitrides. Bondings between metalloids and nitrogen probably have mostly ionic characters as discussed above. In the case of boron

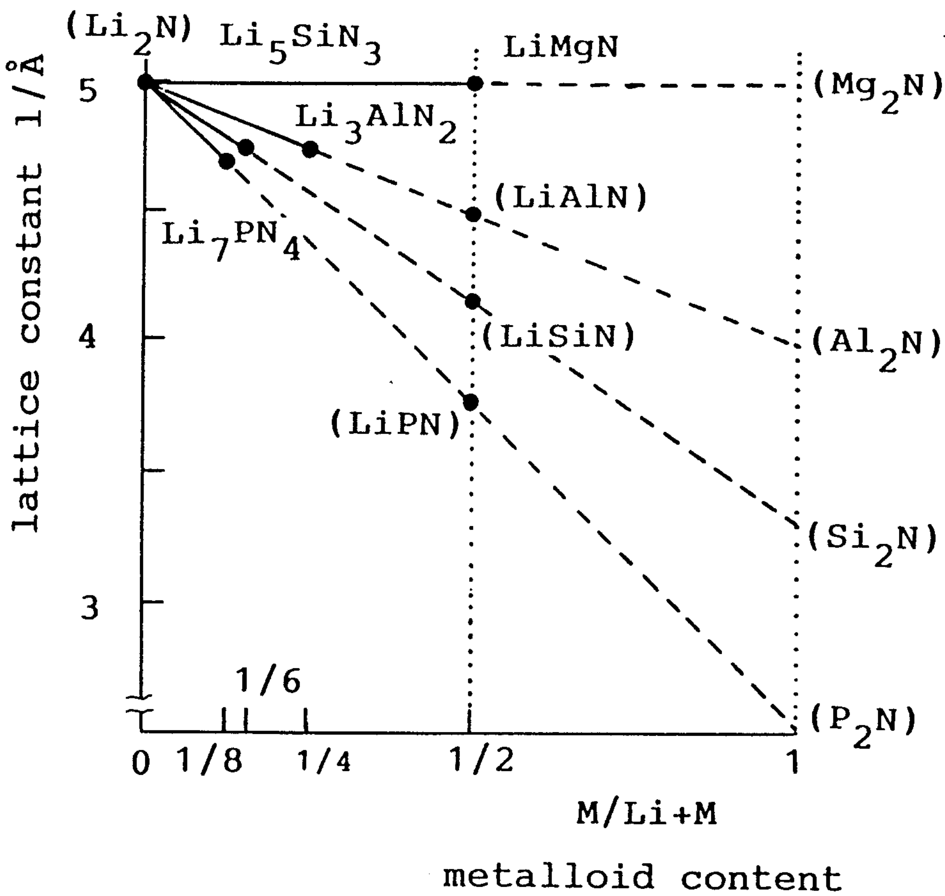

Fig. 37. Lattice constants of imaginary compounds; (LiAlN), (LiSiN) and (LiPN).

and carbon, they are linearly coordinated by two nitrogen atoms. The bondings are so covalent that residual electron densities were observed between nitrogen and boron or carbon atoms. The B-N bond length in α- and β-Li_3BN_2 is 1.34 Å which is the shortest in values observed previously in other crystals.

The structure of α-Li_3BN_2 (low temperature phase) could be also related to the antifluorite structure of Li_3AlN_2 as revealed in Chapter 6, while it contained molecular anion group of $(NBN)^{3-}$. One-third of lithium ions in α-Li_3BN_2 are also linearly coordinated by two nitrogen ions. Another example of two-fold coordination is known only in the Li_3N structure. α-Li_3BN_2 and Li_3N have the same distance of 1.94 Å between nitrogen and lithium. In the case of β-Li_3BN_2 (high temperature phase), all lithium ions are situated in distorted tetrahedra of nitogen ions. The β-phase also has the linear $(NBN)^{3-}$ ions as shown in the case of α-Li_3BN_2. They rotate at the transition between the low and high temperature phases. Pressure induced phase transition had been reported for Li_3BN_2 by DeVries and Fleisher (22). The present study is the first report of thermal induced phase transition for Li_3BN_2 and also for any other kinds of double metal nitrides containing lithium. X-ray diffraction pattern of the high pressure phase did not agree with those of α- and β-Li_3BN_2.

Single crystal growth required for a further structural discussion. Most of the nitrides containing lithium decompose at high temperature. Li_3AlN_2, for example, decomposed to AlN, lithium and nitrogen above 1600 K without melting. $Li_5Si_2N_3$ also changed to Li_2SiN_2 and finally to $LiSi_2N_3$ above 1400 K. Thus it is difficult to grow their single crystal. Li_3BN_2 had a melting point at 1189 K. Crystal structures of α- and β-Li_3BN_2 were determined using their single crystals. Application of high pressure technique will be usefull to suppress the decomposition and to grow single crystals.

7-2. Electrical Properties

Most of the products in the present study were almost pure lithium ionic conductors expect LiMgN and Li_7PN_4. Electronic contribution might be due to an impurity in the case of Li_7PN_2. Figure 38 shows temperature dependences of ionic conductivity in a series of double metal nitrides. Li_8SiN_4 has the highest conductivity in the measured temperature range. Its conductivity was higher by one order of magnitude than that of $Li_9N_2Cl_3$ (12), which had possessed the highest conductivity among lithium ionic conductors having the antifluorite structure (see Chapter 1). The ionic conduction of Li_8SiN_4 had the comparable values in conductivity and in activation energy with those of Li_3N single crystal along c-axis. Judging from the lattice parameters of lithium silicon nitrides, Li_8SiN_4 may have a relatively open crystal structure among them as described in Chapter 3. A number of

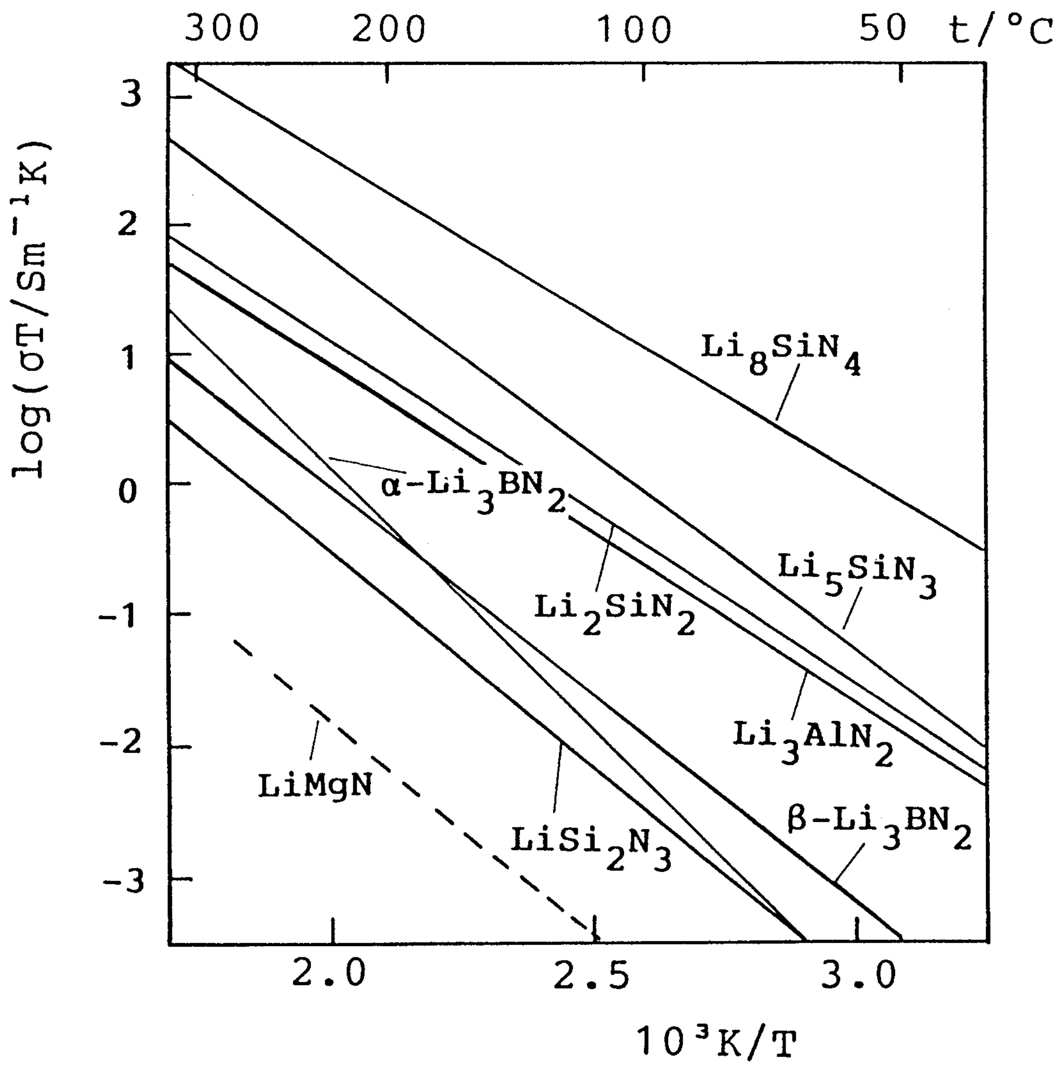

Fig. 38. Ionic conductivity in a series of double metal nitrides containing lithium.

lithium ion in Li_8SiN_4 exceeds that of tetrahecral site in the cubic-close packing of nitrogen ions. The excess number of lithium ions is at least in the octahedral site of the packing. The occupation of lithium ions in the octahedral site may contribute to the high ionic conduction, since lithium ions in the antifluorite structure migrate to the neighbor lithium site through the octahedral site. The same situation is supposed to be in the case of Li_2SiN_2 which might have some lithium ions in the octahedral site of nitrogen hexagonal -close packing as considered in Chapter 3. Li_2SiN_2 has relatively high ionic conductivity, while it has a small number of lithium ions in comparision with Li_3AlN_2 in the cation sites of structure. Li_3AlN_2 and Li_5SiN_3 have the antifluorite or its superstructure. Their ionic conductivities σ were around 10^{-3}-10^{-4} Sm^{-1} at 400 K and their activation energies were around 50-60 kJ/mol.

Both α- and β-Li_3BN_2 had lower conductivities by two order of magnitude than Li_3AlN_2. The activation energy is larger than that of Li_3AlN_2 having an antifluorite derivative structure in which lithium ions are situated in the tatrahedral site of nitrogen cubic close-packing. They migrate through the openning of anion packing. The unit cell volume of Li_3AlN_2 is 849.3 $Å^3$ and the number of formula weight Z equals 16 (15). The volume for one formula weight is 53.08 $Å^3$. α- and β-Li_3BN_2 have the volumes of 56.70 and 57.02 $Å^3$, respectively. The lithium boron nitrides have larger unit volumes than Li_3AlN_2, while boron is smaller than aluminum in ionic radius. In the open structure of Li_3BN_2, linear $(NBN)^{3-}$ molecular ions are linked together by lithium ions. Partial distortion or reorientation of the linear $(NBN)^{3-}$ unit is required for the lithium ion migration in Li_3BN_2. The rotations of $(NBN)^{3-}$ units require a larger activation energy than the simple sway of nitrogen in the antifluorite-type lattice. This might be a reason for the lower conductivity of Li_3BN_2 in comparison with that of Li_3AlN_2.

The conductivity of LiMgN was the lowest among compounds prepared in the present study. Less than 80% of conduction was caused by electron or hole migrations. A significant electronic contribution to the conductivity was also reported in the case of Li_5AlO_4(10, 11). The conductivities of LiMgN and Li_5AlO_4 are in the same order at 500 K. The extremely low ionic conduction of LiMgN is probably caused by obstruction with equivalent number of Mg^{2+} ions to Li^+ ions. These two kinds of cations randomly occupy the cation sites. The radii of magnesium and lithium ions are almost the same: $r(Mg^{2+}) = 0.71$ and $r(Li^+) = 0.73$ Å after Shannon and Prewitt (33). Magnesium ion is however divalint and considered to be strongly bound to nitrogen ions.

The structure of Li_5SiN_3 is another example, in which lithium and silicon ions are statistically distributed to the tetrahedral sites of cubic close-packed nitrogen. In this case, 5/6 of the cation site is occupied by lithium ions. Most of its conduction was caused by lithium ion migration. The conductivity of Li_5SiN_3 is higher at least by three order of magnitude than that of LiMgN. Local structure around lithium is probably fairly distorted due to the difference of ionic radii: $r(Si^{4+}) = 0.4$ and $r(Li^{+}) = 0.73$ Å. This local distortion might form opener conduction path of lithium ion migration and enhance the ionic conduction in addition to the effect of larger number of lithium ions as carriers.

In the above considerations, the ionic conductivity was discussed in relation to crystal structure. An interface resistance between a sample and electrode materials was studied on the conductivity measurement of Li_3AlN_2 and there was no significant difference between carbon and Ag conductive paste electrodes. Lithium ions move from a grain to another grain in a polycrystalline body. Ionic conductivity is affected also by an interface between the grains. Measurement on a single crystal will resolve the contribution of grain boundary to ionic conduction. Consequently, crystal growth is also important for further discussions of ionic conductivity as well as crystal structure.

The following pages present priliminary results of the decomposition voltage study. It is necessary to know the the value of decomposition voltage for each ionic conductor when the ionic conductor is utilized stably as a solid electrolyte in batteries and other electric devices. In spite of this importance, there are only a few examples for the measurements of decomposition voltages. The decomposition voltage of Li_3N was calculated from thermochemical data, while there is no report about the measurement. Hartwig et al. determined the decomposition voltage of $Li_9N_2Cl_3$ with the galvanic cell arrangement which is similar to a Hebb-Wagner polarization cell (26). We also tried to measure the voltage of the compounds prepared in the present study. But the decomposition voltage could not be determined by the method of Hartig et al. We attempted to evaluate the decomposition voltage for Li_3N, Li_3AlN_2 and Li_8SiN_4 by two methods described in the following paragraphs.

Figures 39 and 40 indicate schematic change of current against applied voltage for Li_3N, Li_3AlN_2 and Li_8SiN_4 at 375-385 K. Specimens of these materials were polycrystalline; Li_3AlN_2 and Li_8SiN_4 were sinterd bodies, and Li_3N was a pellet of compressed powder. As shown in Fig. 39, about 2.5-2.6 V was applied to cancel the open circuit voltage generated on a cell:

(−) Li | sample (solid electrolyte) | C (+) .

The currents of this cell were smaller by two to three order of magnitudes than those expected from the total conductivity. The conduction was probably caused by electron or hole migrations and polarizations. Abrupt increases of the currents were observed for Li_3N and Li_8SiN_4 above 2.9 - 3.0 V. Thus the applied voltage on the solid electrolyte was estimated as 0.4-0.5 V. They were caused by the conductions of lithium ions and electrons supplied after the decomposition of Li_3N and Li_8SiN_4. The rate of increasing applied voltage (2 mV/min-2 mV/hr) also gave an influence to the magnitude and amplitude of the changes. Further increasing the voltage,

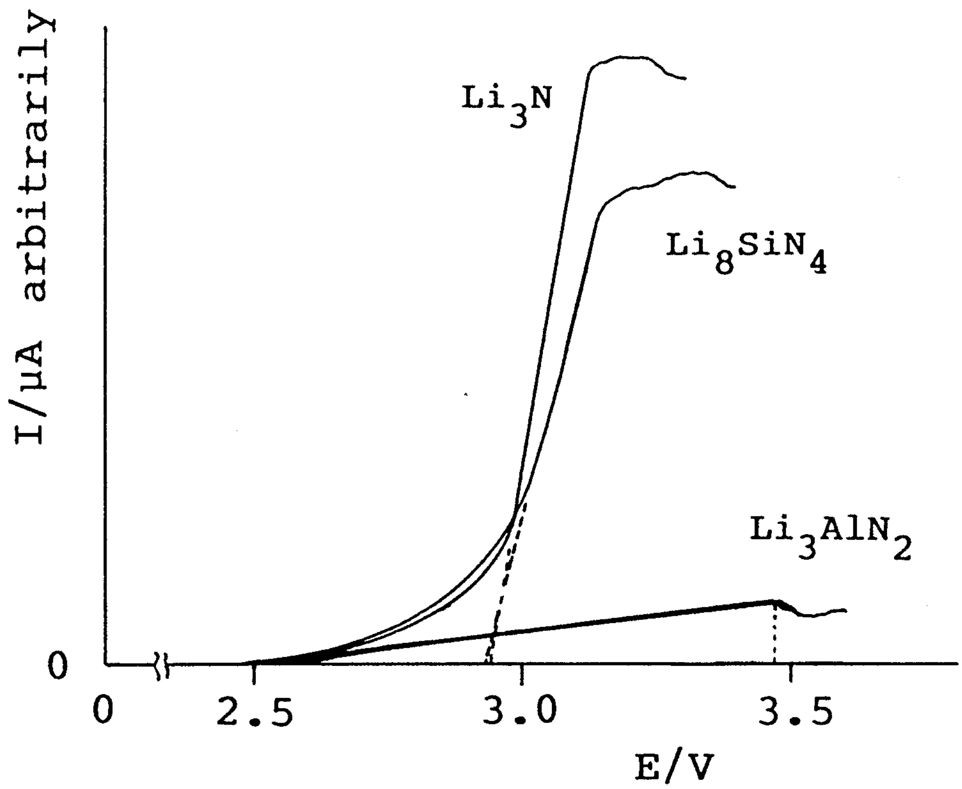

Fig. 39. Current against applied voltage on (-)Li | solid elecrolyte | C(+) cell at 375-385 K.

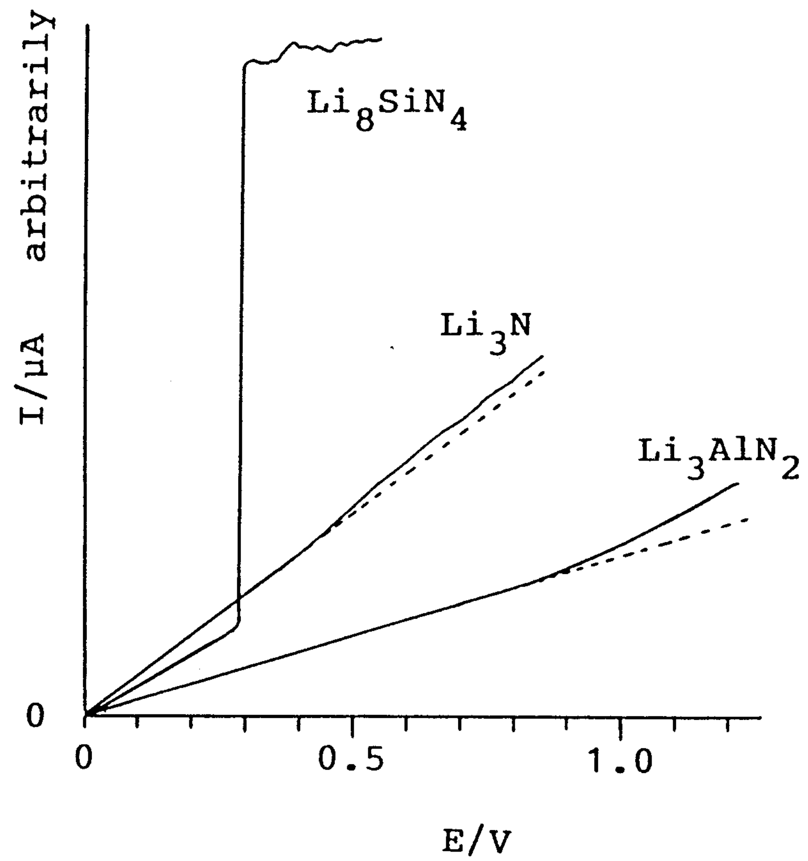

Fig. 40. Current against applied voltage on (-)Li | solid electrolyte | Li(+) cell at 375-385 K.

the conductivity decreased probably due to the production of N_2 gas formed by decomposition of the electrolytes.

In the case of Li_3AlN_2, an abrupt increase of current was not observed as shown in Fig. 37. The linear relation of current against applied voltage continued to 3.45 V and then the conductivity decreased. This phenomenon is probably explained by the formation of decomposition products such as AlN.

Figure 40 shows the results of another experiment using the cell:

$$(-)\ \mathrm{Li} \left| \begin{array}{c} \text{Sample} \\ \text{(solid electrolyte)} \end{array} \right| \mathrm{Li}\ (+) \quad ,$$

in which lithium ion migrations carry the charge. The Ohm's law was observed for each sample at the low applied voltage region. Deviations from the law were observed above 0.4 V for Li_3N and above 0.85 V for Li_3AlN_2 at 380 K. In the case of Li_8SiN_4, a current increased abruptly by one order of magnitude above 0.25-0.4 V.

From these dynamic measurements, the decomposition voltages of Li_3N, Li_3AlN_2 and Li_8SiN_4 were estimated to be about 0.4, 0.85 and 0.25-0.5 V, respectively.

The decomposition votage, $E_{dec.}$, of lithium solid electrolyte is theoretically calculated by the equation:

$$E_{dec.} = \frac{\Delta G_{dec.}}{nF} \quad ,$$

where n is a number of lithium ion released in the reaction, F the Farady constant and $\Delta G_{dec.}$ the free energy change of lithium release reaction.

In the case of Li_3N, the free energy change is equal to the formation free energy of Li_3N, which was presented by Yanco at al. (23);

$$Li_3N \xrightarrow{-\Delta Gf} 3\ Li + 1/2\ N_2$$

$$\Delta G_f\ (kJ/mol) = 0.139T - 163.7 \quad .$$

The decomposition voltage E_{dec} = 0.38 V at 380 K. This value corresponds to that observed in the present study.

There are no thermodynamic data for Li_3AlN_2 and Li_8SiN_4. The decomposition voltage for Li_3AlN_2 was 0.85 V which was larger than 0.4 V for Li_3N. The enhancement was explained in Chapter 2, assuming the decomposition reaction :

$$Li_3AlN_2 \longrightarrow 3\ Li + 1/2\ N_2 + AlN \quad .$$

Li_8SiN_4 may not decompose directly to lithium, nitrogen and silicon nitride;

$$Li_8SiN_4 \longrightarrow 8\ Li + 4/3\ N_2 + Si_3N_4 \quad .$$

The decomposition presumably takes place stepwise through the following reactions;

$$Li_8SiN_4 \longrightarrow 3\ Li + 1/2\ N_2 + 1/3\ Li_{21}Si_3N_{11}$$

$$Li_{21}Si_3N_{11} \longrightarrow 3\ Li + 1/2\ N_2 + Li_{18}Si_3N_{10}$$

$$Li_{18}Si_3N_{10} \longrightarrow 3\ Li + 1/2\ N_2 + 3\ Li_5SiN_3$$

$$Li_5SiN_3 \longrightarrow 3\ Li + 1/2\ N_2 + Li_2SiN_2$$

$$Li_2SiN_2 \longrightarrow 3\ Li + 1/2\ N_2 + 1/3\ LiSi_2N_3$$

$$LiSi_2N_3 \longrightarrow Li + 1/6\ N_2 + 2/3\ Si_3N_4 \quad .$$

The free energy change is probably small at the first reaction because of the low decomposition voltage of Li_8SiN_4. No decomposition product was however detected by X-ray powder diffraction method for Li_8SiN_4 and Li_3AlN_2 after the experiments.

Summary

Summary

(1) Single phase of Li_3AlN_2 was prepared from the mixtures of Li_3N/AlN = 1.2 to 1.5 in molar ratio at 875 and 1175 K. It crystallizes in the cubic system derived from antifluorite-type structure having a lattice parameter a = 9.470(1) Å. Li_3AlN_2 is a pure ionic conductor having conductivity of 5×10^{-6} Sm^{-1} at room temperature and an activation energy of 52 kJ/mol. Its decomposition voltage was 0.85 V at 377 K. The $Li|Li_3AlN_2|TiS_2$ cell could be discharged at a constant current of 45 $\mu A/cm^2$ at 377 K.

(2) Six phases were obtained by the reaction of Li_3N and Si_3N_4.

Phase I, $LiSi_2N_3$, was prepared from the mixture of Li_3N/Si_3N_4 = 1.6 in molar ratio at 1475 K for 1 hr. It crystallizes in the orthorhombic system derived from wurtzite-type structre having lattice parameter a = 9.198(3), b = 5.307(2) and c = 4.779(2) Å.

Phases II to VI were obtained by heating the mixtures having the same composition as the products or containing a slightly excess amount of Li_3N at 1075 K for 10-20 min.

Phase II, Li_2SiN_2, had the same X-ray powder diffraction pattern with that reported by Lang and Charlot (18). The crystal system could not be determined.

Phase III, Li_5SiN_3 crystallizes in the cubic system having a lattice paramter of a = 4.7240(3) Å. Lithium and silicon may statistically occupy the tetrahedral sites of antifluorite structure.

Phases IV, V and VI crystallize in the tetragonal system,

Phase IV, $Li_{18}Si_3N_{10}$; a = 14.168(4), c = 14.353(8) Å

Phase V, $Li_{21}Si_3N_{11}$; a = 9.470(3), c = 9.530(8) Å

Phase VI Li_8SiN_4; a = 10.217(2), c = 9.536(3) Å .

Their crystal structures could not be determined using their X-ray powder diffraction data. The compounds may have antifluorite-type derivative structure, since their unit cells dimensions could be related to that of Li_5SiN_3 antifluorite structure.

Phases I to VI are pure lithium ionic conductors. Conductivities at 400 K and activation energies were $1.9x10^{-5}$ and 64 for $LiSi_2N_3$, $1.1x10^{-3}$ and 53 for Li_2SiN_2, $4.7x10^{-3}$ and 57 for Li_5SiN_3, $2.9x10^{-3}$ and 55 for $Li_{18}Si_3N_{10}$, $8.6x10^{-4}$ and 54 for $Li_{21}Si_3N_{11}$ and $5.0x10^{-2}$ Sm^{-1} and 46 kJ/mol for Li_8SiN_4.

(3) Single phase of LiMgN was prepared by the reaction between Li_3N and Mg_3N_2 in a nitrogen flow above 875 K. An electric contribution to conductivity was relatively high because of its low ionic conduction.

(4) Li_7PN_4 was prepared by the reaction of Li_3N, red phosphorus and nitrogen at 875 K with some amount of unidentified phase. The mixture showed an electric conduction.

(5) Low (α) and high (β) temperature phases of Li_3BN_2 were prepared from the mixture of Li_3N/BN = 1.1 - 1.0 in molar ratio at 1070 and at 1170 K, respectively. The β-phase is a new polymorph of lithium boron nitride. The phase transition temperature is about 1135 K. The melting

point of β-Li_3BN_2 is arround 1189 K. α-Li_3BN_2 crystallizes directly from the undercooled liquid at 1160 K. The structure of α-Li_3BN_2 has tetragonal symmetry, $P4_22_12$, a = b = 4.6435(2), c = 5.2592(5) Å, Z = 2, $D_{calc.}$ = 1.747 Mgm^{-3}. The structure was determined by 208 unique X-ray reflections with Fo > 3σ(Fo) and refined up to R = 0.042 by full-matrix least-squares method. The lattice is composed of Li(1), Li(2) and linear $(NBN)^{3-}$ ions [r(B-N) 1.338(2) Å]. Li(1) ion is also linearly coordinated by two nitrogen atoms [r(Li(1)-N) 1.945(8) Å]. Li(2) ion is at the center of tetrahedron of N atoms [r(Li(2)-N 2.125(18) Å, ∠N-Li-N 103.6(2) and 112.5(9)°]. The structure of β-Li_3BN_2 has monoclinic symmetry, $P2_1/c$, a = 5.1502(2), b = 7.0824(2), c = 6.7908(2) Å, β = 112.956(2)°, Z = 4, D_m = 1.74, $D_{cal.}$ = 1.737 Mgm^{-3}. It was determined using 1325 unique X-ray reflections from a single crystal and refined up to R = 0.023. Two kinds of layers alternate parallel to (100) in the structure. One layer includes Li and B atoms, and the other is composed of only N atoms. N(1) and N(2) are coordinated by six Li and B atoms. Each Li atom is in the distorted tetrahedron of N atoms. Boron is linearly coordinated by two N atoms [r(B-N(1)) 1.3393(5), r(B-N(2)) 1.3361(5) Å, ∠N(1)-B-N(2) 179.12(4)°]. Lithium ionic conductivities of $3x10^{-5}$ and $6x10^{-5}$ Sm^{-1} were measured at 400 K on the polycrystalline samples of α- and β-Li_3BN_2, respectively. Activation energies were 78 and 64 kJ/mol for the α- and β-phases respectively.

Acknowledgements

The author expresses his appreciation and gratitude to Professor M. Koizumi of Osaka University for his encouragement during the course of this investigation. The author is greatly indebted to Dr. S. Kikkawa for his helpful discussions, continuing guidance, and encouragement. The auther would like to thank Professor S. Kawai of Osaka University for his help in the impedance measurement. The author also would like to thank Professor H. Horiuchi of Tokyo Univesity for his considerable assistance and significant suggestions on the crystal structure analysis. The author expresses his thanks to Mr. T. Tanaka in Material Analysis Center of ISIR for his advice in the single crystal X-ray diffraction experiment using the equipment (AFC-5FOS). The author is also indebted to Professor F. Kanamaru and his colleague at ISIR in Osaka University for their discussion and help in computation in structural analysis. In final, the author appreciates the kind cooperation and encouragement of all members at his laboratory.

References

1) P. Hagenmuller and W. van Gool eds., "Solid Electrolytes", Academic Press (1978).

2) Y.-F. Y. Yao and J. T. Kummer, J. Inorg. Nucl. Chem. 29, 2453 (1967).

3) U. v. Alpen, A. Rabenau and G. H. Talat, Appl. Phys. Lett., 30, 621 (1977).

4) A. Rabenau, Solid State Ionics, 6, 277 (1982).

5) W. Weppner, Solid State Ionics, 5, 3 (1981).

6) H. Y.-P. Hong, Mat. Res. Bull., 13, 117 (1978).

7) U. v. Alpen, M. F. Bell and W. Wichelhaus, Electrochim. Acta, 23, 1395 (1978).

8) R. M. Biefeld and R. J. Johnson, Jr., J. Electrochim. Soc., 126, 1 (1979).

9) R. A. Sharma, J. Electrochem. Soc. 119, 1439 (1972).

10) J. R. Raistrick, C. Ho and R. A. Huggins, Mat. Res. Bull. 11, 953 (1976).

11) R. A. Huggins, Electrochim. Acta, 22, 773 (1977).

12) P. Hartwig, W. Weppner and W. Wichelhaus, Mat. Res. Bull., 14, 493, (1979).

13) R. Juza, K. Langer and K. von Benda, Angew. Chem., 80, 373 (1968).

14) R. Juza and F. Hund, Z. Anorg. Allg. Chem., 257, 1 (1948).

15) R. Juza and F. Hund, Z. Anorg. Allg. Chem., 257, 13 (1948).

16) J. Lang, "Nitrogen Ceramicl" p.89, F. L. Riley ed., Nordhoff-Leyden (1977).

17) R. Juza, H. H. Weber and E. Meyer-Simon, Z. Anorg. Allg. Chem., 273, 48 (1948).

18) J. Lang and J.-P. Charlot, Rev. Chem. Miner., 7, 121 (1970).

19) J. David, J.-P. Charlot and J. Lang, Rev. Chem. Miner., 11, 405 (1974).

20) J. David, Y. Laurent, J-P. Charlot and J. Lang, Bull. Soc. Fr. Mineral. Cristallogr., 96, 21 (1973).

21) V. J. Goubeau and W. Anselment, Z. Anorg. Allg. Chem., 310, 248 (1961).

22) R. C. DeVries and J. F. Fleischer, Mat. Res. Bull., 4, 433 (1969).

23) R. M. Yonco, E. Veleckis and V. A. Maroni, J. Neucl. Mater., 57, 317 (1975).

24) W. L. Roth, S. P. Mitoff amd R. N. King, NASA Report, Contract NAS 3-15692 (1972).

25) P. A. G. O'Hare and G. K. Johnson, J. Chem. Thermodyn., 7, 13 (1975).

26) P. Hartwig, A. Rabenau and W. Weppner, J. Less-Common Met., 80, 81(1981).

27) W. Weppner, P. Hartwig and A. Rabenau, J. Power Sources, 6, 251 (1981).

28) J. B. Wagner and C. Wagner, J. Chem. Phys., 26, 1597 (1957).

29) M. S. Whittihgham, J. Electrochim. Soc., 123, 315 (1976)

30) R. Kanno, Y. Takeda and O. Yamamoto, Mat. Res. Bull., 16, 999 (1981).

31) D. H. Bollman and D. M. Mortimore, Anal. Chem. 43, 154 (1971).

32) A. Ichinose and H. Einaga, Yogyo-Kyokai-Shi, 83, 465 (1975).

33) R. D. Shannon and C. T. Prewitt, Acta Cryst., B25, 952 (1969).

34) Y. Laurent and J. Lang, C. R. Acad. Sci., 262, 103 (1966).

35) J. David and J. Lang, C. R. Acad. Sci., 261, 1005 (1965).

36) P. Eckerlin, A. Rabenau and H. Nortmann, Z. Anorg. Allg. Chem., 353, 113 (1967).

37) P. Eckerlin, Z. Anorg. Allg. Chem., 353, 225 (1967).

38) V. A.-P. Palisaar and R. Juza, Z. Anorg. Allg. Chem., 384, 1 (1971).

39) A. E. Maslout, J.-P. Motte and C. Gleitzer, J. Solid State Chem., 7, 250, (1973).

40) J.-F. Brice, J.-P. Motte, A. E. Maslout and J. Aubry, C. R. Acad. Sc. Paris, 273, C 744 (1971).

41) R. Juza, W. Gieren and J. Haug, Z. Anorg. Allg. Chem. 300, 61, (1959).

42) R. S. Pease, Acta Cryst. 5, 356, (1952).

43) D. Billand, E. McRae and A. Herold, Mat. Res. Bull., 14, 857, (1979).

44) R. C. Croft, Austral. J. Chem. 9, 206, (1956).

45) C. Mugiya, N. Ohigashi, Y. Mori and H. Inokuchi, Bull. Chem. Soc. Jpn. 43, 287, (1970).

46) "Interntional Tables for X-ray Crystallography", vol. IV, Kynoch Press, Birmingham, England (1974).

47) C. W. Burnham, An IBM 7090 Computer Program for Least-Squares Refinement of Crystallographic Lattice Constants. Geophysical Laboratory, Carnegie Institution of Washinton, Washigton, D.C. (1962).

48) L. W. Finger, A Fortran IV Computer Program for Structure Factor Calculation and Least-Squares Refinement of Crystal Structures. Geophysical Laboratory, Carnegie Institution of Washington, Washington, D.C. (1972).

49) L. W. Finger, University of Minnesota Pragram for Computing Bond Angles and Distances, and Thermal Ellipsoids with Error Analysis (1968).

50) Y. Iitaka, private communication.

51) C. K. Johnson, ORTEP-II. Report ORNL-3794, second revision. Oak Ridge National Laboratory, Tennessee (1971).

52) F. P. Bundy and R. H. Wentorf, Jr., J. Chem. Phys., 38, 1144 (1963).

53) P. S. Bryan and R. L. Kuczkowski, Inorg. Chem., 10, 200 (1971).

54) H. Hess, Acta Cryst., B 25, 2338 (1969).

55) J. Gaude, P. L'Haridon, J. Guyader and J. Lang, J. Solid State Chem., 59, 143 (1985).

56) F. B. Clippard, Jr. and L. S. Batell, Ionrg. Chem., 9, 2439 (1970).

57) G. J. Bullen and N. H. Clard, J. Chem. Soc. A., 992 (1970).

58) L. S. Bartell and R. A. Bonham, J. Chem. Phys., 31, 400 (1959).

59) R. B. Helmholdt, A. F. J. Ruysink, H. Reynaers and G. Kemper, Acta Cyst., B28, 318 (1972).

60) A. Rabenau and H. Schulz, J. Less-Common Met. 50, 155 (1976).

61) M. G. Down, M. J. Haley, P. Hubberstey, R. J. Pulham and A. E. Thunder, J. C. S. Dalton 1407, (1978).

Appendix I.

Fo-Fc Data of α-Li_3BN_2

H	K	L	F(OBS)	F(CALC)
4	0	0	11.642	11.583
6	0	0	5.412	5.397
9	0	0	0.952	0.000
1	1	0	4.594	4.434
2	1	0	9.042	8.206
3	1	0	1.681	1.558
4	1	0	6.398	6.481
5	1	0	2.521	2.551
6	1	0	4.784	4.756
8	1	0	2.263	2.324
9	1	0	1.401	1.107
2	2	0	21.188	19.960
3	2	0	2.510	2.780
4	2	0	4.919	5.095
6	2	0	3.485	3.456
7	2	0	1.020	1.156
8	2	0	4.191	4.061
3	3	0	4.997	5.093
4	3	0	4.123	4.096
5	3	0	2.947	2.885
6	3	0	2.644	2.436
7	3	0	3.541	3.473
8	3	0	1.479	1.622
4	4	0	6.062	5.980
6	4	0	3.563	3.468
7	4	0	1.199	1.041
5	5	0	5.165	5.057
7	5	0	1.759	1.893
6	6	0	1.994	2.083
1	0	1	9.513	9.292
3	0	1	6.734	6.872
5	0	1	7.283	7.343
7	0	1	2.331	2.324
9	0	1	2.633	2.366
1	1	1	19.205	17.427
2	1	1	1.927	1.885
3	1	1	6.073	6.343
4	1	1	2.118	2.191
6	1	1	1.580	1.656
7	1	1	1.557	1.693
8	1	1	0.751	0.499
9	1	1	2.342	2.292
2	2	1	3.529	3.120
3	2	1	6.611	6.752
4	2	1	3.485	3.630
5	2	1	3.148	3.120
6	2	1	2.342	2.369
7	2	1	4.213	4.179
8	2	1	1.524	1.378
3	3	1	2.835	2.624
5	3	1	0.796	0.584
6	3	1	1.008	0.823
7	3	1	1.277	1.184

H	K	L	F(OBS)	F(CALC)
8	3	1	2.443	2.583
4	4	1	4.000	4.089
5	4	1	3.305	3.151
6	4	1	3.754	3.703
8	4	1	2.118	1.894
6	5	1	1.681	1.684
6	6	1	2.835	2.950
0	0	2	20.056	19.571
2	0	2	9.692	9.855
4	0	2	3.261	3.341
6	0	2	1.602	1.611
8	0	2	1.468	1.471
1	1	2	13.759	14.234
2	1	2	6.207	6.243
3	1	2	7.059	7.168
4	1	2	5.591	5.738
5	1	2	6.880	6.948
6	1	2	4.482	4.448
7	1	2	1.961	1.937
8	1	2	2.263	2.185
9	1	2	1.826	1.910
2	2	2	7.171	7.166
3	2	2	2.263	2.431
4	2	2	1.468	1.367
7	2	2	1.008	1.038
8	2	2	2.611	2.542
3	3	2	10.734	10.724
4	3	2	3.653	3.700
5	3	2	0.919	0.767
6	3	2	2.375	2.311
7	3	2	4.896	4.892
8	3	2	1.233	1.563
4	4	2	1.692	1.645
5	4	2	0.717	0.233
6	4	2	1.277	1.208
7	4	2	1.109	1.059
5	5	2	6.790	6.790
1	0	3	4.908	5.023
3	0	3	4.000	4.109
5	0	3	6.577	6.600
7	0	3	2.039	1.954
1	1	3	9.255	9.677
3	1	3	4.347	4.553
4	1	3	2.129	2.323
5	1	3	0.773	0.538
6	1	3	1.524	1.658
7	1	3	1.535	1.544
2	2	3	2.252	2.210
3	2	3	5.658	5.825
4	2	3	2.846	2.894
5	2	3	2.431	2.398
6	2	3	2.118	2.209
7	2	3	3.944	3.819

H	K	L	F(OBS)	F(CALC)
3	3	3	2.263	2.229
5	3	3	0.683	0.473
6	3	3	0.840	0.851
7	3	3	0.997	0.975
8	3	3	2.398	2.367
4	4	3	3.541	3.668
5	4	3	3.014	2.959
6	4	3	3.328	3.214
6	5	3	1.613	1.641
6	6	3	2.644	2.694
0	0	4	16.717	16.907
2	0	4	1.468	1.493
4	0	4	7.115	7.167
6	0	4	3.698	3.699
1	1	4	0.840	0.515
2	1	4	3.518	3.657
3	1	4	0.964	1.058
4	1	4	4.314	4.357
5	1	4	1.950	1.932
6	1	4	3.675	3.637
8	1	4	1.591	1.877
2	2	4	10.510	10.844
3	2	4	1.748	1.808
4	2	4	2.992	2.986
6	2	4	2.308	2.286
7	2	4	0.728	0.876
8	2	4	3.283	3.087
3	3	4	3.294	3.414
4	3	4	2.745	2.845
5	3	4	2.308	2.272
6	3	4	2.185	2.054
7	3	4	2.712	2.739
4	4	4	3.955	4.019
6	4	4	2.543	2.409
5	5	4	3.978	3.936
1	0	5	3.597	3.626
3	0	5	1.905	1.904
5	0	5	5.300	5.326
7	0	5	1.535	1.452
1	1	5	5.188	5.231
2	1	5	0.717	0.661
3	1	5	2.891	2.970
4	1	5	2.286	2.177
6	1	5	1.513	1.481
7	1	5	1.233	1.216
2	2	5	1.490	1.470
3	2	5	4.527	4.661
4	2	5	2.062	2.105
5	2	5	1.703	1.583
6	2	5	1.681	1.765
7	2	5	3.193	3.136
3	3	5	1.580	1.729
4	4	5	2.880	2.947

H	K	L	F(OBS)	F(CALC)
5	4	5	2.476	2.538
6	4	5	2.543	2.499
6	5	5	1.412	1.384
0	0	6	4.695	4.694
2	0	6	3.462	3.315
4	0	6	1.871	1.931
6	0	6	0.874	1.067
1	1	6	4.706	4.843
2	1	6	2.263	2.234
3	1	6	2.756	2.790
4	1	6	3.126	3.085
5	1	6	3.496	3.437
6	1	6	2.734	2.693
2	2	6	3.115	3.167
3	2	6	1.356	1.294
4	2	6	0.964	0.613
3	3	6	4.930	5.046
4	3	6	1.905	2.026
6	3	6	1.692	1.586
4	4	6	1.064	1.094
6	4	6	1.199	0.737
5	5	6	3.944	3.933
1	0	7	2.812	2.658
3	0	7	1.031	0.955
5	0	7	3.944	3.811
1	1	7	3.350	3.195
2	1	7	0.740	0.806
3	1	7	2.006	1.939
4	1	7	1.681	1.653
2	2	7	0.796	0.985
3	2	7	3.350	3.341
4	2	7	1.535	1.416
5	2	7	0.919	1.043
6	2	7	1.199	1.342
3	3	7	1.233	1.227
4	3	7	0.952	0.543
4	4	7	1.894	2.103
5	4	7	1.726	1.851
0	0	8	5.501	5.318
4	0	8	2.969	2.731
1	1	8	0.840	0.662
2	1	8	1.445	1.399
4	1	8	2.207	2.020
2	2	8	4.034	3.910
3	2	8	0.930	0.858
4	2	8	1.132	0.903
3	3	8	1.524	1.849
4	3	8	0.908	1.328
4	4	8	1.770	1.671
1	0	9	1.994	1.701
1	1	9	2.207	1.930
3	1	9	1.277	1.187
4	1	9	1.524	1.076
2	2	9	0.852	0.613
3	2	9	1.871	2.122
3	3	9	1.266	0.777
0	0	10	2.207	2.026

Appendix II.

Fo-Fc Data of β-Li_3BN_2

Observed and calculated structure factors.

H	K	L	F(OBS)	F(CALC)
-9	0	2	6.585	6.340
-9	1	2	3.206	3.126
-9	1	3	0.394	0.459
-9	2	3	4.003	3.899
-9	1	4	4.432	4.337
-9	2	4	4.591	4.517
-9	3	4	1.307	1.371
-9	1	5	2.751	2.684
-9	2	5	3.217	3.161
-9	3	5	1.646	1.522
-9	0	6	2.127	2.084
-9	1	6	0.635	0.596
-9	2	6	4.046	3.965
-9	1	7	2.261	2.190
-8	1	1	1.930	1.893
-8	2	1	4.029	4.016
-8	3	1	3.249	3.145
-8	4	1	1.261	1.260
-8	5	1	2.814	2.816
-8	0	2	0.481	0.515
-8	2	2	6.243	6.178
-8	3	2	1.739	1.677
-8	5	2	0.501	0.432
-8	6	2	2.704	2.776
-8	1	3	0.817	0.710
-8	2	3	0.672	0.667
-8	3	3	3.730	3.737
-8	4	3	6.777	6.618
-8	5	3	1.122	1.146
-8	0	4	3.487	3.503
-8	2	4	1.316	1.293
-8	3	4	2.846	2.732
-8	4	4	1.838	1.798
-8	5	4	1.475	1.591
-8	6	4	3.203	3.228
-8	1	5	2.638	2.657
-8	2	5	2.594	2.576
-8	3	5	4.942	4.922
-8	4	5	7.953	7.774
-8	5	5	2.333	2.245
-8	6	5	2.948	2.976
-8	0	6	4.217	4.213
-8	1	6	1.696	1.677
-8	2	6	0.594	0.654
-8	3	6	1.107	1.063
-8	4	6	2.490	2.419
-8	5	6	3.409	3.414
-8	6	6	1.869	1.753
-8	1	7	0.565	0.521
-8	2	7	0.467	0.463
-8	3	7	6.066	5.926
-8	4	7	1.643	1.664
-8	5	7	5.953	5.813
-8	0	8	1.385	1.396
-8	1	8	0.533	0.510
-8	2	8	0.400	0.446
-8	3	8	1.783	1.820
-8	4	8	1.467	1.553
-8	1	9	2.012	1.996
-8	2	9	2.719	2.738
-8	3	9	2.197	2.170
-7	1	1	1.023	1.041
-7	2	1	2.214	2.213
-7	3	1	5.264	5.303
-7	4	1	9.826	9.751
-7	5	1	3.887	3.799
-7	6	1	2.751	2.773
-7	7	1	0.736	0.699
-7	0	2	2.864	2.839
-7	1	2	2.861	2.873
-7	3	2	0.409	0.365
-7	4	2	0.803	0.655
-7	5	2	4.269	4.316
-7	6	2	4.664	4.533
-7	7	2	0.403	0.173
-7	8	2	2.325	2.363
-7	1	3	0.672	0.696
-7	2	3	2.223	2.287
-7	3	3	6.774	6.663
-7	4	3	3.722	3.815
-7	5	3	7.945	7.779
-7	6	3	2.507	2.476
-7	8	3	0.933	0.999
-7	0	4	0.994	1.076
-7	1	4	0.388	0.396
-7	2	4	2.623	2.644
-7	3	4	2.838	2.921
-7	4	4	0.768	0.797
-7	5	4	5.194	5.162
-7	6	4	0.893	0.907
-7	7	4	1.780	1.654
-7	8	4	0.751	0.768
-7	1	5	1.884	1.871
-7	2	5	4.139	4.158
-7	3	5	1.252	1.199
-7	4	5	3.916	3.924
-7	5	5	2.336	2.381
-7	6	5	3.826	3.745
-7	7	5	4.116	4.067
-7	8	5	1.406	1.349
-7	0	6	3.617	3.699
-7	1	6	3.722	3.785
-7	2	6	1.046	1.055
-7	3	6	6.895	6.860
-7	4	6	0.435	0.446
-7	5	6	3.898	3.835
-7	6	6	2.933	2.879
-7	7	6	0.716	0.675
-7	8	6	1.748	1.715
-7	1	7	5.823	5.798
-7	2	7	1.977	2.005
-7	3	7	1.754	1.758
-7	4	7	2.472	2.523
-7	5	7	3.768	3.713
-7	6	7	1.096	1.067
-7	7	7	5.368	5.253
-7	0	8	4.380	4.345
-7	1	8	0.632	0.574
-7	2	8	3.719	3.723
-7	3	8	4.264	4.253
-7	4	8	0.429	0.431
-7	5	8	0.417	0.363
-7	6	8	3.011	3.004
-7	1	9	4.339	4.314
-7	2	9	1.290	1.258
-7	3	9	1.014	1.050
-7	4	9	0.420	0.399
-7	5	9	1.704	1.652
-7	0	10	0.728	0.735
-7	1	10	4.719	4.733
-7	2	10	3.261	3.225
-7	3	10	0.530	0.481
-7	1	11	1.327	1.305
-6	1	1	2.678	2.602
-6	2	1	5.510	5.521
-6	3	1	1.043	0.992
-6	4	1	2.278	2.246
-6	5	1	1.070	1.067
-6	6	1	4.884	4.744
-6	7	1	4.866	4.815
-6	8	1	1.333	1.268
-6	0	2	4.151	4.315
-6	1	2	6.440	6.544
-6	2	2	1.846	2.011
-6	3	2	8.275	8.248
-6	4	2	2.522	2.604
-6	5	2	3.267	3.160
-6	6	2	0.748	0.695
-6	7	2	2.240	2.270
-6	8	2	5.061	4.949
-6	9	2	2.090	2.124
-6	1	3	10.431	10.495
-6	2	3	3.206	3.360
-6	4	3	0.362	0.208
-6	5	3	6.272	6.312
-6	6	3	1.501	1.501
-6	7	3	6.362	6.174
-6	8	3	2.185	2.176
-6	0	4	8.327	8.441
-6	1	4	0.513	0.393
-6	2	4	5.214	5.236
-6	3	4	6.582	6.572
-6	4	4	0.655	0.695
-6	5	4	1.481	1.449
-6	6	4	2.968	2.962
-6	7	4	2.177	2.207
-6	8	4	4.806	4.729
-6	9	4	1.090	0.954
-6	1	5	2.771	2.743
-6	3	5	4.206	4.316
-6	4	5	0.797	0.825
-6	5	5	1.075	1.137
-6	6	5	1.501	1.428
-6	7	5	5.107	5.009
-6	8	5	2.927	2.858
-6	9	5	4.658	4.661
-6	0	6	1.655	1.711
-6	1	6	8.403	8.419
-6	2	6	3.527	3.550
-6	3	6	1.496	1.537
-6	4	6	0.635	0.682
-6	5	6	1.985	2.037
-6	7	6	6.003	5.930
-6	8	6	0.328	0.282
-6	9	6	4.122	4.086
-6	1	7	4.014	4.018
-6	2	7	1.188	1.021
-6	3	7	1.061	1.052
-6	4	7	2.371	2.435
-6	5	7	1.901	1.909
-6	8	7	0.814	0.953
-6	0	8	6.637	6.553
-6	1	8	6.301	6.269
-6	2	8	6.136	6.101
-6	4	8	1.058	1.070
-6	5	8	2.003	2.026
-6	6	8	0.307	0.245
-6	7	8	3.252	3.264
-6	8	8	5.948	5.827
-6	1	9	2.162	2.165
-6	2	9	1.936	1.977
-6	4	9	3.336	3.284
-6	5	9	0.493	0.498
-6	6	9	0.513	0.455
-6	7	9	1.081	1.200
-6	0	10	8.921	8.798
-6	1	10	1.180	1.218
-6	2	10	1.759	1.749
-6	3	10	1.916	1.916
-6	4	10	1.232	1.244
-6	5	10	1.435	1.412
-6	1	11	1.954	1.903
-6	2	11	3.101	3.127
-6	3	11	1.162	1.200
-5	1	1	4.762	4.839
-5	2	1	1.823	2.061
-5	3	1	2.510	2.717
-5	4	1	2.298	2.333
-5	5	1	1.101	1.156
-5	6	1	0.330	0.169
-5	7	1	4.255	4.216
-5	8	1	3.293	3.220
-5	9	1	5.208	5.227
-5	10	1	2.426	2.383
-5	0	2	3.890	4.076
-5	1	2	10.860	11.258
-5	2	2	3.298	3.565
-5	3	2	1.223	1.197
-5	4	2	2.264	2.329
-5	5	2	1.843	1.850
-5	6	2	1.617	1.561
-5	7	2	6.171	6.092
-5	9	2	6.374	6.243
-5	1	3	8.301	8.578
-5	2	3	0.530	0.616
-5	3	3	2.985	2.881
-5	4	3	5.023	5.078
-5	5	3	1.409	1.444
-5	6	3	1.365	1.405
-5	7	3	0.446	0.419
-5	8	3	3.301	3.464
-5	9	3	6.803	6.731
-5	10	3	0.441	0.384
-5	0	4	13.608	13.938
-5	1	4	8.733	8.865
-5	2	4	7.892	8.116
-5	3	4	1.977	2.055
-5	4	4	2.258	2.308
-5	5	4	3.611	3.580
-5	6	4	2.333	2.374
-5	7	4	4.811	4.742
-5	8	4	6.014	5.917
-5	9	4	3.501	3.600
-5	10	4	3.484	3.366
-5	1	5	7.672	7.844
-5	2	5	0.681	0.737
-5	3	5	1.820	1.818
-5	4	5	3.032	2.973
-5	5	5	1.298	1.310
-5	6	5	3.339	3.381
-5	7	5	2.562	2.611
-5	8	5	3.324	3.370
-5	9	5	3.365	3.296
-5	10	5	5.229	5.143
-5	0	6	14.188	14.299
-5	1	6	1.461	1.489
-5	2	6	1.910	1.931
-5	3	6	4.168	4.218
-5	4	6	2.539	2.553
-5	5	6	2.501	2.575
-5	6	6	2.281	2.292
-5	7	6	1.185	1.161
-5	8	6	5.400	5.392
-5	9	6	0.336	0.256
-5	10	6	1.377	1.294
-5	1	7	1.029	0.995
-5	2	7	5.730	5.760
-5	4	7	0.609	0.683
-5	5	7	1.110	1.135
-5	6	7	3.904	3.929
-5	7	7	4.687	4.664
-5	8	7	0.933	0.850
-5	9	7	0.316	0.168
-5	0	8	2.009	1.992
-5	1	8	3.011	3.047
-5	2	8	4.565	4.525
-5	3	8	4.038	4.051
-5	4	8	1.406	1.431
-5	5	8	3.858	3.884
-5	6	8	1.267	1.199
-5	7	8	0.991	1.059
-5	8	8	1.910	1.928
-5	1	9	1.869	1.857
-5	2	9	4.907	4.883
-5	3	9	3.933	3.978
-5	4	9	1.130	1.099
-5	5	9	4.307	4.337
-5	6	9	5.388	5.412
-5	0	10	2.722	2.706
-5	2	10	4.490	4.485
-5	3	10	0.823	0.805
-5	4	10	2.252	2.194
-5	5	10	1.675	1.709
-5	6	10	3.290	3.343
-5	1	11	1.284	1.315
-5	2	11	0.896	0.869
-5	3	11	4.266	4.249
-5	4	11	4.040	4.073
-5	5	11	3.414	3.435
-5	0	12	0.916	0.926
-5	1	12	0.965	0.966
-4	1	1	10.310	10.928
-4	2	1	1.145	1.058
-4	3	1	0.330	0.017
-4	4	1	2.501	2.339
-4	5	1	1.765	1.787
-4	6	1	4.893	4.967
-4	7	1	5.440	5.390

Observed and calculated structure factors.

H	K	L	F(OBS)	F(CALC)
-4	8	1	4.284	4.252
-4	9	1	4.313	4.171
-4	10	1	4.884	4.780
-4	11	1	0.391	0.255
-4	0	2	9.098	9.551
-4	1	2	1.154	1.345
-4	2	2	9.194	9.683
-4	3	2	9.081	9.791
-4	4	2	1.901	2.005
-4	5	2	6.263	6.217
-4	6	2	0.693	0.649
-4	7	2	0.942	0.986
-4	8	2	6.982	6.871
-4	9	2	1.183	1.230
-4	10	2	0.890	0.892
-4	11	2	4.493	4.408
-4	1	3	0.913	0.670
-4	2	3	8.133	8.632
-4	3	3	2.881	2.931
-4	4	3	2.785	2.994
-4	5	3	5.478	5.721
-4	6	3	6.026	5.959
-4	7	3	8.205	8.158
-4	8	3	0.664	0.653
-4	9	3	2.243	2.252
-4	10	3	3.533	3.516
-4	11	3	3.020	2.977
-4	1	4	0.925	1.062
-4	2	4	7.058	7.318
-4	3	4	5.458	5.723
-4	4	4	3.003	3.235
-4	5	4	6.620	6.572
-4	6	4	1.101	1.061
-4	7	4	1.287	1.308
-4	8	4	2.064	2.027
-4	9	4	0.861	0.827
-4	10	4	3.826	3.778
-4	11	4	2.061	2.032
-4	1	5	5.632	5.749
-4	2	5	8.669	8.795
-4	3	5	14.585	14.782
-4	4	5	1.800	1.807
-4	5	5	5.185	5.206
-4	6	5	9.101	9.009
-4	7	5	2.255	2.250
-4	8	5	2.936	2.911
-4	9	5	0.385	0.365
-4	10	5	0.739	0.702
-4	11	5	2.965	2.906
-4	0	6	4.910	4.935
-4	1	6	3.046	3.056
-4	2	6	6.266	6.320
-4	3	6	1.133	1.177
-4	4	6	4.046	4.135
-4	5	6	4.336	4.345
-4	6	6	5.214	5.235
-4	7	6	1.423	1.458
-4	8	6	1.687	1.738
-4	9	6	1.846	1.861
-4	10	6	4.119	4.131
-4	1	7	1.898	1.963
-4	2	7	1.119	1.106
-4	3	7	7.177	7.108
-4	4	7	6.313	6.327
-4	5	7	7.437	7.397
-4	6	7	1.861	1.810
-4	7	7	2.438	2.449
-4	8	7	1.704	1.744
-4	9	7	1.354	1.350
-4	0	8	6.223	6.158
-4	1	8	1.127	1.084
-4	2	8	7.742	7.681
-4	3	8	0.896	0.891
-4	4	8	4.032	4.010
-4	5	8	1.449	1.449
-4	6	8	2.751	2.800
-4	7	8	0.461	0.456
-4	8	8	0.646	0.713
-4	9	8	0.441	0.452
-4	1	9	0.823	0.661
-4	2	9	1.919	1.960
-4	3	9	1.319	1.336
-4	4	9	8.913	8.871
-4	5	9	1.754	1.744
-4	6	9	1.956	1.990
-4	8	9	0.438	0.371
-4	0	10	1.183	1.218
-4	1	10	2.046	2.037
-4	2	10	1.362	1.390
-4	3	10	1.139	1.135
-4	4	10	0.609	0.547
-4	5	10	1.629	1.676
-4	6	10	4.261	4.276
-4	7	10	0.330	0.283
-4	1	11	0.568	0.485
-4	2	11	0.907	0.858
-4	3	11	6.875	6.805
-4	4	11	3.461	3.505
-4	5	11	4.490	4.492
-4	1	12	0.962	0.854
-4	2	12	2.426	2.453
-3	1	1	6.913	7.072
-3	2	1	10.791	11.434
-3	3	1	19.156	19.809
-3	4	1	3.953	3.930
-3	5	1	11.524	11.768
-3	6	1	10.179	9.849
-3	7	1	1.591	1.666
-3	8	1	2.864	2.875
-3	9	1	2.351	2.362
-3	10	1	0.475	0.279
-3	11	1	3.864	3.854
-3	12	1	0.472	0.403
-3	0	2	4.409	4.498
-3	1	2	11.342	11.581
-3	2	2	16.205	17.013
-3	3	2	1.383	1.325
-3	4	2	2.145	1.434
-3	5	2	10.443	10.796
-3	6	2	1.675	1.553
-3	7	2	0.971	0.984
-3	8	2	0.429	0.422
-3	9	2	1.696	1.759
-3	10	2	2.803	2.793
-3	11	2	1.884	1.855
-3	12	2	1.403	1.291
-3	1	3	2.194	2.331
-3	3	3	10.269	10.538
-3	4	3	7.579	7.694
-3	5	3	13.286	13.226
-3	6	3	0.530	0.471
-3	7	3	0.777	0.801
-3	8	3	3.235	3.253
-3	9	3	3.275	3.280
-3	10	3	1.087	1.118
-3	11	3	2.948	2.901
-3	12	3	5.084	5.049
-3	0	4	6.666	6.998
-3	1	4	1.545	1.773
-3	2	4	5.866	5.996
-3	3	4	2.443	2.145
-3	4	4	1.812	1.737
-3	5	4	3.681	4.014
-3	6	4	6.994	6.943
-3	7	4	0.762	0.763
-3	8	4	2.443	2.480
-3	9	4	0.704	0.607
-3	10	4	1.458	1.424
-3	11	4	0.675	0.696
-3	1	5	0.568	0.410
-3	2	5	0.467	0.347
-3	3	5	5.878	5.891
-3	4	5	15.680	15.670
-3	5	5	1.339	1.406
-3	6	5	0.762	0.355
-3	7	5	4.553	4.565
-3	8	5	1.725	1.723
-3	9	5	0.997	1.002
-3	10	5	0.719	0.719
-3	11	5	0.319	0.240
-3	0	6	0.452	0.276
-3	1	6	5.333	5.410
-3	2	6	3.472	3.354
-3	3	6	5.927	5.831
-3	4	6	1.052	0.979
-3	5	6	0.838	0.831
-3	6	6	8.029	8.012
-3	7	6	1.200	1.170
-3	8	6	2.214	2.210
-3	9	6	2.907	2.896
-3	10	6	2.725	2.712
-3	11	6	2.525	2.554
-3	1	7	5.620	5.565
-3	2	7	2.759	2.788
-3	3	7	7.739	7.664
-3	4	7	5.237	5.225
-3	5	7	10.649	10.567
-3	6	7	2.916	2.914
-3	7	7	3.472	3.481
-3	8	7	1.441	1.415
-3	9	7	1.316	1.321
-3	10	7	1.148	1.126
-3	1	8	1.568	1.557
-3	2	8	6.052	6.013
-3	3	8	0.261	0.150
-3	4	8	1.400	1.365
-3	5	8	5.403	5.361
-3	6	8	3.472	3.516
-3	7	8	0.858	0.906
-3	8	8	1.078	1.085
-3	9	8	0.562	0.564
-3	1	9	1.020	1.032
-3	2	9	5.324	5.301
-3	3	9	3.397	3.433
-3	4	9	0.577	0.595
-3	5	9	4.342	4.288
-3	6	9	5.388	5.358
-3	7	9	1.032	1.075
-3	8	9	1.064	1.092
-3	0	10	5.162	5.141
-3	1	10	3.380	3.411
-3	2	10	2.817	2.767
-3	3	10	3.423	3.489
-3	5	10	2.417	2.461
-3	6	10	1.026	1.012
-3	7	10	2.316	2.289
-3	1	11	3.081	3.069
-3	2	11	2.423	2.523
-3	4	11	0.530	0.549
-3	5	11	1.554	1.511
-3	0	12	5.921	5.917
-3	1	12	0.878	0.871
-3	2	12	2.774	2.783
-2	1	1	12.159	11.405
-2	2	1	0.812	0.937
-2	3	1	6.855	6.688
-2	4	1	19.257	19.440
-2	5	1	3.496	3.941
-2	6	1	0.496	0.438
-2	7	1	8.121	8.307
-2	8	1	0.481	0.452
-2	9	1	1.174	1.273
-2	10	1	0.916	0.947
-2	11	1	0.838	0.890
-2	12	1	4.922	4.905
-2	0	2	12.455	11.742
-2	1	2	14.330	13.828
-2	2	2	20.866	20.566
-2	3	2	13.724	13.356
-2	4	2	4.513	4.893
-2	5	2	1.872	1.525
-2	6	2	5.869	6.106
-2	7	2	0.783	0.780
-2	8	2	0.881	0.896
-2	9	2	1.713	1.692
-2	10	2	3.040	3.090
-2	11	2	5.858	5.893
-2	12	2	0.751	0.781
-2	1	3	21.106	20.866
-2	2	3	8.852	8.916
-2	3	3	6.768	6.485
-2	4	3	6.321	6.204
-2	5	3	18.486	18.762
-2	6	3	5.924	6.112
-2	7	3	4.866	4.863
-2	8	3	3.646	3.634
-2	9	3	1.487	1.464
-2	10	3	0.951	0.951
-2	11	3	2.284	2.300
-2	12	3	3.930	3.969
-2	0	4	0.223	0.017
-2	1	4	1.359	1.787
-2	2	4	15.666	15.700
-2	3	4	3.640	3.815
-2	4	4	2.855	2.623
-2	5	4	4.388	4.330
-2	6	4	5.716	5.788
-2	7	4	3.342	3.427
-2	8	4	1.496	1.510
-2	9	4	0.670	0.612
-2	10	4	5.724	5.778
-2	11	4	2.278	2.281
-2	12	4	2.003	1.963
-2	1	5	5.808	6.059
-2	2	5	9.649	9.602
-2	3	5	12.110	11.885
-2	4	5	0.258	0.289
-2	6	5	7.119	7.077
-2	7	5	2.394	2.421
-2	8	5	2.330	2.350
-2	9	5	2.985	2.969
-2	10	5	3.003	3.071
-2	11	5	1.501	1.521
-2	0	6	14.275	14.073
-2	1	6	7.356	7.183
-2	2	6	5.423	5.499
-2	3	6	4.614	4.561
-2	4	6	1.667	1.784
-2	5	6	2.339	2.414
-2	6	6	1.125	1.178
-2	7	6	4.469	4.432
-2	8	6	4.965	4.957
-2	9	6	2.493	2.574
-2	10	6	1.507	1.556
-2	11	6	2.901	2.908
-2	1	7	2.649	2.670
-2	2	7	4.919	4.812
-2	3	7	1.438	1.393
-2	4	7	3.756	3.783
-2	5	7	1.275	1.308
-2	6	7	1.974	2.004
-2	7	7	5.046	5.022
-2	8	7	2.942	2.980
-2	9	7	0.478	0.502
-2	10	7	4.081	4.079
-2	0	8	10.110	9.945
-2	1	8	1.203	1.206
-2	2	8	9.750	9.639
-2	3	8	4.501	4.481
-2	4	8	1.646	1.667
-2	5	8	1.446	1.461
-2	6	8	0.496	0.423
-2	7	8	0.629	0.602
-2	8	8	8.747	8.627
-2	1	9	4.180	4.158
-2	2	9	1.443	1.440
-2	3	9	0.470	0.436
-2	4	9	3.939	3.909
-2	5	9	0.635	0.600
-2	6	9	1.127	1.092
-2	7	9	2.229	2.222
-2	8	9	3.632	3.586
-2	0	10	7.423	7.298
-2	1	10	5.707	5.699
-2	2	10	1.484	1.489
-2	3	10	1.159	1.128
-2	4	10	1.872	1.853
-2	5	10	1.362	1.348

Observed and calculated structure factors.

H	K	L	F(OBS)	F(CALC)
-2	6	10	1.041	1.004
-2	7	10	4.072	4.101
-2	1	11	1.487	1.553
-2	2	11	0.571	0.627
-2	3	11	1.270	1.262
-2	4	11	0.339	0.279
-2	5	11	1.933	1.927
-2	0	12	2.667	2.665
-2	1	12	4.122	4.165
-1	1	1	2.582	2.782
-1	2	1	22.866	21.349
-1	3	1	7.930	8.090
-1	4	1	3.058	2.990
-1	6	1	8.608	8.831
-1	7	1	2.522	2.540
-1	8	1	2.513	2.546
-1	9	1	4.785	4.786
-1	10	1	3.878	3.844
-1	11	1	2.035	2.066
-1	12	1	2.771	2.761
-1	0	2	25.318	23.829
-1	1	2	23.515	22.038
-1	3	2	9.408	9.003
-1	4	2	4.936	4.775
-1	5	2	3.806	3.809
-1	6	2	4.953	4.962
-1	7	2	3.939	3.982
-1	8	2	10.553	10.441
-1	9	2	5.852	5.852
-1	10	2	2.481	2.528
-1	11	2	1.200	1.177
-1	2	3	10.634	10.246
-1	3	3	5.701	5.879
-1	4	3	14.652	15.038
-1	5	3	0.449	0.425
-1	6	3	3.081	3.140
-1	7	3	5.455	5.446
-1	8	3	7.177	7.153
-1	9	3	1.284	1.327
-1	10	3	5.423	5.371
-1	11	3	1.713	1.698
-1	12	3	0.910	0.926
-1	0	4	36.581	35.961
-1	1	4	1.658	1.616
-1	2	4	10.614	10.286
-1	3	4	4.852	4.859
-1	4	4	4.142	4.205
-1	5	4	1.119	1.188
-1	6	4	1.385	1.447
-1	8	4	12.292	12.120
-1	9	4	0.296	0.229
-1	10	4	2.722	2.737
-1	11	4	2.307	2.299
-1	12	4	1.687	1.650
-1	1	5	1.577	1.506
-1	2	5	2.107	1.833
-1	3	5	3.069	2.915
-1	4	5	7.211	7.366
-1	5	5	2.423	2.466
-1	6	5	3.675	3.642
-1	7	5	2.936	2.934
-1	8	5	3.693	3.697
-1	9	5	4.078	4.061
-1	10	5	7.113	7.049
-1	11	5	0.325	0.130
-1	0	6	16.878	16.693
-1	1	6	10.139	9.910
-1	2	6	0.528	0.514
-1	3	6	1.545	1.611
-1	4	6	3.838	3.818
-1	5	6	2.325	2.301
-1	6	6	1.217	1.249
-1	7	6	6.666	6.621
-1	8	6	5.223	5.202
-1	9	6	3.855	3.907
-1	10	6	0.751	0.755
-1	1	7	7.733	7.599
-1	2	7	3.519	3.507
-1	3	7	0.948	0.991
-1	4	7	1.597	1.608
-1	5	7	0.817	0.837
-1	6	7	3.145	3.185
-1	7	7	0.377	0.349
-1	9	7	5.081	5.021
-1	10	7	1.287	1.279
-1	0	8	3.843	3.790
-1	1	8	5.461	5.339
-1	2	8	6.101	6.041
-1	3	8	1.374	1.416
-1	4	8	1.145	1.140
-1	5	8	0.345	0.206
-1	6	8	2.440	2.469
-1	7	8	3.096	3.182
-1	8	8	1.417	1.440
-1	9	8	3.985	3.980
-1	1	9	6.226	6.194
-1	2	9	1.014	0.936
-1	3	9	1.725	1.768
-1	4	9	0.832	0.770
-1	5	9	2.806	2.835
-1	6	9	2.910	2.876
-1	7	9	3.591	3.597
-1	8	9	3.127	3.143
-1	0	10	7.405	7.320
-1	1	10	1.104	1.106
-1	2	10	3.206	3.285

H	K	L	F(OBS)	F(CALC)
-1	3	10	5.037	5.002
-1	4	10	1.722	1.703
-1	5	10	2.139	2.147
-1	6	10	2.980	2.987
-1	1	11	2.669	2.696
-1	2	11	1.881	1.938
-1	3	11	1.348	1.336
-1	4	11	2.064	2.126
0	2	0	3.177	3.210
0	4	0	16.709	16.920
0	6	0	6.985	7.052
0	8	0	11.223	11.383
0	10	0	4.748	4.658
0	12	0	1.354	1.428
0	1	1	1.055	1.182
0	2	1	10.863	10.361
0	3	1	1.626	1.385
0	4	1	16.831	17.144
0	5	1	3.826	3.963
0	6	1	2.275	2.293
0	7	1	0.328	0.291
0	8	1	5.565	5.535
0	9	1	3.617	3.635
0	10	1	8.179	8.076
0	11	1	0.919	0.837
0	12	1	2.188	2.222
0	0	2	28.315	26.633
0	1	2	25.953	24.331
0	2	2	4.591	4.861
0	3	2	4.269	4.056
0	4	2	3.417	3.259
0	5	2	0.785	0.803
0	6	2	4.730	4.762
0	7	2	5.197	5.241
0	8	2	10.440	10.465
0	9	2	6.237	6.242
0	10	2	1.458	1.511
0	12	2	0.409	0.376
0	1	3	19.846	19.439
0	2	3	12.553	12.296
0	3	3	6.910	7.322
0	4	3	4.206	4.238
0	5	3	6.423	6.343
0	6	3	7.536	7.617
0	7	3	1.756	1.743
0	8	3	0.481	0.401
0	9	3	4.000	4.056
0	10	3	2.261	2.280
0	11	3	2.823	2.763
0	12	3	1.617	1.640
0	0	4	5.249	5.163
0	1	4	7.098	6.543
0	2	4	14.414	14.357
0	3	4	5.782	5.900
0	4	4	2.956	2.845
0	5	4	0.913	1.008
0	6	4	4.895	4.886
0	7	4	5.374	5.447
0	8	4	0.530	0.469
0	9	4	3.046	3.055
0	10	4	5.168	5.182
0	11	4	2.739	2.731
0	1	5	3.130	3.009
0	2	5	4.890	5.003
0	3	5	12.762	12.635
0	4	5	1.562	1.493
0	5	5	2.017	2.070
0	6	5	6.771	6.744
0	7	5	9.988	9.932
0	8	5	3.667	3.674
0	9	5	4.452	4.481
0	10	5	1.835	1.870
0	11	5	0.348	0.270
0	0	6	10.875	10.624
0	1	6	3.643	3.721
0	2	6	5.835	5.618
0	3	6	10.092	9.945
0	4	6	3.417	3.380
0	5	6	3.046	3.077
0	6	6	6.466	6.403
0	7	6	1.562	1.546
0	8	6	1.742	1.792
0	9	6	1.449	1.458
0	10	6	3.629	3.600
0	1	7	6.907	6.808
0	2	7	3.046	3.009
0	3	7	1.185	1.205
0	4	7	4.559	4.547
0	5	7	3.058	3.072
0	6	7	1.629	1.662
0	7	7	6.698	6.594
0	8	7	1.516	1.554
0	9	7	0.748	0.799
0	10	7	1.739	1.708
0	0	8	2.597	2.621
0	1	8	2.220	2.213
0	2	8	3.977	3.961
0	3	8	5.658	5.611
0	4	8	4.151	4.121
0	5	8	4.220	4.251
0	6	8	0.655	0.130
0	7	8	0.768	0.780
0	8	8	1.977	1.964
0	9	8	0.643	0.689
0	1	9	1.229	1.232
0	2	9	3.400	3.407

H	K	L	F(OBS)	F(CALC)
0	3	9	4.913	4.885
0	4	9	3.035	3.125
0	5	9	4.820	4.796
0	6	9	3.507	3.509
0	7	9	1.759	1.731
0	0	10	1.125	1.097
0	1	10	1.646	1.634
0	2	10	2.661	2.632
0	3	10	0.838	0.888
0	5	10	3.904	3.951
0	1	11	1.246	1.249
1	0	0	5.003	4.998
1	1	0	8.832	9.168
1	2	0	31.480	30.200
1	3	0	11.617	11.364
1	4	0	4.887	4.518
1	5	0	2.151	2.315
1	6	0	6.956	7.078
1	7	0	8.034	8.218
1	8	0	1.003	0.979
1	9	0	0.623	0.320
1	10	0	6.516	6.485
1	11	0	1.672	1.668
1	12	0	2.249	2.297
1	1	1	16.318	15.129
1	2	1	14.411	13.393
1	3	1	18.260	18.184
1	4	1	5.608	5.469
1	5	1	9.034	9.299
1	6	1	9.507	9.705
1	7	1	11.576	11.554
1	8	1	3.707	3.762
1	9	1	2.730	2.781
1	10	1	1.046	1.030
1	11	1	0.797	0.858
1	12	1	3.194	3.236
1	0	2	3.472	3.231
1	1	2	12.437	12.076
1	2	2	22.350	21.965
1	3	2	16.025	15.719
1	4	2	3.272	3.550
1	5	2	0.272	0.264
1	6	2	5.087	5.178
1	7	2	0.904	0.912
1	8	2	2.635	2.692
1	9	2	0.728	0.700
1	10	2	3.435	3.491
1	11	2	7.165	7.165
1	1	3	16.083	15.879
1	2	3	3.924	3.685
1	3	3	0.867	0.755
1	4	3	9.063	9.023
1	5	3	6.292	6.465
1	6	3	3.038	3.102
1	7	3	7.692	7.692
1	8	3	2.872	2.931
1	9	3	0.632	0.628
1	11	3	1.006	1.019
1	12	3	4.808	4.822
1	0	4	1.617	1.952
1	1	4	1.449	1.230
1	2	4	2.087	2.040
1	3	4	8.817	8.536
1	4	4	1.887	1.797
1	5	4	6.675	6.872
1	6	4	4.562	4.583
1	7	4	0.365	0.355
1	9	4	0.661	0.577
1	11	4	2.933	3.008
1	1	5	5.753	5.804
1	2	5	2.159	2.042
1	3	5	12.124	12.038
1	4	5	7.875	7.790
1	5	5	7.116	7.022
1	6	5	0.994	1.010
1	7	5	0.362	0.359
1	8	5	2.023	2.025
1	9	5	2.145	2.206
1	10	5	1.626	1.651
1	11	5	2.710	2.780
1	0	6	3.481	3.533
1	1	6	4.695	4.728
1	2	6	2.055	1.998
1	3	6	0.945	0.877
1	4	6	1.806	1.823
1	5	6	6.953	6.878
1	6	6	1.649	1.649
1	7	6	0.956	0.963
1	8	6	0.449	0.439
1	9	6	2.881	2.875
1	1	7	0.985	0.970
1	2	7	1.583	1.556
1	3	7	8.594	8.479
1	4	7	4.469	4.451
1	5	7	10.614	10.482
1	6	7	1.464	1.465
1	7	7	0.325	0.206
1	8	7	1.081	1.146
1	9	7	3.101	3.141
1	0	8	2.826	2.829
1	1	8	2.481	2.457
1	2	8	0.417	0.211
1	3	8	2.516	2.538
1	4	8	1.948	1.946
1	5	8	5.782	5.745
1	6	8	2.226	2.218

Observed and calculated structure factors.

H	K	L	F(OBS)	F(CALC)
1	7	8	0.774	0.703
1	8	8	0.988	1.038
1	1	9	1.478	1.500
1	2	9	2.629	2.683
1	3	9	1.319	1.330
1	4	9	6.959	6.889
1	5	9	2.072	2.058
1	6	9	2.542	2.611
1	0	10	0.513	0.566
1	1	10	0.971	1.010
1	2	10	1.322	1.325
1	3	10	2.762	2.787
2	0	0	1.235	0.192
2	1	0	1.591	1.550
2	2	0	7.000	6.771
2	3	0	9.440	8.757
2	4	0	5.698	6.070
2	5	0	6.768	7.493
2	6	0	12.475	12.507
2	7	0	0.391	0.409
2	8	0	4.759	4.677
2	10	0	2.327	2.251
2	11	0	2.243	2.270
2	12	0	3.316	3.345
2	1	1	6.861	6.660
2	2	1	0.893	0.624
2	3	1	16.672	17.093
2	4	1	10.826	11.175
2	5	1	11.553	11.585
2	6	1	0.571	0.292
2	7	1	0.858	0.725
2	9	1	3.107	3.149
2	10	1	0.664	0.697
2	11	1	3.003	3.065
2	12	1	3.333	3.324
2	0	2	4.608	4.639
2	1	2	12.023	12.338
2	2	2	10.866	11.307
2	3	2	2.643	2.601
2	4	2	3.136	2.559
2	5	2	11.826	12.051
2	7	2	1.165	1.176
2	8	2	0.855	0.963
2	9	2	2.322	2.293
2	10	2	1.261	1.122
2	11	2	1.162	1.196
2	12	2	0.533	0.533
2	1	3	5.035	5.038
2	2	3	5.200	5.439
2	3	3	9.066	9.093
2	4	3	6.127	6.095
2	5	3	18.092	18.186
2	6	3	5.066	4.863
2	7	3	1.927	1.907
2	8	3	2.881	2.908
2	9	3	5.197	5.099
2	10	3	0.670	0.672
2	11	3	4.336	4.321
2	0	4	4.009	4.089
2	1	4	3.559	3.574
2	2	4	3.304	3.315
2	3	4	3.736	3.902
2	4	4	3.087	3.243
2	5	4	7.637	7.512
2	6	4	1.788	1.825
2	7	4	0.516	0.519
2	8	4	0.487	0.358
2	9	4	1.371	1.420
2	10	4	2.107	2.112
2	11	4	1.574	1.601
2	1	5	9.782	9.791
2	2	5	4.449	4.477
2	3	5	7.574	7.646
2	4	5	9.127	9.055
2	5	5	0.472	0.468
2	6	5	3.568	3.515
2	7	5	2.394	2.400
2	8	5	1.275	1.251
2	9	5	1.058	1.014
2	10	5	1.530	1.535
2	0	6	4.666	4.751
2	1	6	1.304	1.291
2	2	6	2.156	2.199
2	3	6	5.626	5.600
2	4	6	0.997	0.988
2	5	6	2.591	2.615
2	6	6	5.229	5.212
2	8	6	0.429	0.329
2	1	7	4.510	4.464
2	2	7	0.716	0.642
2	3	7	3.530	3.492
2	4	7	2.264	2.308
2	5	7	2.640	2.656
2	6	7	2.133	2.132
2	7	7	5.058	5.051
2	8	7	2.551	2.599
2	0	8	1.362	1.364
2	1	8	2.009	2.077
2	2	8	9.434	9.339
2	3	8	2.554	2.521
2	4	8	0.470	0.430
2	5	8	0.432	0.413
2	6	8	1.826	1.907
2	7	8	2.261	2.314
2	1	9	2.800	2.825
2	2	9	3.597	3.596

H	K	L	F(OBS)	F(CALC)
2	3	9	1.330	1.294
2	4	9	0.525	0.509
2	5	9	1.014	0.992
2	0	10	0.614	0.690
3	0	0	4.098	4.097
3	1	0	2.093	1.963
3	2	0	7.976	8.458
3	3	0	4.020	4.732
3	4	0	3.667	4.317
3	5	0	6.530	6.322
3	6	0	0.255	0.236
3	7	0	3.061	3.116
3	8	0	1.017	0.982
3	9	0	2.287	2.369
3	10	0	3.469	3.473
3	11	0	3.272	3.294
3	12	0	3.371	3.252
3	1	1	11.095	11.545
3	2	1	7.203	7.696
3	3	1	6.623	6.736
3	4	1	7.675	7.937
3	5	1	0.687	0.926
3	6	1	5.072	4.944
3	7	1	4.768	4.766
3	8	1	0.925	0.912
3	9	1	1.380	1.373
3	10	1	3.194	3.136
3	11	1	2.110	2.139
3	0	2	3.646	3.758
3	1	2	0.968	1.099
3	2	2	9.745	10.091
3	3	2	10.202	10.612
3	4	2	2.759	2.840
3	5	2	6.762	6.596
3	6	2	2.098	2.091
3	7	2	1.803	1.858
3	8	2	4.611	4.522
3	9	2	1.472	1.531
3	10	2	1.183	1.198
3	11	2	4.501	4.402
3	1	3	5.864	5.977
3	2	3	0.487	0.424
3	3	3	4.388	4.529
3	4	3	1.130	1.134
3	5	3	1.136	1.045
3	6	3	2.498	2.518
3	7	3	7.142	7.214
3	8	3	5.258	5.279
3	9	3	3.962	3.943
3	10	3	1.939	1.931
3	0	4	9.345	9.442
3	1	4	5.066	5.082
3	2	4	10.405	10.529
3	3	4	3.765	3.763
3	4	4	2.693	2.776
3	5	4	1.962	1.930
3	6	4	3.994	4.020
3	7	4	3.614	3.668
3	8	4	3.011	2.988
3	9	4	2.698	2.718
3	10	4	4.713	4.689
3	1	5	3.472	3.414
3	2	5	5.533	5.513
3	3	5	2.330	2.436
3	4	5	0.377	0.379
3	5	5	1.191	1.170
3	6	5	7.127	7.129
3	7	5	2.185	2.187
3	8	5	1.809	1.848
3	9	5	5.414	5.280
3	0	6	0.475	0.426
3	1	6	7.913	7.818
3	2	6	2.072	2.079
3	3	6	0.499	0.059
3	4	6	2.203	2.173
3	5	6	1.310	1.308
3	6	6	2.171	2.185
3	7	6	5.029	5.018
3	8	6	2.629	2.626
3	1	7	3.180	3.234
3	2	7	3.261	3.275
3	3	7	1.026	1.035
3	4	7	1.759	1.743
3	5	7	0.446	0.445
3	6	7	1.545	1.548
3	7	7	0.478	0.477
3	0	8	9.234	9.006
3	1	8	1.525	1.528
3	2	8	2.156	2.220
3	4	8	0.704	0.700
3	5	8	0.400	0.244
3	1	9	1.041	1.096
3	2	9	2.243	2.262
4	0	0	22.182	22.892
4	1	0	8.487	8.736
4	2	0	4.495	4.956
4	3	0	3.861	4.103
4	4	0	8.559	8.840
4	5	0	3.733	3.696
4	6	0	7.197	7.180
4	7	0	4.919	4.830
4	8	0	3.191	3.179
4	9	0	3.698	3.740
4	10	0	5.843	5.677
4	11	0	2.751	2.747
4	1	1	6.208	6.461

H	K	L	F(OBS)	F(CALC)
4	2	1	4.423	4.690
4	3	1	0.278	0.361
4	4	1	2.927	2.896
4	5	1	2.496	2.463
4	6	1	5.895	5.959
4	7	1	2.232	2.249
4	8	1	2.762	2.836
4	9	1	7.440	7.291
4	10	1	0.872	0.860
4	11	1	1.342	1.279
4	0	2	5.014	5.098
4	1	2	10.611	10.739
4	2	2	6.017	6.173
4	3	2	0.409	0.346
4	4	2	1.493	1.565
4	5	2	1.380	1.331
4	6	2	0.455	0.456
4	7	2	5.675	5.599
4	8	2	0.994	0.971
4	9	2	6.182	6.068
4	10	2	1.322	1.199
4	1	3	9.229	9.286
4	2	3	3.011	3.138
4	3	3	3.348	3.338
4	4	3	2.078	2.062
4	5	3	1.791	1.881
4	6	3	0.774	0.739
4	8	3	1.893	1.852
4	9	3	3.475	3.578
4	10	3	3.556	3.547
4	0	4	12.588	12.444
4	1	4	1.417	1.417
4	2	4	3.788	3.782
4	3	4	3.716	3.717
4	4	4	1.020	1.057
4	5	4	1.481	1.462
4	6	4	0.962	0.945
4	7	4	2.325	2.329
4	8	4	7.032	6.992
4	9	4	1.281	1.209
4	2	5	3.232	3.258
4	3	5	4.295	4.318
4	4	5	3.174	3.125
4	5	5	0.539	0.523
4	6	5	0.455	0.430
4	7	5	5.374	5.211
4	8	5	2.513	2.530
4	0	6	9.692	9.581
4	1	6	5.536	5.526
4	2	6	0.571	0.572
4	3	6	4.632	4.636
4	4	6	1.012	1.010
4	5	6	1.362	1.329
4	6	6	0.878	0.826
4	7	6	1.956	1.952
4	1	7	0.678	0.695
4	2	7	4.156	4.176
4	3	7	0.325	0.193
4	4	7	1.200	1.160
4	5	7	1.217	1.215
4	0	8	0.432	0.348
4	1	8	3.339	3.316
4	2	8	2.183	2.190
5	0	0	12.289	12.602
5	1	0	0.722	0.829
5	2	0	5.142	5.215
5	3	0	7.765	7.836
5	4	0	1.043	1.095
5	5	0	3.400	3.438
5	6	0	2.177	2.052
5	7	0	3.980	4.026
5	8	0	6.791	6.770
5	9	0	0.328	0.166
5	10	0	1.948	1.944
5	1	1	4.330	4.311
5	2	1	3.655	3.750
5	3	1	4.365	4.483
5	4	1	1.997	2.064
5	5	1	2.591	2.657
5	6	1	0.864	0.839
5	7	1	7.907	7.660
5	8	1	2.475	2.532
5	9	1	0.754	0.842
5	10	1	4.006	4.055
5	0	2	6.872	6.840
5	1	2	7.348	7.342
5	2	2	2.183	2.350
5	3	2	7.000	6.904
5	4	2	1.983	2.006
5	5	2	1.756	1.719
5	6	2	0.522	0.203
5	7	2	3.096	3.116
5	8	2	6.339	6.181
5	9	2	2.014	2.082
5	1	3	3.159	3.157
5	2	3	6.095	6.091
5	3	3	1.643	1.649
5	4	3	0.814	0.854
5	5	3	1.206	1.191
5	6	3	5.832	5.711
5	7	3	3.539	3.459
5	0	4	2.113	2.204
5	1	4	3.125	3.170
5	2	4	4.936	4.854
5	3	4	2.226	2.248
5	4	4	1.072	1.084

Observed and calculated structure factors.

H	K	L	F(OBS)	F(CALC)
5	5	4	2.980	3.002
5	6	4	2.330	2.272
5	7	4	2.611	2.542
5	1	5	0.930	0.885
5	2	5	2.742	2.728
5	3	5	5.371	5.361
5	4	5	1.954	1.970
5	5	5	3.988	3.958
5	6	5	2.904	2.799
5	0	6	2.316	2.340
5	1	6	1.603	1.595
5	2	6	4.182	4.129
5	3	6	2.293	2.329
5	4	6	1.156	1.054
6	0	0	5.800	6.032
6	1	0	1.826	1.907
6	2	0	7.910	7.947
6	3	0	3.206	3.193
6	4	0	1.661	1.692
6	5	0	4.901	4.859
6	7	0	2.371	2.287
6	8	0	0.739	0.696
6	9	0	0.690	0.705
6	1	1	0.406	0.351
6	2	1	2.962	2.970
6	3	1	7.336	7.308
6	4	1	3.394	3.458
6	5	1	6.426	6.346
6	6	1	3.101	3.004
6	7	1	1.504	1.529
6	8	1	0.652	0.593
6	0	2	2.003	2.004
6	1	2	2.858	2.843
6	2	2	1.484	1.442
6	3	2	1.029	1.052
6	5	2	3.310	3.378
6	6	2	5.110	5.034
6	1	3	3.275	3.396
6	2	3	1.122	1.132
6	3	3	2.296	2.271
6	4	3	9.391	9.324
6	5	3	5.582	5.482
6	6	3	1.342	1.320
6	0	4	4.545	4.491
6	1	4	0.904	0.870
6	2	4	1.316	1.339
6	3	4	1.078	1.091
6	4	4	1.962	1.962
6	5	4	0.754	0.664
6	1	5	1.272	1.281
6	2	5	0.838	0.796
6	3	5	1.287	1.241
7	0	0	5.119	5.023
7	1	0	0.394	0.352
7	2	0	1.556	1.568
7	3	0	0.528	0.368
7	4	0	2.209	2.209
7	6	0	4.174	4.120
7	1	1	1.956	1.914
7	2	1	0.597	0.612
7	3	1	2.078	2.020
7	4	1	8.217	8.045
7	5	1	2.982	3.017
7	6	1	0.293	0.259
7	0	2	1.783	1.778
7	1	2	0.603	0.538
7	2	2	5.397	5.402
7	3	2	1.017	0.959
7	4	2	0.342	0.381
7	5	2	1.507	1.437
7	2	3	3.197	3.141
7	3	3	4.713	4.653
8	0	0	1.649	1.742
8	1	0	3.449	3.401
8	2	0	3.930	3.810
8	3	0	2.119	2.104
8	4	0	2.820	2.780
8	1	1	1.096	1.094
8	2	1	4.727	4.646
8	3	1	0.806	0.763